MODEL REDUCTION FOR VEHICLE SYSTEMS MODELLING

by

Khanh V. Q. Nguyen

A thesis
presented to the University of Waterloo
in fulfillment of the
thesis requirement for the degree of
Master of Applied Science
in
Mechanical and Mechatronics Engineering

Waterloo, Ontario, Canada, 2014

© Khanh V. Q. Nguyen 2014

I hereby declare that I am the sole author of this thesis. This is a true copy of the thesis, including any required final revisions, as accepted by my examiners.

I understand that my thesis may be made electronically available to the public.

Abstract

The full model of a double-wishbone suspension has more than 30 differential-algebraic equations which takes a remarkably long time to simulate. By contrast, the look-up table for the same suspension is simulated much faster, but may not be very accurate. Therefore, developing reduced models that approximate complex systems is necessary because model reduction decreases the simulation time in comparison with the original model, enables real time applications, and produces acceptable accuracy.

In this research, we focus on model reduction techniques for vehicle systems such as suspensions and how they are approximated by models having lower degrees of freedom. First, some existing model reduction techniques, such as irreducible realization procedures, balanced truncation, and activity-based reduction, are implemented to some vehicle suspensions. Based on the application of these techniques, their disadvantages are revealed. Then, two methods of model reduction for multi-body systems are proposed.

The first proposed method is 2-norm power-based model reduction (2NPR) that combines 2-norm of power and genetic algorithms to derive reduced models having lower degrees of freedom and fewer number of components. In the 2NPR, some components such as mass, damper, and spring are removed from the original system. Afterward, the values of the remaining components are adjusted by the genetic algorithms. The most important advantage of the 2NPR is keeping the topology of multi-body systems which is useful for design purposes.

The second method uses proper orthogonal decomposition. First, the equations of motion for a multi-body system are converted to explicit second-order differential equations. Second, the projection matrix is obtained from simulation or experimental data by proper orthogonal decomposition. Finally, the equations of motion are transferred to a lower-dimensional state coordinate system.

The implementation of the 2NPR to two double-wishbone suspensions and the comparison with other techniques such as balanced truncation and activity-based model reduction also demonstrate the efficiency of the new reduction technique.

Acknowledgements

After more than two years at the University of Waterloo, I have had many chances to learn many interesting topics about modeling and control of vehicle systems. I would like to express my very great appreciation to Prof. Amir Khajepour, who gave me these chances. In addition, for my thesis, I think I would not accomplish the thesis without his help.

I am also particularly grateful for the assistance given by Dr. Thanh-Son Dao, who helped me get more familiar with MapleSim and Maple software. In addition, it is great to work in a large lab with more than 40 talented researchers. I would like to thank my colleagues, especially Saeid Khosravani, for their support. Special thanks also to my friends in Canada. They are friendly, honest, and give me many invaluable and unforgettable memories.

Finally, I would like to offer my special thanks to my beloved parents and my sisters. They always stand by me while I am studying abroad.

Table of Contents

List of Tables **viii**

List of Figures **ix**

1 Introduction **1**

1.1 Objectives 1

1.2 Outline 2

2 Literature Review **3**

3 2-Norm Power-Based Model Reduction for Vehicle Systems **13**

3.1 Extension of Activity-Based Model Reduction 13

3.2 2-Norm Power-Based Model Reduction 15

3.2.1 2-Norm of Power 15

3.2.2 2-Norm Power-Based Model Reduction (2NPR) 17

4 Model Reduction for Multi-body Systems via Proper Orthogonal Decomposition **19**

5 Examples and Comparison **23**

5.1 A 6 DOF Double-Wishbone Suspension with Bushings 23

5.1.1 Geometry 23

5.1.2 Analytical Model 26
5.1.3 Linearization 30
5.2 Improvement on IRP & Balanced Truncation 33
5.3 Application of IRP to the 6 DOF Double-Wishbone Suspension 36
5.4 Application of Balanced Truncation to the 6 DOF Double-Wishbone Suspension 40
5.5 Calculation of Activity in Louca's Method 46
5.6 2-Norm Power-based Reduction 48
5.7 Application of Model Reduction Techniques to 5 DOF Double-Wishbone Suspension 61
5.8 Application of Model Reduction Techniques to a Piston-Crank System . . 64
5.9 MapleSim Template of Model Reduction 66

6 Conclusion and Future Work **68**
6.1 Discussion 68
6.2 Summary and Thesis Contribution 69
6.3 Future Work 69

APPENDICES **71**

A Definitions **72**
A.1 Moments of a Transfer Function 72
A.2 QR Decomposition 72

B Linear System Control **73**
B.1 Linear State-Space Systems 73
B.2 Optimization in Hilbert Space 74
B.3 Signals 75
B.4 The Controllability Gramian 75
B.5 The Observability Gramian 77

C Least Squares Estimation (LSE) for Nonlinear Systems **78**

D Parameter Estimation for Nonlinear Systems via Genetic Algorithms **80**

E Dynamics of a 6 DOF Planar Double-Wishbone Suspension **82**

E.1 Analytical Model 82

E.2 Baumgarte Constraint Stabilization 91

F Demo of Using MapleSim Template of Model Reduction **94**

References **95**

List of Tables

5.1 Parameters of 6 DOF Double-Wishbone Suspension 25

5.2 Poles of Linear System with 16 States and Reduced Order System with 12 States 37

5.3 Hankel Singular Values of $[I_r, A_r, B_r, C_r]$ 42

5.4 Activities of All Components at $t = 4$ (seconds) 47

5.5 2-Norms of Power of Each Component at $t = 4$ (seconds) 50

5.6 Equivalent Values of 5 Remaining Components in 2 DOF Suspension . . . 56

5.7 Values of m_2 and m_3 64

E.1 Poles of Linear System $\left[\hat{I}, \hat{A}, \hat{B}, \hat{C}\right]$ 90

E.2 Poles of $[I, A, B, C]$ and $\left[\hat{I}, \hat{A}, \hat{B}, \hat{C}\right]$ Models 93

List of Figures

2.1 Recent Model Reduction 4

2.2 Interconnected System: Linear Subsystem $\sum_{lin}$ and Nonlinear Subsystem $\sum_{nl}$ 7

3.1 Comparison of Energy-Based Metrics 16

3.2 2-Norm Power-Based Reduction 17

5.1 Double-Wishbone Suspension [15] 24

5.2 Suspension Geometry of Planar Double-Wishbone Suspension 24

5.3 Displacement of Chassis in Analytical Model 27

5.4 ADAMS Model of Planar Double-Wishbone Suspension 28

5.5 Comparison of Chassis Displacement in Analytical and ADAMS Models . . 29

5.6 Chassis Displacement of Linear and Nonlinear Models 32

5.7 Comparison of Nonlinear Model, Linear Model with 16 States, and Linear Model with 12 States 39

5.8 Output Error Between 6 DOF Suspension and Reduced Model with 12 States 39

5.9 Comparison of Nonlinear System with Reduced Systems of Order 12 & 11 . 42

5.10 Comparison of Nonlinear System with Reduced Systems with Order of 2 . 43

5.11 Output Error of Reduced Models with 2 States & 12 States 44

5.12 Comparison of Nonlinear System and Reduced Order Models 45

5.13 Comparison of Nonlinear System and Reduced Order Models 45

5.14 Activity of All Components in 6 DOF Suspension in $t \in [0, 4]$ (second) . . 46

5.15 2-Norm of Power of All Components in $t \in [0, 4]$ (second) 51
5.16 Reduced Model with 5 DOF 52
5.17 Comparison of Chassis Displacement Between 6 DOF and 5 DOF Model . 52
5.18 Reduced Model with 4 DOF 53
5.19 Chassis Displacement in Reduced 4 DOF Model 53
5.20 Reduced Model with 3 DOF 54
5.21 Chassis Displacement in Reduced 3 DOF Model 54
5.22 Reduced Model with 2 DOF 55
5.23 Chassis Displacement in 2-DOF Models 55
5.24 Chassis Displacement After Applying Genetic Algorithms 57
5.25 Comparison of Two 4 DOF Reduced Models without Mass of Chassis and without Gravity of Wheel 58
5.26 Comparison of 2NPR and Truncation Methods 59
5.27 Output Error of Reduced Model with 2 States & 2 DOF Model of 2NPR . 60
5.28 5 DOF Planar Double-Wishbone Suspension 61
5.29 Vertical Displacement of Wheel Center: Truncation Methods and 2NPR . . 62
5.30 Activity of Gravity of Upper Arm (Ag3) and Mass of Lower Arm (Am1) . 63
5.31 Comparison of Systems without Mass of Upper Arm $m1$ and without Gravity of Upper Arm g_3 63
5.32 Schematic of Piston-Crank Assembly 64
5.33 2-Norm of Power of All Components 65
5.34 Displacement of Piston in Reduced Model Before Finding Equivalent Values of Remaining Components 65
5.35 MapleSim Template of Model Reduction 66
5.36 MapleSim Template of Model Reduction 67

6.1 Equivalent Components of Mechanical And Electrical Circuits [65] 70

D.1 Parameter Estimation via Genetic Algorithms 81

E.1 Chassis Displacement of Linear and Nonlinear Models 89
E.2 Comparison of Chassis Displacement between Two Analytical Models (equations (E.33) & (E.28)) 92

Chapter 1

Introduction

1.1 Objectives

Model reduction is a technique that reduces the number of degrees of freedom, or differential equations (DEs), or components from a system. The first advantage of model reduction is to decrease simulation time. Model reduction can also enable real-time implementation. Furthermore, reduced models are extremely useful for the control and design of vehicles.

Singular value-based truncation and Krylov-based reduction are two most common reduction techniques nowadays. The principle of singular value-based truncation is to remove less important states by comparing their singular values and simplify the system to a fewer number of equations. For example, in balanced truncation, Hankel singular values represent the importance of each state (how states affect the system responses), so the states that Hankel singular values are relatively smaller than others are removed. On the other hand, the Krylov-based reduction approximates the transfer function of a system by matching moments (described in Appendix A.1). The projection matrices of Krylov-based reduction are derived by applying Arnoldi algorithm or Lanczos process to construct "an orthogonal basis of Krylov subspace". These two techniques are very effective in linear systems. However, they have disadvantages for nonlinear systems, and there are very few studies for model reduction in vehicle systems or complex suspensions.

In summary, the above factors briefly highlight the importance of developing a model reduction for vehicle systems. The first goal of this thesis is to apply and extend previous studies of model reduction, such as irreducible realization procedure (IRP), balanced truncation, and activity-based model reduction to vehicle systems. In addition, two new

reduction methods for nonlinear systems are proposed. They are called 2-norm power-based model reduction and model reduction for multi-body systems via proper orthogonal decomposition. These two methods can be applied to vehicle systems as well as multi-body systems in general.

1.2 Outline

The thesis is organized as follows:

Chapter 1 introduces the main goals of the thesis and research outline.

Chapter 2 briefly presents the literature review.

Chapter 3 describes improvements in a previous reduction technique called activity-based reduction, and suggests a new model reduction based on 2-norm of power, least squares estimation and genetic algorithms. This method is called 2-norm power-based model reduction (2NPR).

Chapter 4 introduces a new reduction method for multi-body systems via proper orthogonal decomposition.

The application of several model reduction methods to some vehicle systems, such as a 6 DOF planar double-wishbone suspension with bushings, and a piston-crank system, is investigated in Chapter 5. First, the analytical model of the 6 DOF planar double-wishbone suspension is derived, and verified by an ADAMS model. Based on two commonly-used singular value-based reduction, namely irreducible realization procedure (IRP) and balanced truncation, the linear model with the order of 16 is successfully approximated by a model having only two states. In addition, the new model reduction, 2NPR, can simplify the 6 DOF suspension to a 2 DOF nonlinear model by eliminating components less affecting to system behavior (which 2-norms of power are smaller than others) and finding equivalent values of the remaining components. The 2NPR is also compared with IRP and balanced truncation methods.

Finally, Chapter 6 discusses the disadvantages of truncation and the advantages of 2NPR, and summarizes the thesis contribution and future work.

Chapter 2

Literature Review

In the first chapter, the outline and the motivation of model reduction for vehicle systems were discussed. The aim of this chapter is to relate this research to previous studies to evaluate their strengths and weaknesses.

The most commonly-used model reduction techniques are shown in Figure 2.1. These model reduction techniques can be categorized into four types, namely singular value-based truncation, Krylov susbspace-based reduction, statistic-based reduction, and physical reduction.

First, truncation and singular perturbation are two most popular methods for linear systems. The basics of truncation and singular perturbation are to transform a linear system into new coordinates where new states are sorted in a certain order, such as in decreasing Hankel singular values; and then shorten these new states with truncation or singular perturbation methods [2]. In order to sort the states, most authors used singular value decomposition (SVD) [26], or QR decomposition, or RQ decomposition [72]. Sections 5.2, 5.3, and 5.4 will discuss in detail two most commonly used truncation methods for linear systems.

There are three main characteristics of a linear system, namely controllability, observability, and stability. Some truncation method can apply to uncontrollable or unobservable systems to make them controllable and observable [72, 11]. For example, irreducible realization procedure (IRP) is one of the most commonly-used model reduction that separates the uncontrollable or unobservable states of the original system, and remove these states to create a new reduced controllable and observable system. However, this truncation is only available to uncontrollable or unobservable systems since they cannot reduce the order of linear controllable and observable systems. Moreover, defining finite controllability

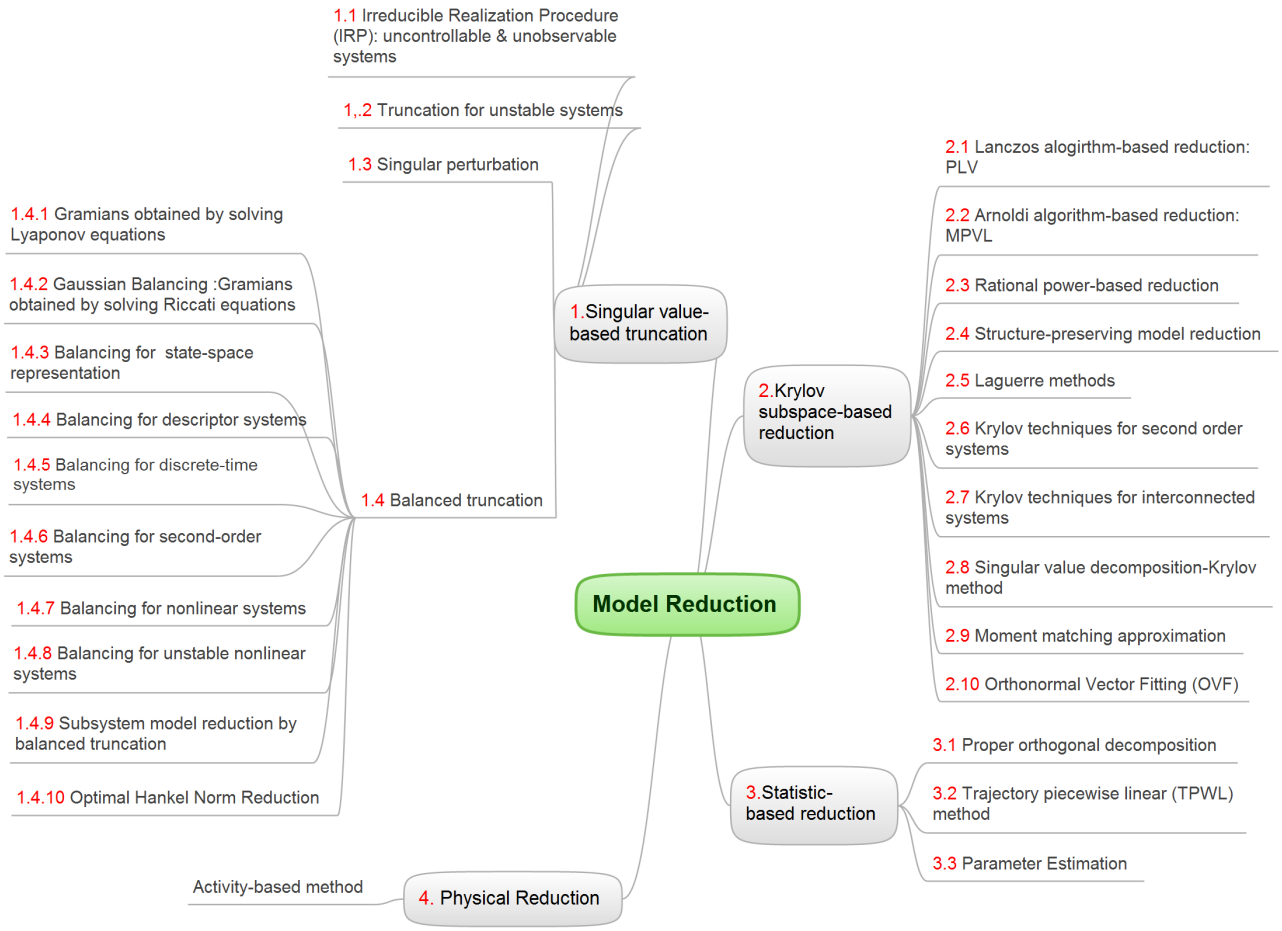

Figure 2.1: Recent Model Reduction

and observability Gramians (Appendix B) for balanced truncation in unstable systems is extremely difficult. In 1999, Zhou introduced new Gramians in the frequency domain, and developed a new balancing truncation for unstable systems [81].Another method to define the Gramians of unstable systems is to use time-limited Gramians [2]. In general, linear systems are usually reduced by IRP or Zhou's truncation in [81] in order to make the systems controllable, observable and stable before being reduced by other methods. For example, Chapter 5 will suggest that the 6 DOF planar double-wishbone suspension should be reduced by IRP first, and simplified by balanced truncation afterwards.

In contrast to uncontrollable or unobservable or unstable systems, many truncation methods, such as balanced truncation and Gaussian balancing, have been developed for

stable, controllable and observable systems. In this area, Bruce Moore is a pioneer in this area introducing controllability and observability Gramians (Appendix B), and balanced truncation for state-space representations [44]. The main goal of balanced truncation is to remove states that have less effect on the system behaviors. It is achieved by transforming the states into new states associated to the largest Hankel singular values. Furthermore, the Lyapunov's equations are solved to obtain controllability Gramian P and observability Gramian Q. Hankel singular values are the singular values of the square root of the product of the controllability Gramian and the observability Gramian ($\sqrt{PQ}$). In addition, the invertible projection matrix T is calculated based on the controllability and observability Gramians. The error bound of balanced truncation is also determined as follows [40]:

$$\|G - G_r\|_\infty \leq 2(\sigma_{l+1} + \cdots + \sigma_m), \tag{2.1}$$

where G, G_r, and σ_i ($i = \{l+1, l+2, \cdots, m\}$) are, respectively, the transfer function of the original system and the reduced system, and Hankel singular values corresponding to the states that are removed. Later, many studies have widely investigated, and extended balanced truncation in order to improve error bounds, simulation time, and Gramians functions. For instance, linear-quadratic Gaussian (LQG) balancing truncation uses Riccati equations in order to find the Gramians and the transformation matrix [27, 28, 29]. It is not limited to asymptotically stable systems like Lyapunov-based balanced truncation, and the error bound of LQG balancing truncation is much smaller than that of balanced truncation. However the disadvantage of LQG is that it is difficult to numerically solve Riccati equations, especially for the generalized algebraic Riccati equations [33, 77].

Truncation methods have been extended to descriptor systems [67, 26, 42]. For example, LQG for descriptor systems solves the generalised algebraic Riccati equations to obtain the Gramians. Mockel also successfully illustrated this truncation by reducing the discretization model of the flow of an incompressible fluid with 869 states to a model that has only 38 states [26]. Nevertheless, the computation of most truncation methods for descriptor systems is quite complicated.

Al-Saggaf et al. also proposed balanced truncation for discrete-time systems as well as defined its error bound [70]. In this method, the Gramians are the solutions of Lyapunov equations for discrete-time systems. In addition, balanced truncation for linear time-varying systems has been developed by Verriest [75] and Shokoohi [66]. Its error bounds were determined by Lall [32] and Sandberg [60].

Some balanced truncation methods have been studied for second-order systems by using position and velocity Gramians [43, 78, 51]. By comparing four structure-preserving second-order balanced truncation methods with Meyer's truncation in [43] and Chahlaoui's

method in [78], Ries argued that position-velocity singular values-based truncation preserves the stability of symmetric second-order systems. However, all balanced truncation methods for second-order system do not fully preserves stability in the reduced models [51].

Truncation is also developed for nonlinear systems. Based on the input and output energy functions, Scherpen extended balanced truncation for stable nonlinear systems [61]. He defined the controllability and observability functions of a nonlinear system as metrics measuring the importance of states. These functions are solutions of Lyapunov and Hamilton-Jacobi equations. An algorithm to transform a stable nonlinear system into a balanced form was also presented. Scherpen continued to develop balancing for unstable nonlinear systems [63] and H_∞ balancing for nonlinear system [62]. However Scherpen's methods are not intrinsic because their singular value functions are not unique [23], and these controllability and observability functions still depend on inputs. Hence, Krener introduced a more intrinsic reduction for nonlinear systems than Scherpen's methods [31]. Based on a Taylor series, the normal forms of the controllability and observability functions are defined, and quite similar to Scherpen's. Another approach of truncation for nonlinear systems is to use empirical Gramians. A constant controllability Gramian is calculated by the data obtained from many different directions of inputs. In addition, the data observed from many different initial values distributed on a unit sphere is used to estimate a constant observability Gramian [57]. After that, the transformation matrix T is computed, and the balanced truncation is applied in the same way for linear systems. The advantage of this method is that it requires only simple matrix computations, and the reduced model is nonlinear. Its implementation in some models demonstrates the efficiency of the empirical Gramians-based truncation. For example, Liu applied the empirical Gramian balanced truncation to a classical 2 DOF quarter car model, and an exhaust gas recirculation valve [35]. Although the reduced models of these techniques still depend on the inputs, their methods of defining these normal forms or using empirical Gramians are potentially useful for our studies to decrease the influence of inputs on our reduction method that will be described in Chapter 3.

While most reduction methods focus only on linear systems or nonlinear systems, Besselink had a different approach for nonlinear systems. It is interesting to know that some nonlinear systems can be decomposed into a linear subsystem with relatively higher order and a nonlinear subsystem with relatively lower order (Figure 2.2), then only the linear subsystem is reduced by truncation methods, for example balanced truncation or LQG balancing [6]. The condition of the nonlinear system stability and the error bound of this method are also defined.

The system that Besselink decomposed into two subsystems looks quite similar to in-

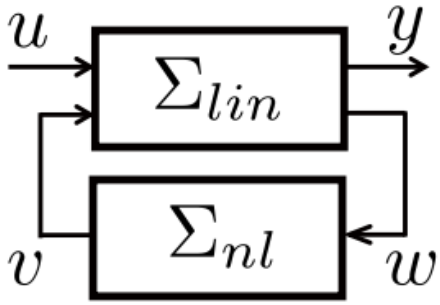

Figure 2.2: Interconnected System: Linear Subsystem $\sum_{lin}$ and Nonlinear Subsystem $\sum_{nl}$

terconnected systems. The studies of balanced truncation in interconnected systems have been investigated in [18, 49, 71].

The second type of model reduction is based on Krylov subspace, and it is typically applied to large electronic circuits. The basics of Krylov subspace-based reduction are to approximate the transfer function of linear systems by matching a finite number of its moments (described in Appendix A.1). In order to satisfy this moment matching property, Krylov subspaces are determined to construct projection matrices.

Pillage developed an approximation method related to Krylov subspace [48]. His method is called asymptotic waveform evaluation (AWE). Developing from AWE, Feldmann introduced Pade approximation via Lanczos (PLV) algorithm to compute Pade approximation via Lanczos process for single-input single-output systems [16], and MPVL extended to multiple-input multiple-output systems [17]. A Krylov subspace based Lanczos process for model order reduction, and an overview of the development of Krylov subspace techniques were also reported in [4]. On the other hand, there are different Krylov subspace-based techniques using Arnoldi algorithm to replace Lanczos process, for example PRIMA for RLC interconnect circuits [1]. The Krylov techinques based on Arnoldi algorithm and Lanczos process were briefly described in [59]. The third algorithm in Krylov subspace-based truncation is rational power [24]. The later studies of Krylov subspace-based truncation have developed not only the accuracy of reduction, but also the preservation of the system properties. Some examples of these developments are a rational Krylov method [20], an algorithm for the construction of structure-preserving projection matrices in Krylov subspace [80], and Laguerre method [30].

Krylov subspace techniques are available for not only linear systems, but also for second-order, semi-second-order nonlinear systems. For interconnected systems, Vandendorpe

suggest ISBT algorithm based on Krylov subspace and Gramian in order to reduce each subsystem and to preserve their interconnected structure [71]. This algorithm also was combined some other model reduction and applied to large-scale systems.

Third, the statistic-based reduction includes the proper orthogonal decomposition (POD), the trajectory piecewise-linear method (TPWL), and parameter estimations. These techniques are fairly similar to linear statistical methods: their reduced models are based on the statistical data generated by different inputs and different time.

For POD, the importance of each state is determined by the data collected from different initial values. Considering a nonlinear system:

$$\begin{aligned} \dot{x} &= f\left(x, u\right) \\ y &= h\left(x\right), \end{aligned} \tag{2.2}$$

where u, x, and y, respectively, are input vector, state vector, and output vector. Three main steps of POD are described as follows:

- obtain snapshots of the state vector from simulation or experiments: $X = \left[x\left(t_0\right)\ x\left(t_1\right) \cdots x\left(t_N\right)\right]$, $x\left(t\right) \in \mathbb{R}^N$
- calculate the singular value decomposition of X: $X = U\Sigma V^T$. This decomposition is possible because X is a numerical matrix.
- transform the model to a new state coordinate system: $\hat{x} = U^T x$.

$$\dot{\hat{x}} = U^T f\left(U\hat{x}, u\right), \tag{2.3}$$

- truncate some states of the new system: let a projection matrix, $\bar{U}$, be the first K columns of U, when $K < N$ and N is the numbers of states in the nonlinear system (equation (2.2)). The lower-dimensional state coordinates $\bar{x}$ is defined as: $\bar{x} = \bar{U}\hat{x}$. The nonlinear model is transferred to the new lower-dimensional state coordinate system:

$$\dot{\bar{x}} = \bar{U}^T U^T f\left(U\bar{U}\bar{x}, u\right), \tag{2.4}$$

This method is applied mostly in fluid mechanics, for example turbulence flows, as a model reduction tool and a model analysis tool based on principal component analysis [12, 5]. In addition, POD was recently extended to structural dynamics [34], and high order model obtained from the discretization of PDE's [3]. However, reduced models of

POD depend on initial conditions, so they are only valuable for small changes of the initial conditions.

Rewieski developed a novel model reduction based on linearization collected from many different training trajectories, and called trajectory piecewise-linear method (TPWL) [52]. In other words, TPWL uses weighting funcations at certain points along the trajectory to approximate nonlinear functions. The procedure of TPWL is described as follows:

- simulate the nonlinear system with a training input $u_0(t)$

$$\begin{aligned} \dot{x} &= f(x,u) \\ y &= g(x,u), \end{aligned} \tag{2.5}$$

- choose many points on the training trajectory (x_0^i, u_0^i)
- apply Taylor's Series to linearize the nonlinear system around point i (x_0^i, u_0^i)

$$\begin{aligned} \dot{x} &\simeq f\left(x_0^i, u_0^i\right) + A_i\left(x - x_0^i\right) + B_i\left(u - u_0^i\right) \\ y &\simeq g\left(x_0^i, u_0^i\right) + C_i\left(x - x_0^i\right) + D_i\left(u - u_0^i\right), \end{aligned} \tag{2.6}$$

  where A_i, B_i, C_i and D_i are partial derivatives of f and g with respect to x and u

- rewrite equations (2.6) as a local linearization

$$\begin{aligned} \dot{x} &\simeq f_i(x,u) \\ y &\simeq g_i(x,u), \end{aligned} \tag{2.7}$$

  where

$$\begin{aligned} f_i(x,u) &= f\left(x_0^i, u_0^i\right) + A_i\left(x - x_0^i\right) + B_i\left(u - u_0^i\right) \\ g_i(x,u) &= g\left(x_0^i, u_0^i\right) + C_i\left(x - x_0^i\right) + D_i\left(u - u_0^i\right). \end{aligned} \tag{2.8}$$

- choose a weighting function $w_i(x,u)$ at each point i in order to obtain the global linearization

$$\begin{aligned} \dot{x} &\simeq \sum_i w_i(x,u) f_i(x,u) = \hat{f}(x,u) \\ y &\simeq \sum_i w_i(x,u) g_i(x,u) = \hat{g}(x,u). \end{aligned} \tag{2.9}$$

  The nonlinear system has been approximated by the linear model (2.9).

- apply reduction techniques to reduce the order of the linear model. For instance, Rewieski used Krylov subspace method to transform the state coordinates $z = Wx, W \in R^{\hat{n}xn}$

$$\begin{aligned} \dot{z} &= \sum_i w_i \left(W^T z, u\right) W f_i \left(W^T z, u\right) \\ y &\simeq \sum_i w_i \left(W^T z, u\right) g_i \left(W^T z, u\right). \end{aligned} \tag{2.10}$$

TPWL has successfully applied to nonlinear analog circuits, MEMS, and biomems components [73, 74], fluid dynamics [22], heat-transfer models [79]. However, TPWL still cannot well approximate many nonlinear functions [10].

Similar to POD and TPWL, parameter estimation uses the simulation data of the original models to find equivalent parameters of standard models. Kim et al. developed a parameter identification process in order to determine the equivalent vehicle parameters of a quarter-car model that have almost same behaviour as a real suspension [9]. From the real experimental vehicle, its behavior is measured, such as acceleration of chassis and knuckle $\ddot{z}_s, \ddot{z}_u$, suspension deflection z_{sus}, and tyre forces f_t. For the quarter-car model, the spring stiffness k_s, nonlinear damping rates for extension b_1 and compression b_2, sprung mass m_s, and unsprung mass m_u are unknown and considered as variables. In the first step, the equations of motion of the quarter-car model are derived as follows:

$$m_s\ddot{z}_s + k_s z_{sus} + 0.5\left[1 + sgn(\dot{z}_{sus})\right] b_1 \dot{z}_{sus} + 0.5\left[1 - sgn(\dot{z}_{sus})\right] b_2 \dot{z}_{sus} = 0 \tag{2.11}$$

$$m_u\ddot{z}_u - k_s z_{sus} - 0.5\left[1 + sgn(\dot{z}_{sus})\right] b_1 \dot{z}_{sus} - 0.5\left[1 - sgn(\dot{z}_{sus})\right] b_2 \dot{z}_{sus} - f_t = 0. \tag{2.12}$$

Let $\theta = \begin{bmatrix} m_s & m_u & k_s & b_1 & b_2 \end{bmatrix}^T$ be a variable vector of equations (2.11) and (2.12), and rewrite these equations in the linear form:

$$\theta^T \phi_1 = 0 \tag{2.13}$$

$$\theta^T \phi_2 - f_t = 0, \tag{2.14}$$

where $\phi_1 = \begin{bmatrix} \ddot{z}_s \\ 0 \\ z_{sus} \\ \frac{1+sgn(\dot{z}_{sus})}{2}\dot{z}_{sus} \\ \frac{1-sgn(\dot{z}_{sus})}{2}\dot{z}_{sus} \end{bmatrix}$ and $\phi_2 = \begin{bmatrix} 0 \\ \ddot{z}_u \\ -z_{sus} \\ -\frac{1+sgn(\dot{z}_{sus})}{2}\dot{z}_{sus} \\ -\frac{1-sgn(\dot{z}_{sus})}{2}\dot{z}_{sus} \end{bmatrix}$.

Let $\widehat{\theta} = \left[\widehat{m}_s \ \widehat{m}_u \ \widehat{k}_s \ \widehat{b}_1 \ \widehat{b}_2\right]^T$ be an approximation of the variable vector, ϵ_1 and ϵ_2 be errors:

$$\epsilon_1 = \widehat{\theta}^T \phi_1 \tag{2.15}$$

$$\epsilon_2 = \widehat{\theta}^T \phi_2 - f_t. \tag{2.16}$$

The objective function E is

$$E = \sum_{k=1}^{N} \left[\epsilon_1^2(k) + \epsilon_2^2(k)\right]. \tag{2.17}$$

E minimizes iff $\frac{\delta E}{\delta \widehat{\theta}} = 0$. Hence, the equivalent parameters of the quarter-car model are calculated from:

$$\widehat{\theta} = \left\{\sum_{k=1}^{N} \left[\phi_1(k)\,\phi_1^T(k) + \phi_2(k)\,\phi_2^T(k)\right]\right\}^{-1} \left\{\sum_{k=1}^{N} \phi_2^T(k)\, f_t(k)\right\}. \tag{2.18}$$

In general, the reduced models of statistic-based reduction techniques depend on inputs because the statistical data is varied by inputs. Therefore, these reduced models are only acceptable in a certain domain where inputs slightly change from the nominal inputs.

The last category of model reduction techniques is the physical reduction. Among energy-based metrics, such as root mean square (RMS) of power and energy [55], Louca introduced activity which is the time integral of the absolute value of power, and defined as follows [37]:

$$A = \int_{t_0}^{t_0+T} |P(\tau)|\, d\tau, \tag{2.19}$$

where $P(t)$ is the power. The activity of an element reflects the importance of this element in dynamical systems because it represents energy transaction in this element over a particular time T. In addition, activity is different from energy because energy is just the time integral of power.

According to Louca, activity is simpler in computation and clearer in physical interpretation than RMS power. Second, a new model order reduction algorithm based on activity and bond graphs was proposed. In other words, the bond graphs of a system are used to calculate the power of each energy component. The activity of each element is then calculated from equation (2.19) in the bond graphs. Because the activity reflects the importance of components, less important components have relatively smaller activity. Therefore, the system is reduced by removing these less important componets in the bond

graphs, and afterwards reconstructed an equivalent dynamical system. Finally, in order to evaluate the algorithm, Louca applied it to some models such as a nonlinear quarter car model [37], a tracctor-semitrailer [36], and an integrated hybrid vehicle model consisting of an engine, drivertrain, hydraulics [38].

In contrast to most of the previous reduction, for example balanced truncation and proper orthogonal decomposition, where reduced models are just the set of equations or matrices, the activity-based reduction still preserves the topology of mechanical systems. Additionally, activity is a potentially useful tool for systems design because it possibly describes how much each element affects system behavior. However, because the relative activity of each element varies with the change of inputs, the reduced models of this reduction still depend on the system inputs like other reduction techniques for nonlinear system.

In summary, model reduction techniques for linear systems have been studied for a long time since 1981, but model reductions for nonlinear systems are relatively new, having been developed in the past decade, and still have some disadvantages such as depending on inputs. In addition, there are very few studies of model reduction applications to vehicle systems. Therefore, this thesis is devoted to develop two new model reduction methods more suitable for vehicle systems and specifically for suspensions. The first method is called 2-norm power-based model reduction (2NPR) which combines a new energy-based metric (called 2-norm of power) and genetic algorithms or least squares estimation. In some multi-body systems, the new energy metric is more accurate in term of estimating element importance than the activity-based method.

Furthermore, POD is very common in model reduction for partial differential equations, and has been applied to fluid mechanics, structural mechanics, and heat transfer. However, for there are very few studies of POD for multi-body systems, which are modeled as differential-algebraic equations. Therefore, the second proposed method is model reduction for multi-body systems via POD.

Chapter 3

2-Norm Power-Based Model Reduction for Vehicle Systems

The models of vehicle systems as well as multi-body systems in general are often described by nonlinear algebraic- differential equations that the current reduction methods may not directly applicable. For example, in order to apply balanced truncation (Section 5.4), the system needs to be linear, controllable and observable. POD is only applicable for partial differential equations (PDEs) and ordinary differential equations (ODEs). Therefore, the preliminary studies in this chapter will look into the extension of the activity-based method to handle non-bond graph formulation, a new measure based on the 2-norm of power, and a new model reduction combining a new energy metric and genetic algorithms.

3.1 Extension of Activity-Based Model Reduction

Louca introduced activity for bond-graph models as follows [37]:

$$A = \int_{t_0}^{t} |P(\tau)| \, d\tau = \int_{t_0}^{t} |e(\tau) f(\tau)| \, d\tau, \tag{3.1}$$

where $P(t)$ is the power, $e(\tau)$ is the element effort, and $f(\tau)$ is the element flow. He also introduced a model order reduction algorithm (MORA) or activity-based model reduction to eliminate relatively less important components in the bond graphs. This section extends Louca's studies from bond-graph modelings to the conventional representation of physical dynamic systems.

First, in order to determine the activity of components in the conventional representation of physical dynamic systems, the power of the components needs to be defined. Louca defined the power as the product of an element effort and the element flows in the bond-graph modeling:

$$P(t) = e(t)f(t). \tag{3.2}$$

On the other hand, in the conventional representation, the power of a component such as an applied force, torque, mass, spring, or damper is defined by the time derivative of work or energy:

$$P(t) = \frac{dW}{dt} = \frac{dE}{dt}, \tag{3.3}$$

where W, E, respectively, are the work and energy of a component.

From equation (3.3), the power $P(t)$ of some components in multi-body systems is derived as follows:

- applied forces

$$P(t) = F^T v, \tag{3.4}$$

- applied torques

$$P(t) = \tau^T \omega, \tag{3.5}$$

- gravity (or the mass affects to the potential energy)

$$P(t) = mg^T v, \tag{3.6}$$

- moment of inertia (the mass affects to the angular kinetic energy)

$$P(t) = \omega^T I \dot{\omega}, \tag{3.7}$$

- mass (the mass affects to the translational kinetic energy)

$$P(t) = mv^T \dot{v} \tag{3.8}$$

- springs

$$P(t) = kL\dot{L} \tag{3.9}$$

- dampers

$$P(t) = C\dot{L}^2, \tag{3.10}$$

where $F = \begin{bmatrix} F_x & F_y & F_z \end{bmatrix}^T$, $\tau = \begin{bmatrix} \tau_x & \tau_y & \tau_z \end{bmatrix}^T$, respectively, are the applied force and the applied torque; $\omega = \begin{bmatrix} \omega_x & \omega_y & \omega_y \end{bmatrix}^T$, $v = \begin{bmatrix} v_x & v_y & v_z \end{bmatrix}^T$, are the angular velocity, and translational velocity; m is the mass of the object; I is the moment of inertia tensor; g is the acceleration vector of gravity; k and C, respectively, are the spring constant and the damping coefficient; L is the distance that spring is stretched or compressed away from its rest position.

After calculating the activity of all components, MORA will be applied to obtain reduced models.

3.2 2-Norm Power-Based Model Reduction

This section will introduce a new energy-based metric and a new algorithm to reduce nonlinear systems called 2-norm power-based reduction, which combines a new enery metric, least square estimation and genetic algorithms.

3.2.1 2-Norm of Power

In order to determine the importance of components in multi-body systems, some energy metrics have been studied, such as Rosenberg and Zhou with RMS power [55], and Louca with activity [37]. Louca argued that the activity of a component presents the amount of energy flowing through this component, and it is better than other previous metrics in term of calculation and accuracy, such as the root mean square of power and energy. A new metric, namely 2-norm of power, is proposed to evaluate the importance of each component.

The law of conservation of energy demonstrates the total work of all components in a multi-body system is conserved over time. Therefore, total power of all components in the multi-body system is equal zero over time. At any arbitrary time point, the larger the magnitude of power of a component is, the stronger effect it has on the system. That is the main reason why power is used to determine the effect of each component to a multi-body response. However, power varies by time, so the question is how to compare the power of each component for a period of time.

In order to compare the power over a time period, the 2-norm of power is introduced in this thesis.

It is also straightforward to demonstrate that if the power of a component A is higher than that of a component B in a period of time, the 2-norm power of component A is higher than that of component B.

Figure 3.1 demonstrates different energy-based metrics of an oscillation power $P(t) = sin(\frac{\Pi}{2}t)$

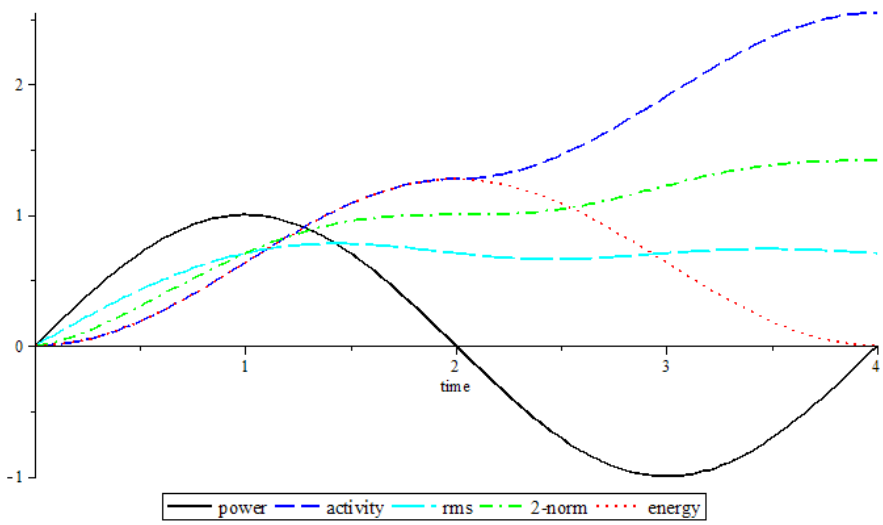

Figure 3.1: Comparison of Energy-Based Metrics

The general formula of the 2-norm of power is defined as follows:

$$\|P\|_2 = \sqrt{\int_{t_0}^{t} [P(\tau)]^2 \, d\tau}. \tag{3.11}$$

If the data is collected from experimental tests, based on Riemann sum, 2-norm of power can be determined by the following formula:

$$\|P\|_2 \simeq \sqrt{\sum_{i=1}^{N-1} [P(t_i)]^2 (t_{i+i} - t_i)}, \tag{3.12}$$

where N is the number of points on the trajectory, $P\,(t_i)$ is the measurement of power at the time t_i, $i \in \{1, 2, 3, ..., N\}$.

3.2.2 2-Norm Power-Based Model Reduction (2NPR)

A new model reduction technique called 2-norm power-based model reduction (2NPR) is proposed in this section. The fundamentals of the 2-norm power-based reduction are to compare the relative 2-norm of power among components, then remove components less important to system behavior, and finally find the equivalent values of the remaining components.

Considering a multi-body system (equations (C.1) and (C.2)), u is the vector and q is the state vector. Choosing the set of N different input vectors: $\mathcal{U} = \left\{u^{(1)}, u^{(2)}, \cdots, u^{(N)}\right\}$, the flow chart of 2NPR is shown in Figure 3.2.

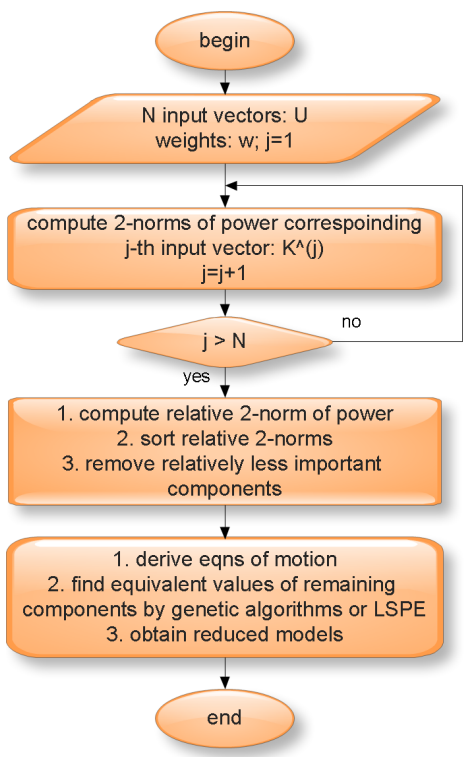

Figure 3.2: 2-Norm Power-Based Reduction

The procedure of 2NPR for a system is described as follows:

- Assign a weight $\varpi^{(j)}$ for each input vector $u^{(j)}, j \in \{1, \cdots, N\}$, such that $\sum_{j=1}^{N} \varpi^{(j)} = 1$.

- Compute the 2-norm of power of every component for each input vector $u^{(j)}, j \in \{1, 2, \cdots, N\}$: based on Section 3.2.1, the 2-norm of power of the ith component $\kappa_i^{(j)}$ corresponding to the input vector $u^{(j)}$ is determined. Let $\mathcal{K} = \left\{\kappa_i^{(1)}, \kappa_i^{(2)}, \cdots, \kappa_i^{(N)}\right\}$ be the set of N 2-norms of power of the ith component corresponding with N input vectors. The 2-norm of power of the ith component for the data generated from the input set $\mathcal{U}$ is defined as follows:

$$\kappa_i = \sum_{j=1}^{N} \varpi_j \kappa_i^{(j)}. \tag{3.13}$$

- Compute the relative 2-norm power κ_{ri} of the ith component for the input set $\mathcal{U}$ as follows:

$$\kappa_{ri} = 100 \frac{\kappa_i}{\kappa_{total}}, \tag{3.14}$$

  where $\kappa_{total} = \sum_{i=1}^{N} \kappa_i$ is the sum of 2-norms power of all components in the system.

- Compare and sort the relative 2-norm power among components in decreasing order.

- Remove less important components whose relative 2-norm power is relatively smaller than others. There is a threshold to determine whether output errors are acceptable. However, the new equations of motion of reduced models should be numerically solved after removing these components.

- Derive the equations of motion of the reduced models by Lagrange's equations.

- Find the equivalent values of the remaining components by the Least Square Estimation (LSE) in Appendix C, or Genetic Algorithms in Appendix D in order to compensate the energy lost by removing some components and to minimize the squared error with the original model .

Noting that there are three different components for each body in the multi-body system: the gravity (equation (3.6)), the moment of inertia (equation (3.7)), and the mass that only affects to kinetic energy (equation (3.8)). Therefore, if a mass is eliminated, the corresponding gravity component will be removed, but the moment of inertia will be still available.

It is better to evaluate the advantages and disadvantages of this method after implementing it to some vehicle systems. Therefore, the evaluation of this method will be discussed later in this thesis (Sections 5.6 and 6.1).

Chapter 4

Model Reduction for Multi-body Systems via Proper Orthogonal Decomposition

POD was developed more than 100 years ago [47]. It has been successfully applied to turbulent flows, structure mechanics, heat transfer, MEMS, and battery simuation because POD can reduce the number of partial differential equations (PDE), and ordinary differential equations (ODE). However, there are very few studies of POD for multi-body systems.

Some studies about POD for differential-algebraic equations (DAEs) have been investigated last decade. Most of them do not take into account the Lagrange's multipliers [54, 41, 34, 68, 76], so these methods are inapplicable for constrained multibody systems, such as the 6 DOF suspension in Section 5.1. Recently, other studies started to consider Lagrange's multipliers in the equations of motion [8, 58]. These studies assume that these Lagrange's multipliers can be measured by experiment [69], or the eigenvalues related to Lagrange's multipliers are minus infinite [19]. However, for complex multibody systems, the Lagrange's multipliers are unknown variables in the equations of motion, so they cannot be measured by experiment. The proposed method in this section can apply to any DAEs of multibody systems without the measurement of Lagrange's multipliers. This section will propose a new model reduction method based on POD that is more suitable for multi-body systems.

The model reduction for multi-body systems via POD has two main steps. First, DAEs of the equations of motion in a multi-body system are converted to the following explicit

second-order differential equation:

$$\ddot{q} = f\left(t, q, \dot{q}\right) \tag{4.1}$$

Second, POD is applied to equation (4.1) to obtain new reduced models with fewer number of differential equations.

In order to convert the equations of motion for a multi-body system to equation (4.1), the following procedures are proposed:

- The equations of motion of every multi-body system have the following form [25]:

$$\begin{bmatrix} M & \Phi_q^T \\ \Phi_q & 0 \end{bmatrix} \begin{bmatrix} \ddot{q} \\ \lambda \end{bmatrix} = \begin{bmatrix} Q_B\left(q, \dot{q}\right) \\ \gamma \end{bmatrix}, \tag{4.2}$$

  where q is the state vector, M is the system mass matrix, Φ_q is the Jacobian matrix of constraint equations, λ is Lagrange's multipliers, and $\gamma = -\left(\Phi_q \dot{q}\right)_q \dot{q} - 2\Phi_{qt}\dot{q} - \Phi_{tt}$ or $\gamma = \left[-\left(\Phi_q \dot{q}\right)_q \dot{q} - 2\Phi_{qt}\dot{q} - \Phi_{tt}\right] - 2\alpha\left(\Phi_q \dot{q} + \Phi_t\right) - \beta^2\Phi$ (Baumgarte constraint stabilization). These equations of motion are derived from the Lagrange's equations (4.3) and the constraint equations (4.4):

$$\frac{d}{dt}\left(\frac{\partial L}{\partial \dot{q}}\right) - \frac{\partial L}{\partial q} + \Phi_q^T \lambda = Q \tag{4.3}$$

$$\Phi = 0. \tag{4.4}$$

  The number of Lagrange's multipliers is equal to the number of states q minus the degrees of freedom. Because equations (4.3) and (4.4) for many multi-body systems maynot be numerically solved, the constraint equation (4.4) is replaced by its second time derivatives:

$$\Phi_q \ddot{q} = -\left(\Phi_q \dot{q}\right)_q \dot{q}, \tag{4.5}$$

  or by Baumgarte constraint equation:

$$\Phi_q \ddot{q} = \left[-\left(\Phi_q \dot{q}\right)_q \dot{q} - 2\Phi_{qt}\dot{q} - \Phi_{tt}\right] - 2\alpha\left(\Phi_q \dot{q} + \Phi_t\right) - \beta^2\Phi, \tag{4.6}$$

  where $\alpha > 0$ and $\beta \neq 0$ are constant. Noting that the notation of this section is as same as Haug's notation in [25].

- The next step is to remove Lagrange's multipliers from equation (4.2). Because the Jacobian matrix, Φ_q, may not be constant in many multi-body systems, and contains the states q, it is extremely difficult to find the QR decomposition of the symbolic Jacobian matrix, Φ_q. The transpose of the symbolic Jacobian matrix, Φ_q^T, is replaced by the value of this transpose at the nominal point, $\Phi_{q^*}^T$, where q^* is the nominal position of the system. Consequently, equation (4.2) is approximated by the following equation:

$$\begin{bmatrix} M & \Phi_{q^*}^T \\ \Phi_q & 0 \end{bmatrix} \begin{bmatrix} \ddot{q} \\ \lambda \end{bmatrix} = \begin{bmatrix} Q_B\left(q, \dot{q}\right) \\ \gamma \end{bmatrix}. \tag{4.7}$$

  Let (Q_1, R_1) be the QR decomposition of Φ_{q*}^T and $Q_1 = (Q_{11} \;\; D)$, where matrix Q_{11} is first r columns of matrix Q_1, r is the number of Lagrange's multipliers, and D consists of other columns of Q_1. Hence, $D^T \Phi_{q*}^T = 0$.

  Multiplying both sides of equation (4.7) with D^T, Lagrange's multipliers are removed, and equations (4.3) and (4.4) are simplified to:

$$\begin{bmatrix} D^T M \\ \Phi_q \end{bmatrix} \ddot{q} = \begin{bmatrix} D^T Q_B\left(q, \dot{q}\right) \\ \gamma \end{bmatrix}, \tag{4.8}$$

  Finally, equation (4.8) is rewritten in the second-order differential equation form:

$$\ddot{q} = \begin{bmatrix} D^T M \\ \Phi_q \end{bmatrix}^{-1} \begin{bmatrix} D^T Q_B\left(q, \dot{q}\right) \\ \gamma \end{bmatrix}. \tag{4.9}$$

Equation (4.9) has the same form as equation (4.1) does. If M and Φ_q are constant, the inverse matrix of $\begin{bmatrix} D^T M \\ \Phi_q \end{bmatrix}$ in equation (4.9) can be easily obtained. However, if the system mass matrix M is a function of q, its symbolic inverse may not be possible. The inverse matrix of $\begin{bmatrix} D^T M \\ \Phi_q \end{bmatrix}$ is usually calculated by its adjugate matrix. In case the symbolic matrix $\begin{bmatrix} D^T M \\ \Phi_q \end{bmatrix}$ is complicated, instead of using its adjugate matrix, the matrix can be approximated by $\begin{bmatrix} D^T M \\ \Phi_{q^*} \end{bmatrix}$ or $\begin{bmatrix} D^T M^* \\ \Phi_q \end{bmatrix}$, or $\begin{bmatrix} D^T M^* \\ \Phi_{q^*} \end{bmatrix}$, where $M^* = M_{q=q^*}$.

After converting the equations of motion of a multi-body system into the explicit second-order differential equation (4.9), POD is used to find the reduced models of the

multi-body system. Assuming the state vector $q \in \mathbb{R}^N$, from the simulation or experiments, the set of N-dimesional state vector q (called empirical data) is obtained. Let $U = \left\{q^{(1)}, q^{(2)}, \ldots, q^{(m)}\right\}$ be the empirical data, where $m \in \mathbb{N}^+$. The main goal of POD is to find the most accurate subspace W with the lower dimension K ($K < N$) of the empirical data U.

Let $\varphi_1, \varphi_2, \ldots, \varphi_K$ be the orthogonal basis of the subspace W, so each vector $q^{(i)}$ in the empirical set U is approximated by the following expression:

$$q^{(i)} \approx \sum_{j=1}^{K} < q^{(i)}, \varphi_j > \varphi_j, \tag{4.10}$$

where $< q^{(i)}, \varphi_j >$ is the inner product in the Euclidean space $\mathbb{R}^N$ (or the dot product).

The objective function is the total error defined as follows:

$$E = \sum_{i=1}^{m} \|q^{(i)} - \sum_{j=1}^{K} < q^{(i)}, \varphi_j > \varphi_j\|_2^2. \tag{4.11}$$

Let $C = UU^T$ be the covariance matrix of the empirical data. It can be mathematically proved that the error (equation (4.11)) is rewritten as follows [7]:

$$E = \sum_{i=1}^{m} \|q^{(i)}\|_2^2 - \sum_{j=1}^{K} \varphi_j^T C \varphi_j = \sum_{i=1}^{m} \|q^{(i)}\|_2^2 - \sum_{j=1}^{K} \psi_j, \tag{4.12}$$

where ψ_j with $j \in \{1, \ldots, K\}$ are the first K largest eigenvalues of the covariance matrix C, and φ_j with $j \in \{1, \ldots, K\}$ are their corresponding eigenvectors.

Denote $T = [\varphi_1, \ldots, \varphi_N]$, and $\bar{T} = [\varphi_1, \ldots, \varphi_K]$. Note that $\bar{T}^T \bar{T}$ is a unit matrix.

The new state vector of the reduced system is determined as follows:

$$\bar{q} = \bar{T}^T q. \tag{4.13}$$

Equations of motion of the multi-body system (equation (4.9)) are transferred by the projection matrix $\bar{T}$:

$$\ddot{\bar{q}} = \bar{T}^T \begin{bmatrix} D^T M \\ \Phi_q \end{bmatrix}^{-1} \begin{bmatrix} D^T Q_B \left(\bar{T}\bar{q}, \bar{T}\dot{\bar{q}}\right) \\ \gamma \end{bmatrix}. \tag{4.14}$$

Equation (4.14) is the new reduced model having only K differential equations ($K < N$).

In summary, this section introduced the model reduction for any constrained multi-body systems via POD. This method also considers Lagrange's multiplier in the equations of motion.

Chapter 5

Examples and Comparison

In an effort to evaluate the efficiency of the 2-norm power-based reduction, a 6 DOF planar double-wishbone suspension, a 5 DOF suspension, and a piston-crank system are modeled; and then IRP, the balanced truncation, the activity-based model reduction, and the 2NPR are implemented.

5.1 A 6 DOF Double-Wishbone Suspension with Bushings

This section briefly introduces the analytical model of a 6 DOF planar double-wishbone suspension with bushings, and the method of linearizing its algebraic-differential equations to a state-space representation.

5.1.1 Geometry

A double-wishbone suspension in vehicle has more than 30 degrees of freedom (Figure 5.1), so it is complicated to derive its equations of motion. Therefore, in order to implement model reduction techniques, a 6 DOF planar double-wishbone suspension is suggested (Figure 5.2).

The chassis with its centre of mass O_{CH} is only able to move in the vertical direction. The upper arm is ED; the lower arm is AB; and the knuckle is DB fixed to KW. A revolute joint between the wheel HH' and the knuckle KW at the point W has no effect

Figure 5.1: Double-Wishbone Suspension [15]

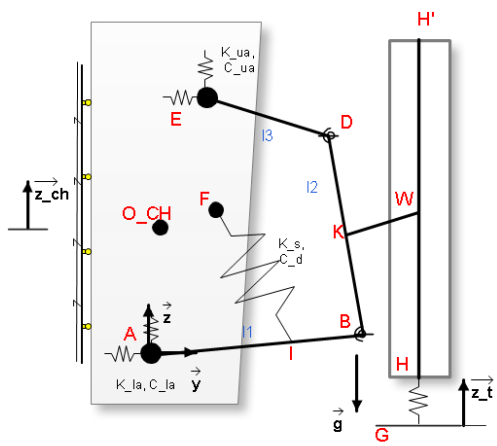

Figure 5.2: Suspension Geometry of Planar Double-Wishbone Suspension

on the planar double wishbone suspension. The tire is described as a spring GH. In many models of a double-wishbone suspension, the upper arm ED connects to the chassis though the revolute joint at E. However, in this suspension model with bushings, vertical and horizontal springs at point E are described as a bushing at E. Similarly, vertical and horizontal springs at A are modelled with a bushing. Please note that IF represents both the spring and damper. The geometric parameters of the suspension are shown in Table 5.1.

Let y_A, z_A, α_1, α_2, y_E, z_E, α_3 and z_{CH} be respectively the horizontal displacement of

Table 5.1: Parameters of 6 DOF Double-Wishbone Suspension

Suspension parameters	Symbols	Values
Mass of chassis	m_{CH}	400 kg
Mass of wheel	m_W	40 kg
Inertia of wheel	I_{xW}	800000 kg.mm^2
Length of lower arm	l_1	260 mm
Length of spindle	l_2	280 mm
Length of upper arm	l_3	180 mm
Distance between points B and F	l_f	200 mm
Mass of lower arm	m_1	8.3 kg
Mass of spindle	m_2	21.8 kg
Mass of upper arm	m_3	3.4 kg
Inertia of lower arm	J_{XX1}	97400 kg.mm^2
Inertial of spindle	J_{XX2}	90000 kg.mm^2
Inertial of upper arm	J_{XX3}	10000 kg.mm^2
Stiffness of lower arm bushing in x, y directions	k_{LA}	497500 $\frac{\mathrm{N}}{\mathrm{m}}$
Stiffness of upper arm bushing in x, y directions	k_{UA}	303000 $\frac{\mathrm{N}}{\mathrm{m}}$
Damping factor of lower arm bushing in x, y directions	c_{LA}	9015 $\frac{\mathrm{Ns}}{\mathrm{m}}$
Damping factor of upper arm bushing in x, y directions	c_{UA}	4560 $\frac{\mathrm{Ns}}{\mathrm{m}}$
Nominal stiffness of suspension spring	k_s	43300 $\frac{\mathrm{N}}{\mathrm{m}}$
Damping factor of shock damper	c_d	2565 $\frac{\mathrm{Ns}}{\mathrm{m}}$
Stiffness of tire	k_t	310000 $\frac{\mathrm{N}}{\mathrm{m}}$
Road profile	z_t	$50\sin(\pi t)$ mm

point A, the vertical displacement of point A, the angle of link AB, the angle of link BD, the horizontal and vertical displacements of point E, the angle of link ED, and the vertical displacement of the chassis at point O_{CH}. The vertical movement of point G representing the displacement of the road is an input of this suspension. The output, namely the vertical displacement of chassis (z_{CH}), is determined by solving Lagrange's equations and constraint equations.

5.1.2 Analytical Model

The equations of motion are derived from Lagrange's equations and constraint equations via Baumgarte constraint stabilization. All details of the formulas are described in Appendix E.

The equations of motion are finally re-written in a descriptor form:

$$\begin{bmatrix} M & \Phi_q^T \\ \Phi_q & 0 \end{bmatrix} \begin{bmatrix} \ddot{q} \\ \lambda \end{bmatrix} = \begin{bmatrix} Q_B \\ \hat{\gamma} \end{bmatrix}, \tag{5.1}$$

where $q = [y_A, z_A, \alpha_1, \alpha_2, y_E, z_E, \alpha_3, z_{CH}]^T$, M is a 8×8 matrix, Φ_q is a 2×8 matrix.

In this planar double-wishbone suspension, the number of links is five, namely ED, AB, the knuckle, the chassis, and ground; the number of lower pairs is three. Based on Gruebler's equation, the number of degrees of freedom is six. However, there are eight variables. Consequently, two constraint equations are needed. These equations can be derived from the geometrical constraints:

$$\overrightarrow{AB} + \overrightarrow{BD} + \overrightarrow{DE} = \overrightarrow{AE}. \tag{5.2}$$

Let $[y_{A0}, z_{A0}, \alpha_{10}, \alpha_{20}, y_{E0}, z_{E0}, \alpha_{30}, z_{CH0}]^T$ be an initial position q_0. The initial conditions are choosen as follows:

$$\begin{aligned} q_0 &= [0, 0, 0, 1.623, 2.768, 77.73, 345.2, 200]^T \\ \dot{q}_0 &= 0 \end{aligned}$$

The input (the vertical displacement of the tire) is $50 \sin(\pi t)$ mm.

The output (the vertical displacement of the chassis) is described in Figure 5.3 by solving the equations of motion. In order to verify the analytical model, an ADAMS model is developed (Figure 5.4). The results of the analytical model are equal to those of ADAMS model (Figure 5.5).

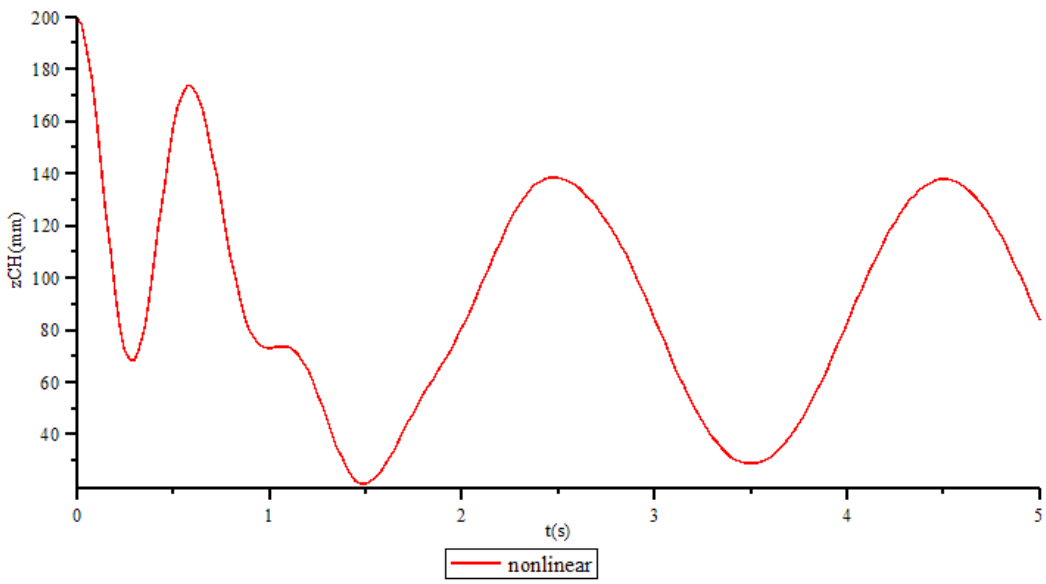

Figure 5.3: Displacement of Chassis in Analytical Model

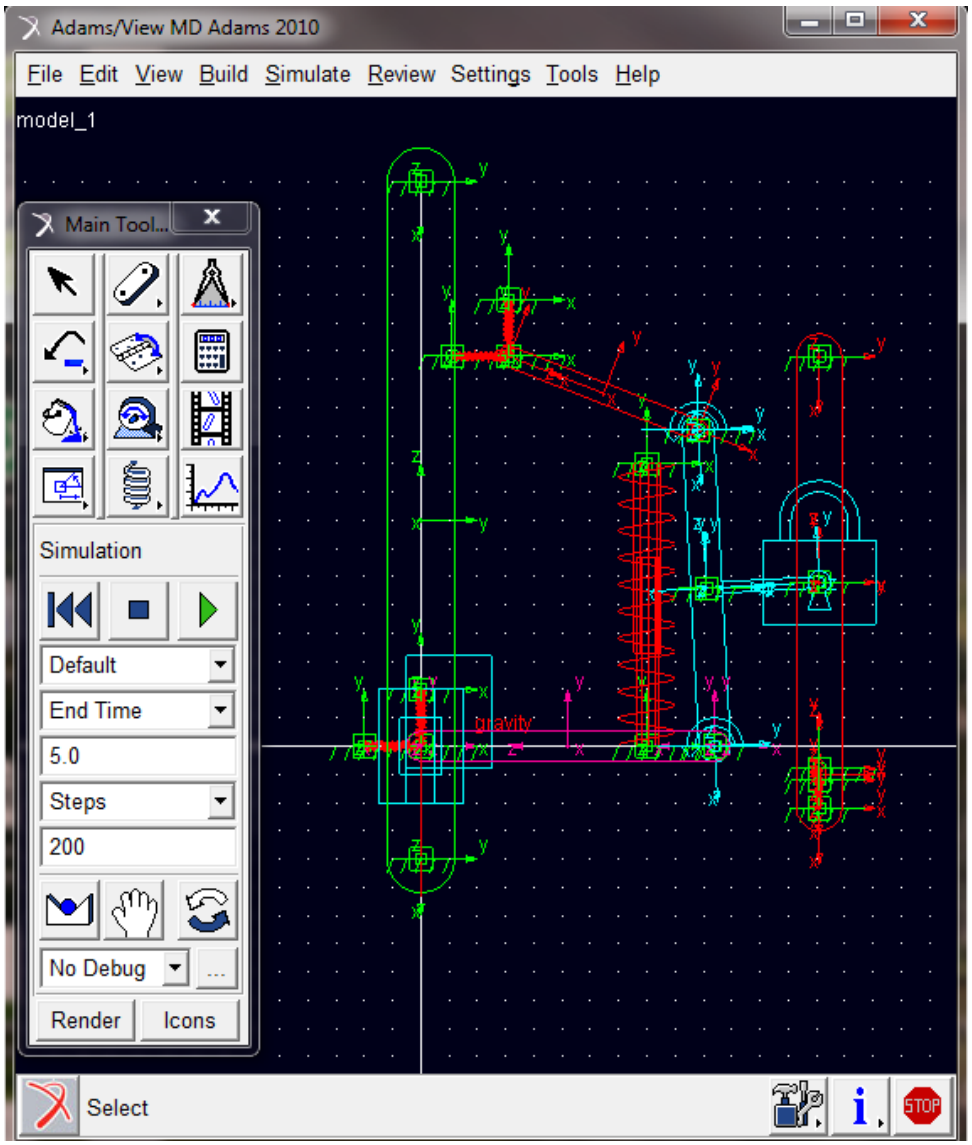

Figure 5.4: ADAMS Model of Planar Double-Wishbone Suspension

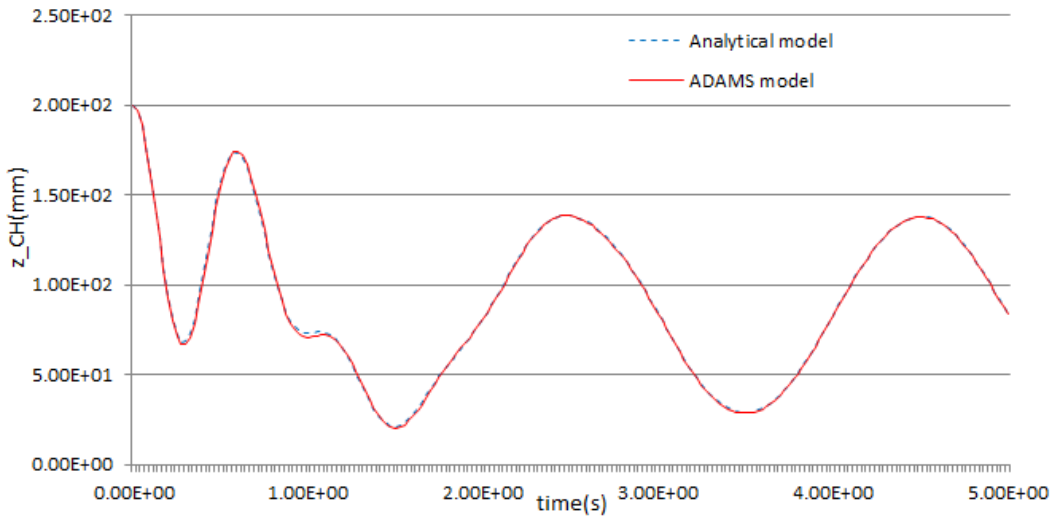

Figure 5.5: Comparison of Chassis Displacement in Analytical and ADAMS Models

5.1.3 Linearization

The linearization of differential-algebraic equations to a state-space representation is slightly different from that of other differential equations. Due to the existence of Lagrange's multipliers, the differential-algebraic equations are linearized to a descriptor system, which is more difficult to apply most model reduction techniques. Therefore, these multipliers need to be removed from the equations. QR decomposition is one of the most common methods to eliminate Lagrange's multipliers [64]. In this section, the linearization of nonlinear differential-algebraic equations for multi-body systems is introduced.

Based on the results of Chapter 4, the equations of motion (equation (5.1)) can be converted to equation (5.3):

$$\begin{bmatrix} D^T M \\ \Phi_q \end{bmatrix} \ddot{q} = \begin{bmatrix} D^T Q_B \\ \hat{\gamma} \end{bmatrix}. \tag{5.3}$$

Let $y = \begin{bmatrix} q & \dot{q} & \ddot{q} & u \end{bmatrix}^T$and $h(y) = \begin{bmatrix} D^T M \\ \Phi_q \end{bmatrix} \ddot{q} - \begin{bmatrix} D^T Q_B \\ \hat{\gamma} \end{bmatrix}$,where u is inputs (or displacement of tire z_t).
The nominal position satisfies the condition $h(y^*) = 0$.
Applying Taylor's series :

$$h(y) \approx h(y^*) + \frac{\partial h}{\partial q}|_{y^*}\Delta q + \frac{\partial h}{\partial \dot{q}}|_{y^*}\Delta \dot{q} + \frac{\partial h}{\partial \ddot{q}}|_{y^*}\Delta \ddot{q} + \frac{\partial h}{\partial u}|_{y^*}\Delta u. \tag{5.4}$$

Equation (5.1) becomes

$$\frac{\partial h}{\partial q}|_{y^*}\Delta q + \frac{\partial h}{\partial \dot{q}}|_{y^*}\Delta \dot{q} + \frac{\partial h}{\partial \ddot{q}}|_{y^*}\Delta \ddot{q} + \frac{\partial h}{\partial u}|_{y^*}\Delta u = 0. \tag{5.5}$$

Hence, the state-space representation of the 6 DOF double wishbone suspension, $[I, A, B, C]$, is obtained as follows:

$$\begin{aligned} \dot{X} &= AX + Bu \\ Y &= CX, \end{aligned} \tag{5.6}$$

where $X = \begin{bmatrix} \Delta q \\ \Delta \dot{q} \end{bmatrix}$, $B = \begin{bmatrix} 0 \\ -(\frac{\partial h}{\partial \ddot{q}}|_{y^*})^{-1}\frac{\partial h}{\partial u}|_{y^*} \end{bmatrix}$,
$A = \begin{bmatrix} 0 & I_8 \\ -(\frac{\partial h}{\partial \ddot{q}}|_{y^*})^{-1}\frac{\partial h}{\partial q}|_{y^*} & -(\frac{\partial h}{\partial \ddot{q}}|_{y^*})^{-1}\frac{\partial h}{\partial \dot{q}}|_{y^*} \end{bmatrix}$,
$C = [0, 0, 0, 0, 0, 0, 0, 1, 0, 0, 0, 0, 0, 0, 0, 0]$, $Y = z_{CH}$.

$$
A = \begin{bmatrix}
0 & 0 & 0 & 0 & 0 & 0 & 0 & 0 & 1 & 0 & 0 & 0 & 0 & 0 & 0 & 0 \\
0 & 0 & 0 & 0 & 0 & 0 & 0 & 0 & 0 & 1 & 0 & 0 & 0 & 0 & 0 & 0 \\
0 & 0 & 0 & 0 & 0 & 0 & 0 & 0 & 0 & 0 & 1 & 0 & 0 & 0 & 0 & 0 \\
0 & 0 & 0 & 0 & 0 & 0 & 0 & 0 & 0 & 0 & 0 & 1 & 0 & 0 & 0 & 0 \\
0 & 0 & 0 & 0 & 0 & 0 & 0 & 0 & 0 & 0 & 0 & 0 & 1 & 0 & 0 & 0 \\
0 & 0 & 0 & 0 & 0 & 0 & 0 & 0 & 0 & 0 & 0 & 0 & 0 & 1 & 0 & 0 \\
0 & 0 & 0 & 0 & 0 & 0 & 0 & 0 & 0 & 0 & 0 & 0 & 0 & 0 & 1 & 0 \\
0 & 0 & 0 & 0 & 0 & 0 & 0 & 0 & 0 & 0 & 0 & 0 & 0 & 0 & 0 & 1 \\
-35713.4 & 46369.7 & -698346.9 & -552402.7 & -689.1 & 103.1 & -12.3 & -50388.3 & -595.8 & 951.3 & 9859.6 & 3.6 & -10.4 & 1.6 & 0.643 & -952.9 \\
46871.9 & -123205.3 & 86979.2 & -253666.9 & 497.7 & -221.6 & 15.1 & 121899.9 & 897 & -2301 & -24808.8 & -2.23 & 7.48 & -3.341 & -0.7915 & 2304.3 \\
-202.6 & 512.5 & -4133.89 & -23.86 & -18.639 & 6.15 & -0.474 & -525.06 & -3.8887 & 9.7077 & 78.852 & 0.0889 & -0.28019 & 0.092808 & 0.02487 & -9.80056 \\
-51.1021 & -40.2139 & -1551.8 & -2729.87 & 37.79 & 7.7567 & 0.1039 & 14.90994 & -0.56629 & -0.3525 & 13.10049 & -0.2309 & 0.568 & 0.116 & -0.00545 & 0.23608 \\
197.38 & 810.895 & -161803.4 & 95250.58 & -27516.81 & 63822.4 & -1026.94 & -64242.37 & -18.915 & -8.962 & -4453.496 & -443.244 & -415.69 & 959.8 & -42.469 & -950.86 \\
638.875 & 1506.65 & 396425.7 & 176287.85 & 63822.40 & -245202.74 & 3743.66 & 245445.6 & 3.7540 & 0.2520 & 1128.367 & -193.2 & 959.8 & -3689.4 & 160.3 & 3689.19 \\
-9.862 & -21.687 & -7412.76 & -2535.8 & -389.3 & 1418.2 & -23.099 & -1424.2 & -0.14927 & -0.045 & -39.26 & 1.239 & -5.8549 & 21.3279 & -2.8934 & -21.282 \\
10.7299 & 1351.3 & 18634.035 & -0.0 & 0.0 & 757.5 & -0.0 & -2108.79 & -0.0 & 28.95 & 1164.65 & -0.0 & 0.0 & 11.4 & -0.0 & -40.35
\end{bmatrix},
$$

$$
B = \begin{bmatrix}
0 \\ 0 \\ 0 \\ 0 \\ 0 \\ 0 \\ 0 \\ 0 \\ 3915.42 \\ 1527.011 \\ 6.36 \\ 17.54 \\ -390.9 \\ -1749.5 \\ 27.687 \\ -0.0
\end{bmatrix}, \quad C = \begin{bmatrix} 0 & 0 & 0 & 0 & 0 & 0 & 0 & 1 & 0 & 0 & 0 & 0 & 0 & 0 & 0 & 0 \end{bmatrix}.
$$

The linear model has 16 first-order diferential equations, so its order is 16. The output of the linear model (equation (5.6)) in comparison with the nonlinear model (equation (5.1)) is shown in Figure 5.6. The error between the state-space representation and the nonlinear model is acceptable. The linear model is used in the next sections for IRP and balanced truncation. However, the 2-norm power-based reduction directly applies to the nonlinear model.

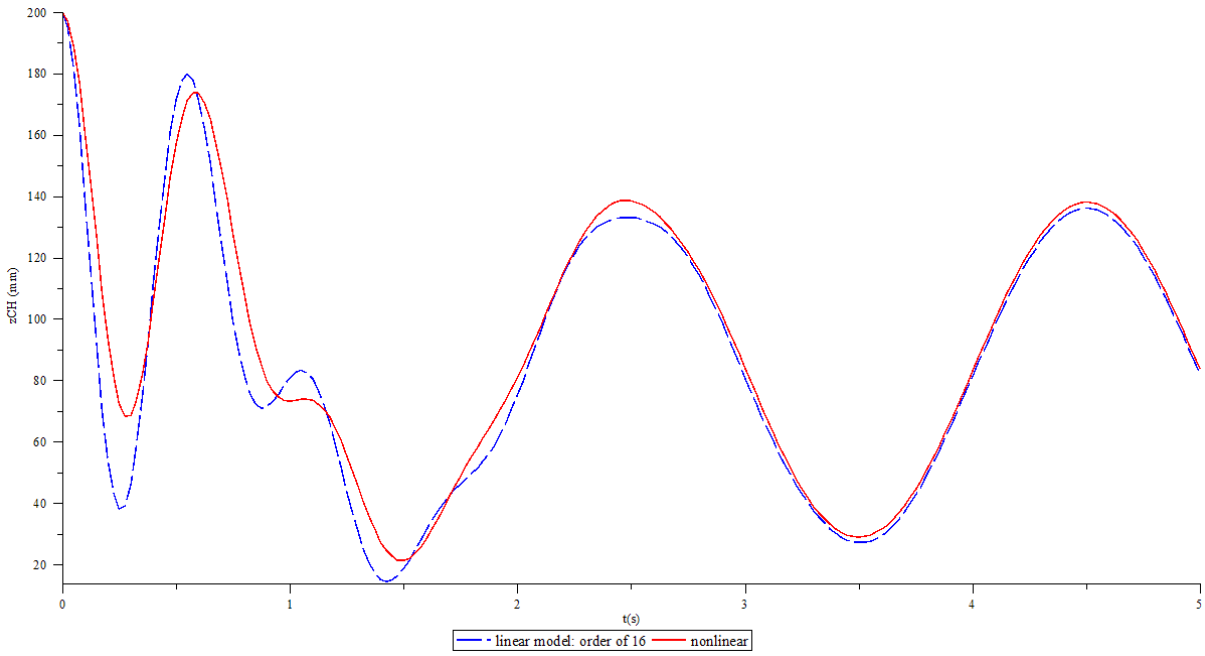

Figure 5.6: Chassis Displacement of Linear and Nonlinear Models

5.2 Improvement on IRP & Balanced Truncation

Initial conditions are extremely important in solving differential equations. In other words, the simulation of reduced models is impossible without the initial values of new reduced states. One of the main problems in many truncation methods for linear systems is to approximately determine the initial values of new states. In balanced truncation and irreducible realization procedure (IRP), many authors such as Varga in [72], Antoulas in [2], and Mockel in [26] just calculated the error bounds without simulating new reduced models in order to verify truncation methods. Therefore, two methods of approximating the initial values in truncation methods are proposed in this section.

One of the methods is based on the transformation matrix. Let X_0 and T be, respectively, the initial values of original states and the transformation matrix. The approximated initial values of r reduced states, namely X_r , are the first r columns of the vector X_0T. The most difficult step of this method is to obtain the transformation matrix T. While the transformation matrix T is easily obtained from the formula $T = RU^{-1/2}$ in balanced truncation, it is slightly complex for IRP. Considering the realization $[E, A, B, I]$ in which outputs are the states of the original system $[E, A, B, C]$ (equation (5.8)), its reduced output matrix, $C_r^{'}$, is obtained after applying IRP. It can mathematically prove that matrix $C_r^{'}$, is the transformation matrix of IRP in the system $[E, A, B, C]$. The algorithm 5.2 of finding the transformation matrix T in IRP is improved from Varga's algorithm 1 in [72]. After calculating the transformation matrix T, the initial conditions of new states in reduced models are defined as follows:

$$X_r\,(0) = X(0)T. \tag{5.7}$$

Algorithm 5.2: This algorithm is for finding the new initial values of reduced models in IRP for the following descriptor system:

$$\begin{aligned} E\dot{X} &= AX + Bu, \\ Y &= CX. \end{aligned} \tag{5.8}$$

Note that the matrix E can be singular. If E is invertible, the descriptor system can be converted to the state-space representation.

1. Transform E to the upper-triangular matrix (U-T) by using RQ decomposition: finding the orthogonal matrix Z_0 such that EZ_0 is an upper-triangular matrix, and transform to the new system:
   $EZ_0 \to E$, $AZ_0 \to A$, $CZ_0 \to C$, $C^{'}Z_0 \to C^{'}$, where $C^{'} = I_n$ is an identity matrix of size n.

2. Initial data: $j = 1, r = 0, n_0 = m, E_0 = E, A_0 = A, B_0 = B, Q = I_n$, and $Z = Z_0$.

3. Compute the orthogonal matrices Q_j and Z_j:

   - apply QR decomposition to B_{j-1} to find Q_j:

$$Q_j^T B_{j-1} = \begin{array}{c} n_j\{ \\ \rho_j\{ \end{array} \begin{pmatrix} \overbrace{A_{j,j-1}}^{n_{j-1}} \\ 0 \end{pmatrix}, \quad A_{j,j-1} \in \mathbb{R}^{n_j \times n_{j-1}}. \tag{5.9}$$

   - apply RQ decomposition to $Q_j^T E_{j-1}$ to determine Z_j:

$$Q_j^T E_{j-1} Z_j = \begin{array}{c} n_j\{ \\ \rho_j\{ \end{array} \begin{pmatrix} \overbrace{E_{j,j}}^{n_j} & \overbrace{E_{j,j+1}}^{\rho_j} \\ 0 & E_j \end{pmatrix}, \quad E_{j,j} \in \mathbb{R}^{n_j \times n_j}, E_{j,j+1} \in \mathbb{R}^{n_j \times \rho_j}, E_j \in \mathbb{R}^{\rho_j \times \rho_j}. \tag{5.10}$$

   - compute:

$$Q_j^T A_{j-1} Z_j = \begin{array}{c} n_j\{ \\ \rho_j\{ \end{array} \begin{pmatrix} \overbrace{A_{j,j}}^{n_j} & \overbrace{A_{j,j+1}}^{\rho_j} \\ B_j & A_j \end{pmatrix}, \quad A_{j,j} \in \mathbb{R}^{n_j \times n_j}, E_{j,j+1} \in \mathbb{R}^{n_j \times \rho_j}, \quad B_j \in \mathbb{R}^{\rho_j \times n_j}, A_j \in \mathbb{R}^{\rho_j \times \rho_j}. \tag{5.11}$$

4. For i from 1 to $(j-1)$, determine $A_{i,j}$ and $E_{i,j}$ by

$$A_{i,j} Z_j = [A_{i,j} | A_{i,j+1}], E_{i,j} Z_j = [E_{i,j} | E_{i,j+1}], \tag{5.12}$$

5. Update the transformation, C' and C matrices:

$$Q = Q \begin{bmatrix} I_r & 0 \\ 0 & Q_j \end{bmatrix}, Z = Z \begin{bmatrix} I_r & 0 \\ 0 & Z_j \end{bmatrix}, C = C \begin{bmatrix} I_r & 0 \\ 0 & Z_j \end{bmatrix}, C' = C' \begin{bmatrix} I_r & 0 \\ 0 & Z_j \end{bmatrix}, \tag{5.13}$$

6. Update $r = r + n$. If $\rho_j = 0$, then $k = j$ and stop; else go to step 7

7. If $n_j = 0$, then $k = j - 1$ and stop; else, increase j by 1 and go to step 3.

The second approximation method for calculating the new initial conditions uses a pseudo-inverse matrix and the relationship between the output Y and the state X: $Y = CX$. Let C_r and Y_0 respectively be the output matrix of the reduced model and the initial values of the output. The initial values of the new reduced states, X_{r0}, are defined as follows:

$$X_{r0} = (C_r^T C_r)^{-1} C_r^T Y_0. \tag{5.14}$$

In term of minimizing a root mean square, $(C_r^T C_r)^{-1} C_r^T Y$ is the best approximation of the initial values of the reduced states [21]. However, matrix $C_r^T C_r$ can be singular in some systems, such as the linear model of the 6 DOF suspension (equation 5.6), so equation (5.14) is not applicable to this model.

In summary, depending on the number of outputs and new reduced states, and the difficulty of finding the transformation matrix, one of these two methods is chosen. For example, in the balanced truncation, the transformation matrix is straightforwardly derived, and the number of the new reduced states is usually small; so the first method can give a better approximation. On the contrary, it is quite complex to determine the transformation matrix in the irreducible realization procedure, and the number of reduced states is relatively large. Therefore, the second method is more suitable.

5.3 Application of IRP to the 6 DOF Double-Wishbone Suspension

Balanced truncation is one of the most popular model order reduction techniques. However, balanced truncation is only applicable to controllable, observable, and asymptotically stable systems while the linear model (equation 5.6) is uncontrollable. Therefore, this section demonstrates how to apply IRP to remove the uncontrollable states of the linear model (equation 5.6).

First, the order of the linear system $[I, A, B, C]$ (equation (5.6)) is 16, and $\text{rank}(A) = 16$, so the system has 16 poles. From Table 5.2, all real parts of these poles are negative, so the linear system is asymptotically stable. Furthermore,

$$\text{rank}([B\ AB\ A^2B\ ...\ A^{15}B]) = 12 < 16, \tag{5.15}$$

and

$$\text{rank}\begin{bmatrix} C \\ CA \\ \vdots \\ CA^{15} \end{bmatrix} = 16, \tag{5.16}$$

so the system is uncontrollable and observable, and has four uncontrollable poles.

Table 5.2: Poles of Linear System with 16 States and Reduced Order System with 12 States

$[I, A, B, C]$	$[I_r, A_r, B_r, C_r]$
-3894.4	-3894.4
-2565.2	-2565.2
$-86.82 + 90.757i$	$-86.82 + 90.757i$
$-86.82 - 90.757i$	$-86.82 - 90.757i$
$-89.87 + 59.361i$	$-89.87 + 59.361i$
$-89.87 - 59.361i$	$-89.87 - 59.361i$
$-11.096 + 55.427i$	$-11.096 + 55.427i$
$-11.096 - 55.427i$	$-11.096 - 55.427i$
-56.417	-56.417
-67.6	-67.6
$-1.665 + 11.1i$	$-1.665 + 11.1i$
$-1.665 - 11.1i$	$-1.665 - 11.1i$
$-1 + 0.47\,10^{-4}i$	
$-1 - 0.47\,10^{-4}i$	
$-1 + 0.227\,10^{-4}i$	
$-1 - 0.227\,10^{-4}i$	

Second, applying IRP in [72] and the algorithm 5.2 which is described in Section 5.2, a reduced order model $[I_r, A_r, B_r, C_r]$ with the order of 12 (having 12 first-order differential equations) and the initial conditions of new states are obtained:

$$\begin{aligned} \dot{X} &= A_r X + B_r u \\ Y &= C_r X, \end{aligned} \tag{5.17}$$

where

$$A_r = \begin{bmatrix} -645.24 & 1180.9 & 957.7 & -858.8 & 2247.5 & 10270.0 & -6496.3 & 4801.7 & -7206.2 & 17467.0 & -379010.0 & 30150.0 \\ 1236.9 & -3401.7 & -1217.8 & 1000.7 & -3287.2 & 908.7 & -4055.9 & 2035.5 & -4288.7 & 30884.0 & 261860.0 & 256280.0 \\ 0.0 & -106.8 & -240.1 & -926.7 & 345.7 & -5343.6 & 9251.8 & 7259.2 & -9650.7 & 66112.0 & -149670.0 & 40578.0 \\ 0.0 & 0.0 & -308.4 & -2629.7 & 1047.3 & -12594.0 & 5861.4 & -1390.7 & -17615.0 & 159050.0 & -172310.0 & -31734.0 \\ 0.0 & 0.0 & 0.0 & -489.1 & 226.3 & -1356.5 & -1164.3 & -2668.8 & -2215.1 & 26770.0 & -9934.4 & -15784.0 \\ 0.0 & 0.0 & 0.0 & 0.0 & -4.37 & -7.35 & -124.08 & -53.77 & 23.91 & -173.58 & 2783.3 & -1305.1 \\ 0.0 & 0.0 & 0.0 & 0.0 & 0.0 & 31.37 & -24.298 & 44.66 & -11.275 & -94.952 & 904.89 & -361.21 \\ 0.0 & 0.0 & 0.0 & 0.0 & 0.0 & 0.0 & -61.10 & -73.67 & 27.247 & -40.017 & 741.31 & -383.79 \\ 0.0 & 0.0 & 0.0 & 0.0 & 0.0 & 0.0 & 0.0 & 50.9 & -18.727 & -32.25 & 591.27 & -324.33 \\ 0.0 & 0.0 & 0.0 & 0.0 & 0.0 & 0.0 & 0.0 & 0.0 & 6.65 & -57.373 & 26.781 & -27.919 \\ 0.0 & 0.0 & 0.0 & 0.0 & 0.0 & 0.0 & 0.0 & 0.0 & 0.0 & -2.807 & -32.296 & -15.66 \\ 0.0 & 0.0 & 0.0 & 0.0 & 0.0 & 0.0 & 0.0 & 0.0 & 0.0 & 0.0 & -17.816 & -58.47 \end{bmatrix}$$

$$B_r = \begin{bmatrix} -4569.1 \\ 0.0 \\ 0.0 \\ 0.0 \\ 0.0 \\ 0.0 \\ 0.0 \\ 0.0 \\ 0.0 \\ 0.0 \\ 0.0 \\ 0.0 \end{bmatrix}$$

$$C_r = \begin{bmatrix} 5.551 \times 10^{-17} & 1.0408 \times 10^{-17} & 0.0000525 & -0.00108 & 0.00627 & -0.13448 & -0.1863 & 0.1323 & 0.5048 & 0.356 & -0.2862 & -0.6827 \end{bmatrix}.$$

Based on Table E.1, IRP removes four uncontrollable states, namely $-1+0.47\,10^{-4}i$, $-1-0.47\,10^{-4}i$, $-1+0.227\,10^{-4}i$, and $-1-0.227\,10^{-4}i$, from the original linear system. Therefore, the reduced order model is controllable, observable and asymptotically stable. Figure 5.7 also shows the output of the reduced model (equation (5.17)), the linear model with the order of 16 (equation(5.6)), and the nonlinear model (equation (5.1)).

The output error between the nonlinear 6 DOF suspension and the reduced model with the order of 12 is shown in Figure 5.8

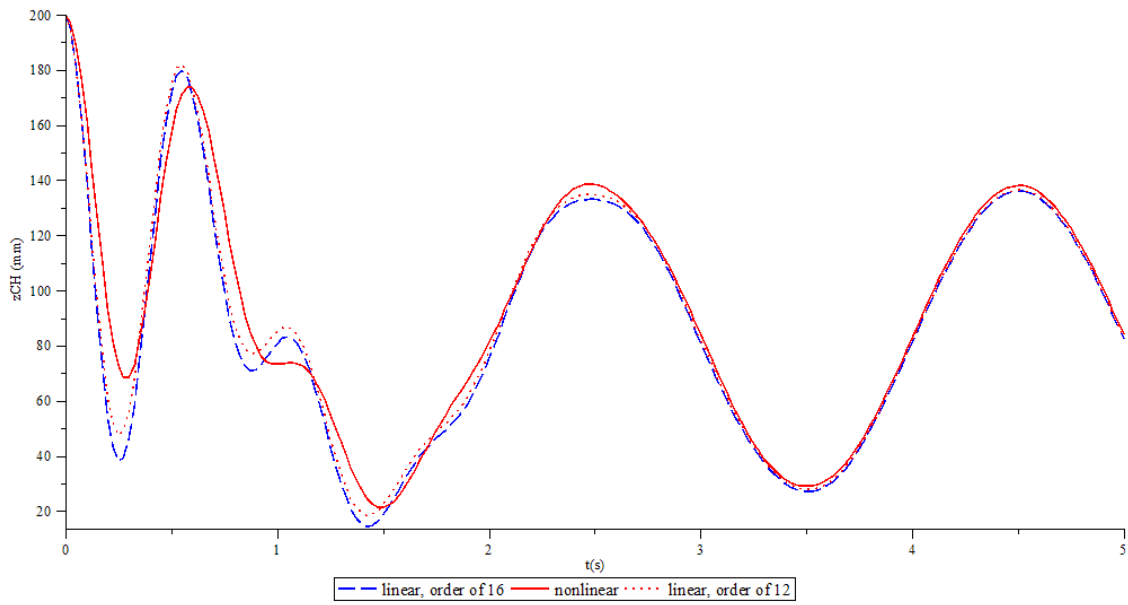

Figure 5.7: Comparison of Nonlinear Model, Linear Model with 16 States, and Linear Model with 12 States

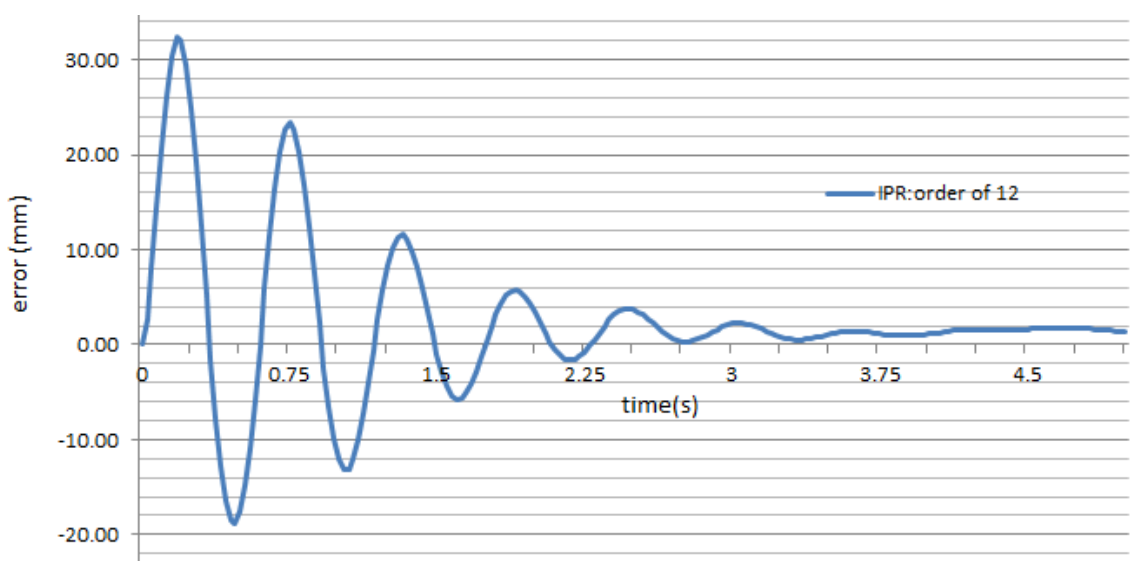

Figure 5.8: Output Error Between 6 DOF Suspension and Reduced Model with 12 States

5.4 Application of Balanced Truncation to the 6 DOF Double-Wishbone Suspension

Because the system $[I, A, B, C]$ is uncontrollable, the balanced truncation cannot be applied to this system. However, after eliminating the uncontrollable states via IRP, the reduced order system $[I_r, A_r, B_r, C_r]$ is controllable, observable and asymptotically stable. According to the lemma 9.3.1 of [40], the realization $[I_r, A_r, B_r, C_r]$ can be transformed to a balanced realization, and its order can be reduced by the balanced truncation.

The Hankel singular values of a state-space representation are defined as the square root of eigenvalues of the product of its controllability Gramian and observability Gramian:

$$\sigma_i = \sqrt{\lambda_i(PQ)}. \tag{5.18}$$

The basis of balanced truncation is to remove states that have relatively smaller Hankel singular values. The balanced truncation procedure for the state-space representation ,$[I_r, A_r, B_r, C_r]$, are described as follows:

1. Solve the Lyapunov's equations (5.19 & 5.20) to find the controllability and observability Gramians P, Q:

$$A_r P + P A_r^T + B_r B_r^T = 0, \tag{5.19}$$
$$A_r^T Q + Q A_r + C_r^T C_r = 0. \tag{5.20}$$

2. Find Cholesky factorization: $RR^T = P$.

3. Compute the singular value decomposition (SVD): $R^T Q R = U \Sigma^2 U^T$, where U is orthogonal, Σ is a diagonal matrix. The main purpose of SVD is to sort the Hankel singular values in descending order.

4. Determine the projection matrix $T = RU\Sigma^{\frac{-1}{2}}$.

5. Transfer the coordinates of the system, and obtain a new model $[\overline{I}, \overline{A}, \overline{B}, \overline{C}]$:

$$
\begin{aligned}
\bar{A} = T^{-1}A_rT &= \begin{array}{c c} & \begin{array}{cc} r & n-r \end{array} \\ \begin{array}{c} r \\ n-r \end{array} & \begin{pmatrix} \bar{A}_{1,1} & \bar{A}_{1,2} \\ \bar{A}_{2,1} & \bar{A}_{2,2} \end{pmatrix} \end{array}, \bar{A}_{1,1} \in \mathbb{R}^{r\times r}, \bar{A}_{1,2} \in \mathbb{R}^{r\times(n-r)} \\
\bar{B} = T^{-1}B_r &= \begin{array}{c c} & m \\ \begin{array}{c} r \\ n-r \end{array} & \begin{pmatrix} \bar{B}_1 \\ \bar{B}_2 \end{pmatrix} \end{array}, \bar{B}_1 \in \mathbb{R}^{r\times m} \\
\bar{C} = C_rT &= \begin{pmatrix} \bar{C}_1 & \bar{C}_2 \end{pmatrix}, \bar{C}_1 \in \mathbb{R}^{p\times r}, \\
\bar{I} &= I_r,
\end{aligned}
\tag{5.21}
$$

where n is the order of the system $[I_r, A_r, B_r, C_r]$ and r is the reduced order.

6. Apply the truncation (equation (5.22)) to remove less important Hankel singular values, and obtain a reduced order model $[I_{r2}, A_{r2}, B_{r2}, C_{r2}]$:

$$
\begin{aligned}
A_{r2} &= \bar{A}_{1,1}, \quad B_{r2} = \bar{B}_1 \\
C_{r2} &= \bar{C}_1, \qquad I_{r2} = \bar{I}.
\end{aligned}
\tag{5.22}
$$

In the linear system $[I_r, A_r, B_r, C_r]$ (equation (5.17)), 12 Hankel singular values are calculated by the balanced truncation procedure in Table 5.3. There are two significant Hankel singular values in this model, so it can be reduced to a reduced model consisting of 2 states.

Choosing $r2 = 11$, the reduced model with order of 11 is derived from the balanced truncation (Figure 5.9). The error bound between the linear model of order 12 and order 11 is computed:

$$
\|G - G_r\|_\infty \leq 2(\sigma_{12}) = 4.699\,10^{-9}. \tag{5.23}
$$

Table 5.3: Hankel Singular Values of $[I_r, A_r, B_r, C_r]$

Hankel Singular Values
2.01488
1.49675
0.06860
0.05330
0.00400
0.00123
$5.8\ 10^{-5}$
$7.5\ 10^{-6}$
$4.4\ 10^{-7}$
$4.710^{-8} + 2.0510^{-8}I$
$4.710^{-8} - 2.0510^{-8}I$
$2.3\ 10^{-9}$

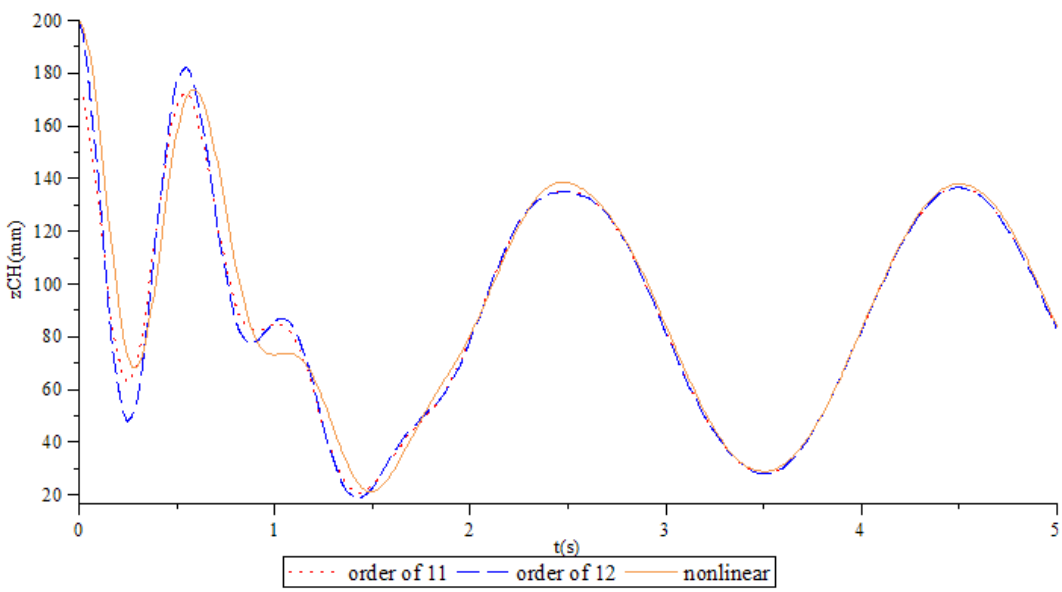

Figure 5.9: Comparison of Nonlinear System with Reduced Systems of Order 12 & 11

Balanced truncation can reduce the order of the linear system from 11 to 2, while their errors are acceptable (Figure 5.12, & 5.13). For example, the reduced model with order of 2 $[I_{r2}, A_{r2}, B_{r2}, C_{r2}]$ (Figure 5.10) is calculated as follows:

$$\begin{aligned} A_{r2} &= \begin{bmatrix} -1.864 & -11.178 \\ 11.178 & -1.492 \end{bmatrix}, \\ B_{r2} &= \begin{bmatrix} -2.741 \\ 2.113 \end{bmatrix}, \\ C_{r2} &= \begin{bmatrix} -2.741 & -2.113 \end{bmatrix}. \end{aligned} \tag{5.24}$$

This reduced model has two first-order differential equations, so its degree of freedom is one. This model is also equal to a 1 DOF quarter-car model.

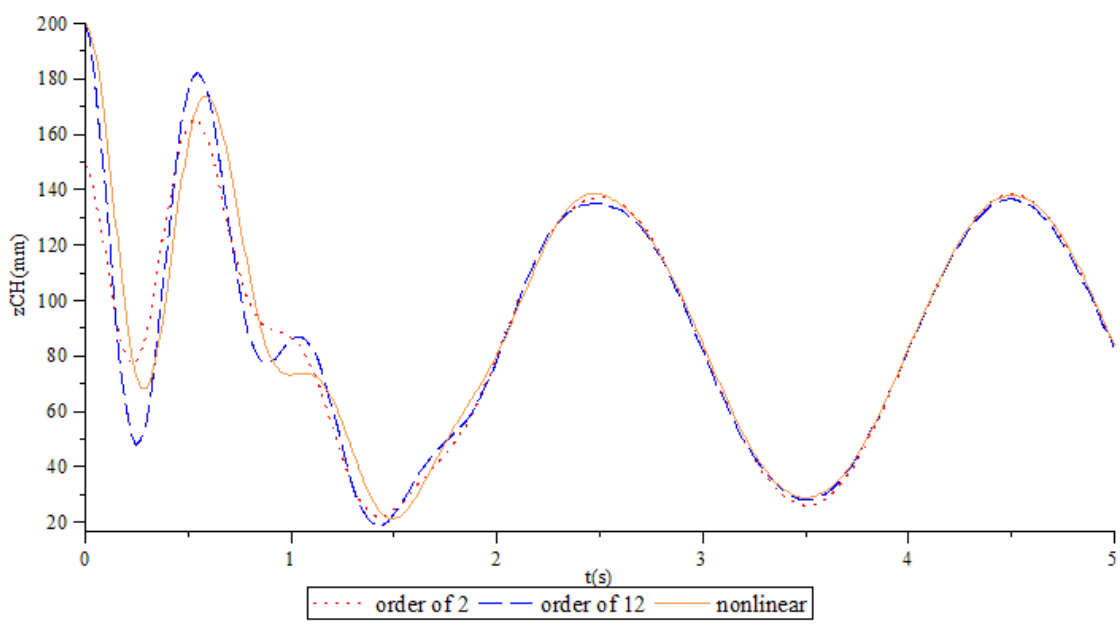

Figure 5.10: Comparison of Nonlinear System with Reduced Systems with Order of 2

The error bound between the linear model of order 12 and order 2 is determined:

$$\|G - G_r\|_\infty \leq 2(\sigma_3 + \cdots + \sigma_{12}) = 0.2544. \tag{5.25}$$

The output error between the nonlinear 6 DOF suspension and the reduced model with the order of 2 is shown in Figure 5.11

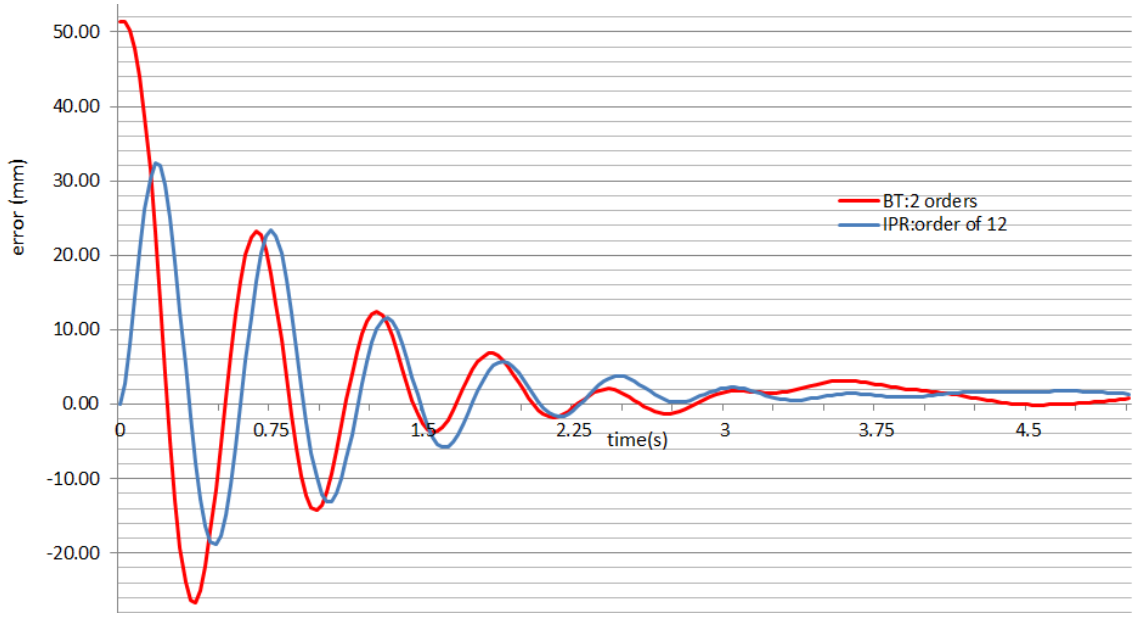

Figure 5.11: Output Error of Reduced Models with 2 States & 12 States

Other reduced models with different orders are also obtained by balanced truncation. From Figures 5.12 and 5.13, the reduced models approximate well the nonlinear 6 DOF suspension in the steady-state period. However, in the transient period, especially the initial value, the output errors between the 6 DOF suspension and the reduced models cannot be ignored.

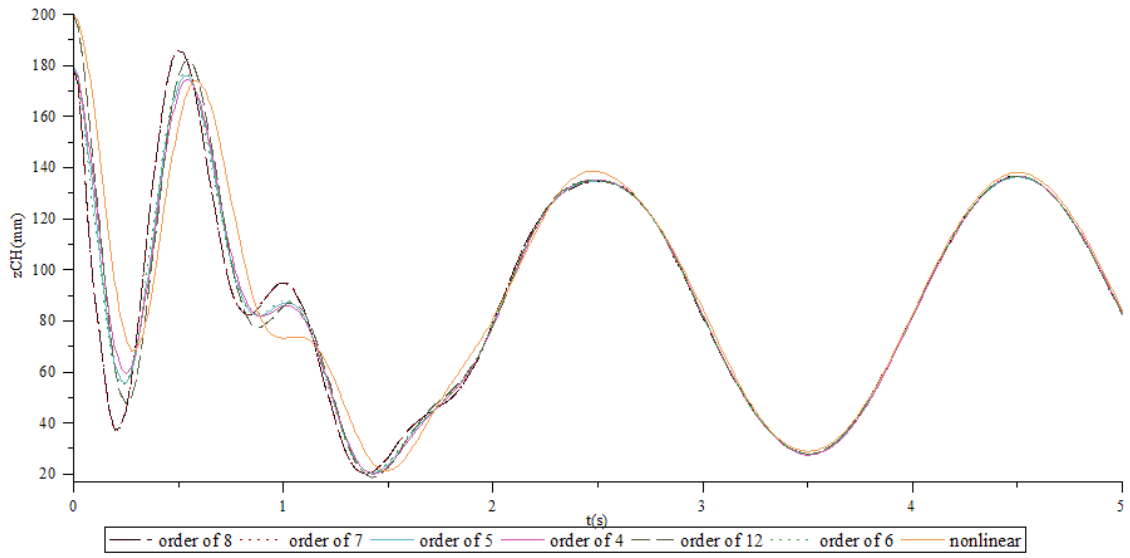

Figure 5.12: Comparison of Nonlinear System and Reduced Order Models

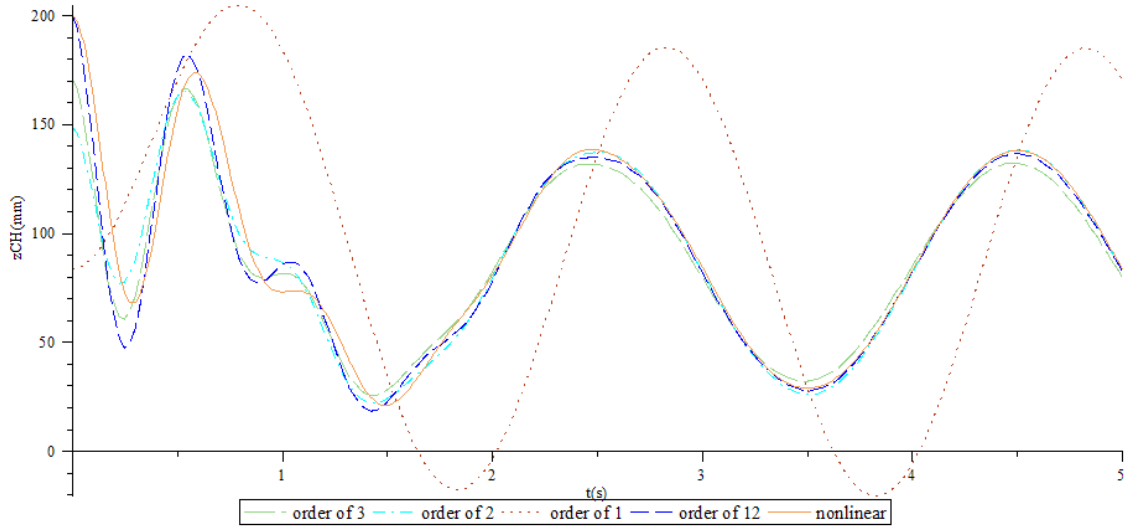

Figure 5.13: Comparison of Nonlinear System and Reduced Order Models

5.5 Calculation of Activity in Louca's Method

The common thing between Louca's method (MORA) [37] and the 2NPR is that components that are relatively less important to the system response are removed in order to obtain reduced models. While MORA uses the activity as the energy metric to determine the importance of components, the 2NPR uses 2 norm as the energy metric. In order to evaluate which metric can represent the importance of components in multi-body systems better, the calculation of the activity of all components is first described.

Based on Section 3.1, the activity of all components during the time interval $[0, 4]$ (second) is calculated and shown in Figure 5.14. In addition, the activity and relative activity (activity indexes) at time $t = 4$ seconds are computed and shown in Table 5.4. In addition,. Comparisons between Louca's method and the 2NPR will be discussed later in this chapter.

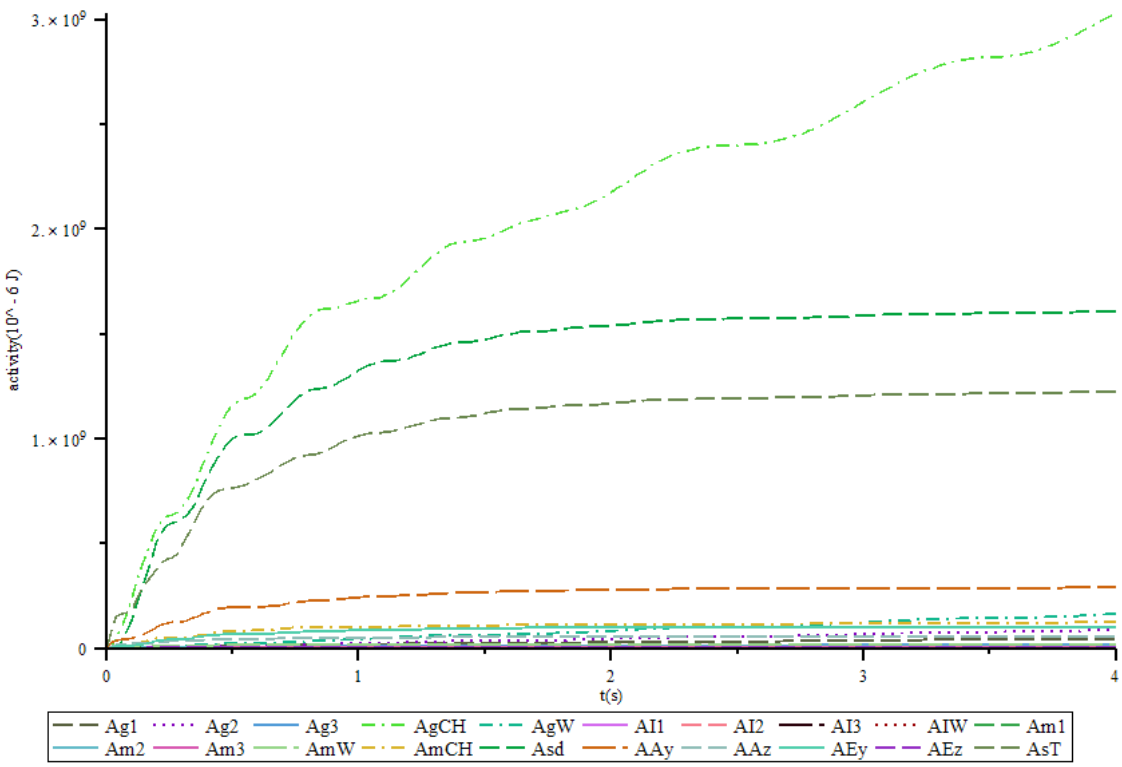

Figure 5.14: Activity of All Components in 6 DOF Suspension in $t \in [0, 4]$ (second)

Table 5.4: Activities of All Components at $t = 4$ (seconds)

notation	components	activity	activity index
A_{gCH}	gravity of chassis	$3.03272365100546 * 10^9$	44.46
A_{sd}	suspension spring & damper	$1.60954275742940 * 10^9$	23.6
A_{sT}	tire spring	$1.22645607781828 * 10^9$	17.98
A_{Ay}	horizontal spring & damper at A	$2.90086067130067 * 10^8$	4.25
A_{gW}	gravity of wheel	$1.63769500859663 * 10^8$	2.40
A_{mCH}	mass of chassis	$1.24829583358167 * 10^8$	1.83
A_{Ey}	horizontal spring & damper at E	$1.03575147527846 * 10^8$	1.52
A_{g2}	gravity of knuckle	$8.88766675408656 * 10^7$	1.30
A_{Az}	vertical spring & damper at A	$5.62041544204703 * 10^7$	0.82
A_{g1}	gravity of lower arm	$4.56627695655444 * 10^7$	0.67
A_{mW}	mass of wheel	$2.06366651800508 * 10^7$	0.30
A_{g3}	gravity of upper arm	$1.91095206635904 * 10^7$	0.28
A_{m2}	mass of knuckle	$9.35221009906156 * 10^6$	0.14
A_{IW}	moment of inertia of wheel	$7.96499535658839 * 10^6$	0.1168
A_{Ez}	vertical spring & damper at E	$7.86056729446393 * 10^6$	0.1152
A_{m1}	mass of lower arm	$7.49056449075160 * 10^6$	0.1098
A_{m3}	mass of upper arm	$3.21531185631446 * 10^6$	0.0471
A_{I1}	moment of inertia of lower arm	$2.43246021876212 * 10^6$	0.0357
A_{I2}	moment of inertia of upper arm	$8.96061977616198 * 10^5$	0.0131
A_{I3}	moment of inertia of knuckle	$5.29589701816148 * 10^5$	0.0078

5.6 2-Norm Power-based Reduction

Based on the 2-norm of power, the importance of each component to the system response is evaluated. The reduced models with fewer degrees of freedom are developed by removing relatively less important components. This section demonstrates how to apply the 2-norm power-based reduction in Section 3.2.2 to the 6 DOF double-wishbone suspension.

Considering the nonlinear model of the 6 DOF double-wishbone suspension (equation (5.1)), the input of the model is the road profile. In order to decrease the dependency of reduced models to the input, the set of input $\mathcal{U}$ can be defined based on the set of possible road profile in reality. For instance, $\mathcal{U}$ is the set of trigonometric functions, heaviside step function, and exponetial sine. However, in this example, the input set is defined as $\mathcal{U} = \{z_t(t) = 50\sin(\pi t)(mm)\}$.

Because the size of the input set is one, no weight is required. The formulas of 2-norm of power of some components are derived as follows:

- gravity of chassis

$$K_{gCH} = \sqrt{\int_{t_0}^{t} {m_{CH}}^2 g^2 \left(\dot{z}_{CH}\right)^2 \, d\tau}, \tag{5.26}$$

- gravity of wheel

$$K_{gW} = \sqrt{\int_{t_0}^{t} {m_W}^2 g^2 \left(\dot{z}_A + l_1 \cos\left(\alpha_1\right) \dot{\alpha}_1 + \left(\left(1/2\, l_2 + y_{KW}\right) \cos\left(\alpha_2\right) - z_{KW} \sin\left(\alpha_2\right)\right) \dot{\alpha}_2\right)^2 \, d\tau}, \tag{5.27}$$

- gravity of lower arm

$$K_{g1} = \sqrt{\int_{t_0}^{t} {m_1}^2 g^2 \left(\dot{z}_A + \frac{1}{2}\, l_1 \cos\left(\alpha_1\right) \dot{\alpha}_1\right)^2 \, d\tau}, \tag{5.28}$$

- gravity of knuckle

$$K_{g2} = \sqrt{\int_{t_0}^{t} {m_2}^2 g^2 \left(\dot{z}_A + l_1 \cos\left(\alpha_1\right) \dot{\alpha}_1 + \left(\frac{1}{2}\, l_2 + y_{C2}\right) \cos\left(\alpha_2\right) \dot{\alpha}_2 - z_{C2} \sin\left(\alpha_2\right) \dot{\alpha}_2\right)^2 \, d\tau}, \tag{5.29}$$

- gravity of upper arm

$$K_{g3} = \sqrt{\int_{t_0}^{t} {m_3}^2 g^2 \left(\dot{z}_A + l_1 \cos\left(\alpha_1\right) \dot{\alpha}_1 + l_2 \cos\left(\alpha_2\right) \dot{\alpha}_2 + \frac{1}{2} l_3 \cos\left(\alpha_3\right) \dot{\alpha}_3 \right)^2 d\tau}, \tag{5.30}$$

- moment of inertial of lower arm

$$K_{I1} = \sqrt{\int_{t_0}^{t} {J_{XX1}}^2 \left(\dot{\alpha}_1\right)^2 \left(\ddot{\alpha}_1\right)^2 \, d\tau}, \tag{5.31}$$

- moment of inertial of knuckle

$$K_{I2} = \sqrt{\int_{t_0}^{t} {J_{XX2}}^2 \left(\dot{\alpha}_2\right)^2 \left(\ddot{\alpha}_2\right)^2 \, d\tau}, \tag{5.32}$$

- moment of inertial of upper arm

$$K_{I3} = \sqrt{\int_{t_0}^{t} {J_{XX3}}^2 \left(\dot{\alpha}_3\right)^2 \left(\ddot{\alpha}_3\right)^2 \, d\tau}, \tag{5.33}$$

- mass of wheel

$$K_{mW} = \sqrt{\int_{t_0}^{t} {J_{XXw}}^2 \left(\dot{\alpha}_2\right)^2 \left(\ddot{\alpha}_2\right)^2 \, d\tau}, \tag{5.34}$$

After that, the 2-norm of power of each component and their relative 2-norms during the time interval $[0, 4]$ (second) (Table 5.5 and Figure 5.15) are calculated by the first and third methods described in Section (3.2.1). For the first method, computer takes around 4276 seconds ≈1 hour and 10 minutes. On the other hand, the computer obtains all 2-norm of power within 56 seconds for the third method. In addition, the 2-norm of power in these two methods are almost equal each other.

Table 5.5: 2-Norms of Power of Each Component at $t = 4$ (seconds)

Notation	Components	2-norm	Relative 2-norm
K_{gCH}	gravity of chassis	$2.192 * 10^9$	33.35351
K_{sd}	suspension spring & damper	$1.817 * 10^9$	27.65042
K_{sT}	tire spring	$1.3955 * 10^9$	21.23334
K_{Ay}	horizontal spring & damper at A	$4.197 * 10^8$	6.38637
K_{mCH}	mass of chassis	$1.4996 * 10^8$	2.281696
K_{Ey}	horizontal spring & damper at E	$1.3087 * 10^8$	1.99125
K_{Az}	vertical spring & damper at A	$1.306 * 10^8$	1.98714
K_{gW}	gravity of wheel	$9.1688 * 10^7$	1.395069
K_{IW}	moment of inertia of wheel	$5.6328 * 10^7$	0.857056
K_{g2}	gravity of knuckle	$4.9823 * 10^7$	0.75807
K_{mW}	mass of wheel	$4.1924 * 10^7$	0.637885
K_{g1}	gravity of lower arm	$2.827 * 10^7$	0.4301392
K_{m1}	mass of lower arm	$1.8398 * 10^7$	0.2799372
K_{g3}	gravity of upper arm	$1.2064 * 10^7$	0.1835658
K_{m2}	mass of knuckle	$1.194 * 10^7$	0.1817006
K_{Ez}	vertical spring & damper at E	$9.884 * 10^6$	0.150395
K_{I2}	moment of inertia of knuckle	$6.3369 * 10^6$	0.0964188
K_{m3}	mass of upper arm	$4.6053 * 10^6$	0.07007
K_{I1}	moment of inertia of lower arm	$4.11801 * 10^6$	0.06266
K_{I3}	moment of inertia of upper arm	$8.73397 * 10^5$	0.013289

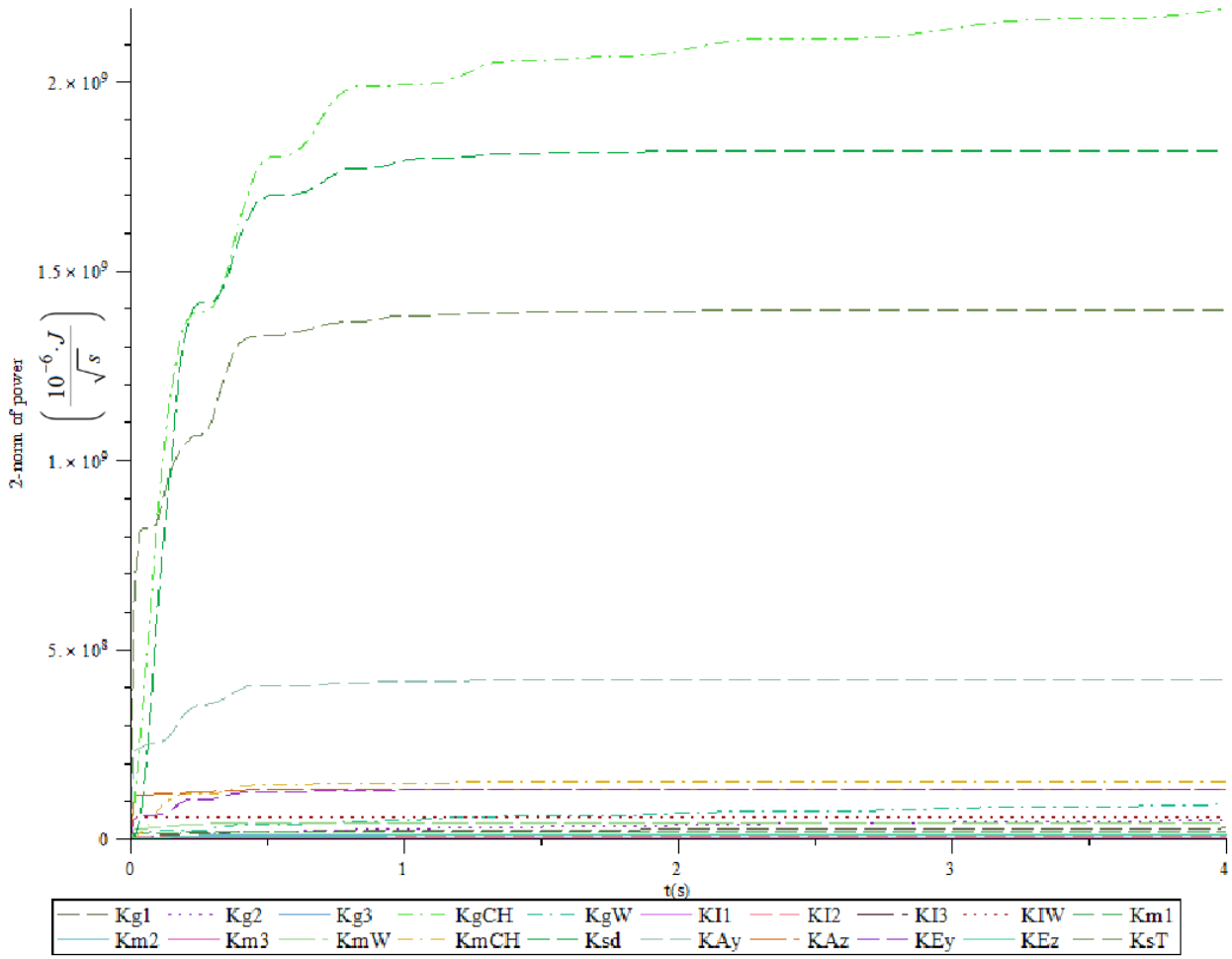

Figure 5.15: 2-Norm of Power of All Components in $t \in [0, 4]$ (second)

From Table 5.5, the moments of inertia of the upper arm, lower arm and knuckle; mass and gravity of upper arm; and the vertical spring-damper at E can be removed from the system because the 2-norms of their power are so small in comparison with other components. Therefore, in the reduced model (Figure 5.16), $I_1 = I_2 = I_3 = 0$, $m_3 = 0$, and the bushing at E is replaced by a prismatic joint and the horizontal spring-damper element. In addition, the reduced model has five links, three lower pairs, and one higher pair; so its degrees of freedom are $3 \times (5 - 1) - 3 \times 2 - 1 = 5$. The equations of motion for the 5 DOF reduced model are derived by Lagrange's equations in the same way for the 6 DOF system that is described in Section (5.1.2). The remaining relative energy, namely

99.6%, is still remarkable high, so there are slightly small differences between the chassis displacement of the 5 DOF reduced model and the 6 DOF system (Figure 5.17).

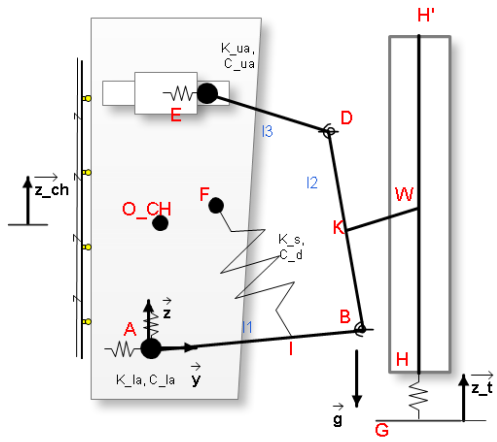

Figure 5.16: Reduced Model with 5 DOF

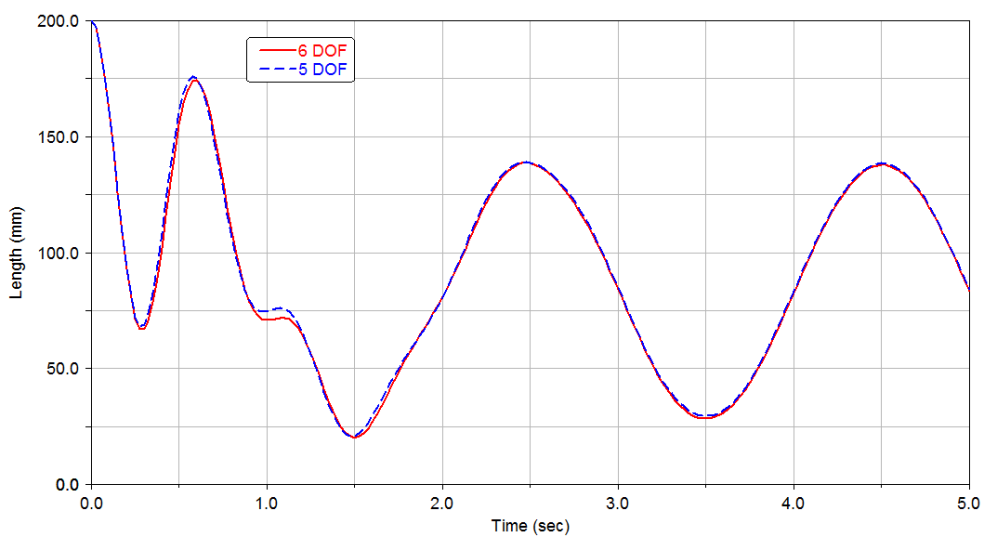

Figure 5.17: Comparison of Chassis Displacement Between 6 DOF and 5 DOF Model

Similarly, a reduced system is obtained by continuing to remove components where the 2-norms of power are small: knuckle mass m_2, upper arm gravity g_3, lower arm mass m_1, lower arm gravity g_1, wheel mass m_W, knuckle gravity g_2, wheel gravity g_W, vertical spring and damper at A. The bushing at A is replaced by a prismatic joint and a horizontal spring-damper element, so the reduced system has four degrees of freedom (Figure 5.18). Using Lagrange's equations, the equations of motion for the 4 DOF reduced model are derived. The remaining relative 2-norm is 93%, the error in chassis displacement is still acceptable (Figure 5.19).

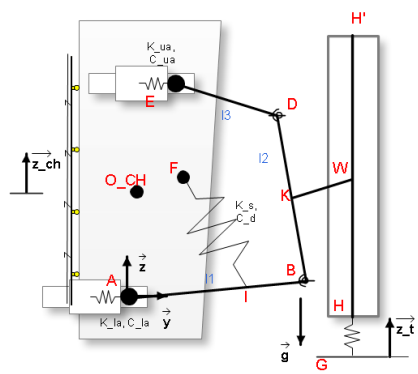

Figure 5.18: Reduced Model with 4 DOF

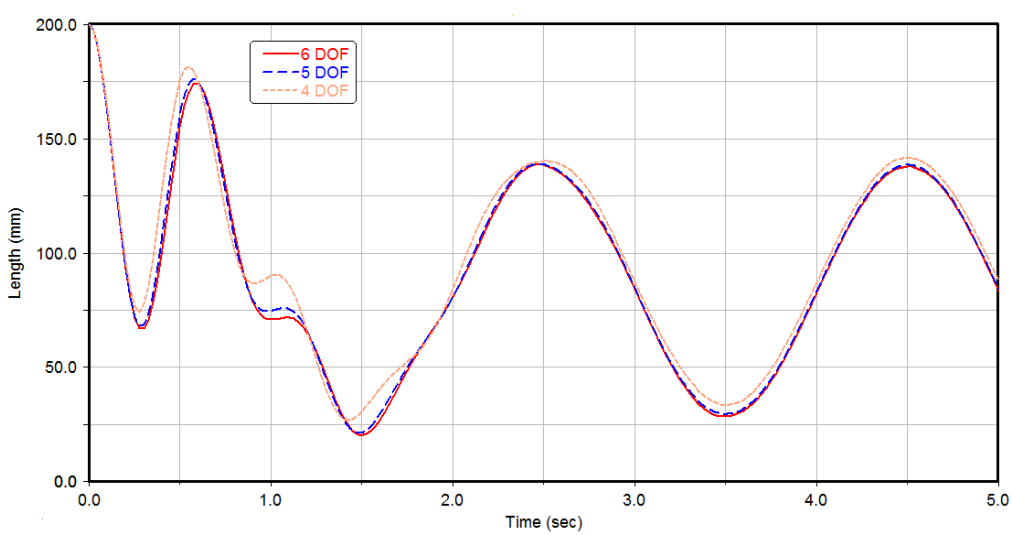

Figure 5.19: Chassis Displacement in Reduced 4 DOF Model

Continuing to remove the horizontal and damper at E, the degrees of freedom are reduced to three. The joint at point E now becomes a revolute joint without bushing (Figure 5.20). The remaining relative 2-norm is 90.9%, and the chassis displacement is compared with that of other reduced systems (Figure 5.21).

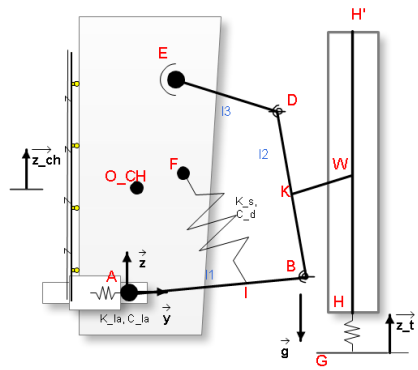

Figure 5.20: Reduced Model with 3 DOF

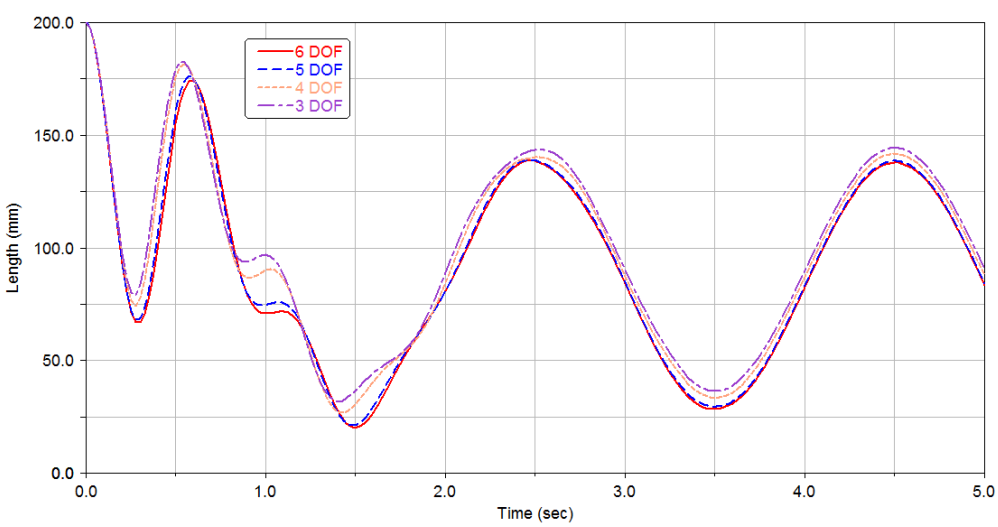

Figure 5.21: Chassis Displacement in Reduced 3 DOF Model

The 2 DOF model is developed by continuing to remove the horizontal spring and damper at A, and other components except for the chassis mass m_{CH}, the suspension spring-damper element, the tire spring and the moment of inertia of the wheel I_{xW} (Figure

5.22). In other words, the 2 DOF reduced model has only 5 components, namely m_{CH}, k_s, c_d, k_t, and I_{xW}. Noting that the wheel mass, m_W, and the wheel moment of inertia, I_{xW}, are two different components in the 2NPR. As discussed in Section (3.2.2), when removing less important components from a system, the equations of motion of the reduced system should still be able to be numerically solved. For this 2 DOF model, without I_{xW} its equations of motion cannot be numerically solved. That is the reason why the 2 DOF reduced model still keeps the moment of inertia of the wheel even though its 2-norm of power K_{IW} is small (Table 5.5). After deriving the equations of motion from Lagrange's equation, the chassis displacement z_{CH} of the 2 DOF reduced model is determined and shown in Figure 5.23. Using QR decomposition described in Chapter 4 to remove Lagrange's multipliers, this 2 DOF reduced model has only four differential equations in the form (4.8) with four variables $\alpha_1, \alpha_2, \alpha_3$, and z_{CH}. The relative 2-norm of power of the remaining components is 82%, so the error of this chassis displacement is larger than that of the 3 DOF system.

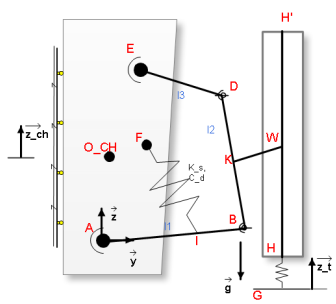

Figure 5.22: Reduced Model with 2 DOF

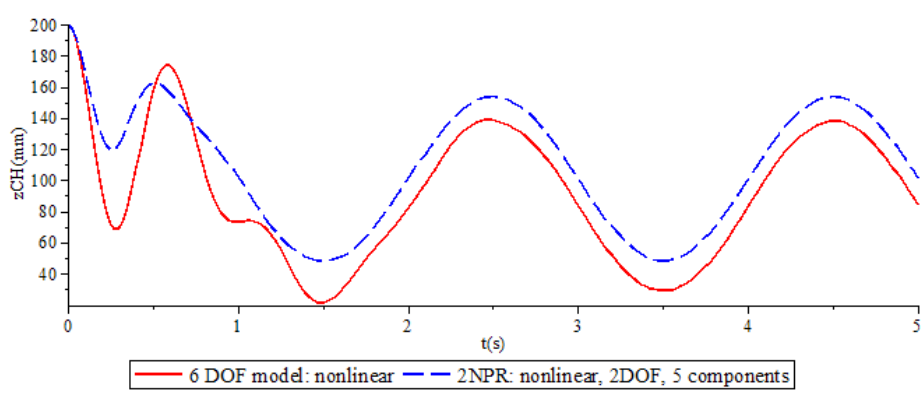

Figure 5.23: Chassis Displacement in 2-DOF Models

Finding Equivalent Values of Remaining Components via Genetic Algorithms: After removing relatively less important components to system response, the values of the remaining components need to be adjusted in order to compensate energy lost by removing other components and to minimize the squared error between the reduced model and the original model. Choosing a random initial population with 8 individuals, the crossover probability is 0.55, the mutation probability is 0.05, and the number of evolutions is 10. Applying the parameter estimation via genetic algorithms (PEvGA) in Appendix D, the equivalent parameters of the 2 DOF reduced model are determined (see Table 5.6).

Table 5.6: Equivalent Values of 5 Remaining Components in 2 DOF Suspension

Components	6 DOF Suspension	2 DOF Model in 2NPR via GAs
Mass of chassis m_{CH} (kg)	400	400.0045777
Stiffness of tire k_t ($\frac{\mathrm{N}}{\mathrm{m}}$)	310000	2.103088426 10^5
Nominal stiffness of suspension spring k_s ($\frac{\mathrm{N}}{\mathrm{m}}$)	43300	33300
Damping factor of shock damper c_d ($\frac{\mathrm{Ns}}{\mathrm{m}}$)	2565	1765
Inertia of wheel I_{xW} (kg.mm^2)	800000	800000

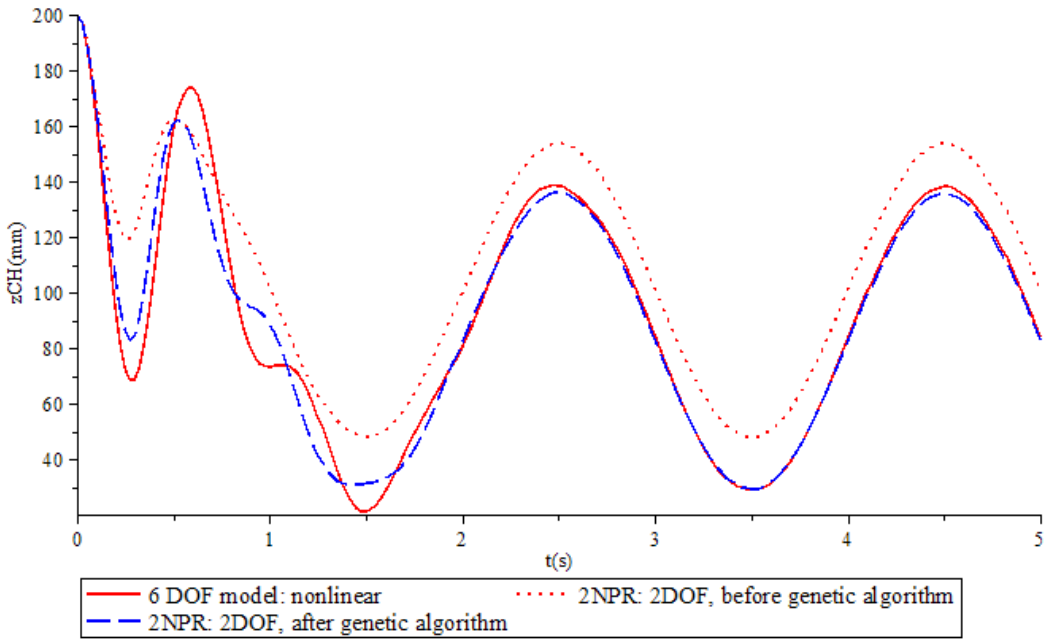

Figure 5.24: Chassis Displacement After Applying Genetic Algorithms

The output of this new 2 DOF reduced model with the estimated parameters is the dash blue line in Figure 5.24. The new 2 DOF model is more accurate than the 2DOF reduced model without parameter estimation.

In summary, the 2NPR reduces the 6 DOF suspension (Figure 5.2) into a 2 DOF model with its geometry shown in Figure 5.22 and its values of 5 remaining components in Table 5.6. From Figure 5.24, the output of the 2 DOF reduced model (the blue dash line) is very accurate in the steady-state period. In addition, the computation time of this 2 DOF model in $[0, 5]$ (s) is 232 seconds in comparison with 4118 seconds for the 6 DOF suspension.

Comparison of 2-Norm of Power with Activity: Comparing two energy metrics, namely activity and 2-norm of power, in term of representing the effect of a component to the system response, a 4 DOF reduced model without the kinetic energy of chassis (related to chassi mass, m_{CH}) and a 4 DOF reduced model that removes the potential energy of the wheel (related to wheel gravity, g_W) are considered. The geometry of these 4 DOF models are shown in Figure 5.19.

From Table 5.4, the activity of the wheel gravity, namely $1.6\ 10^8$, is larger than that of the chassis mass, namely $1.2\ 10^8$: $A_{g_W} > A_{m_{CH}}$. According to Louca in [37], the reduced model that removes the gravity of wheel has larger error than the reduced model without the mass of chassis.

However, Figure 5.25 shows that the error of the 4 DOF model without the gravity of wheel is smaller than that of the 4 DOF model without the mass of chassis.

On the other hand, from Table 5.5, the 2-norm of power of m_{CH} is larger than that of g_W. In other words, the 2-norm of power measures the component importance more accurately than the activity for the 6 DOF suspension.

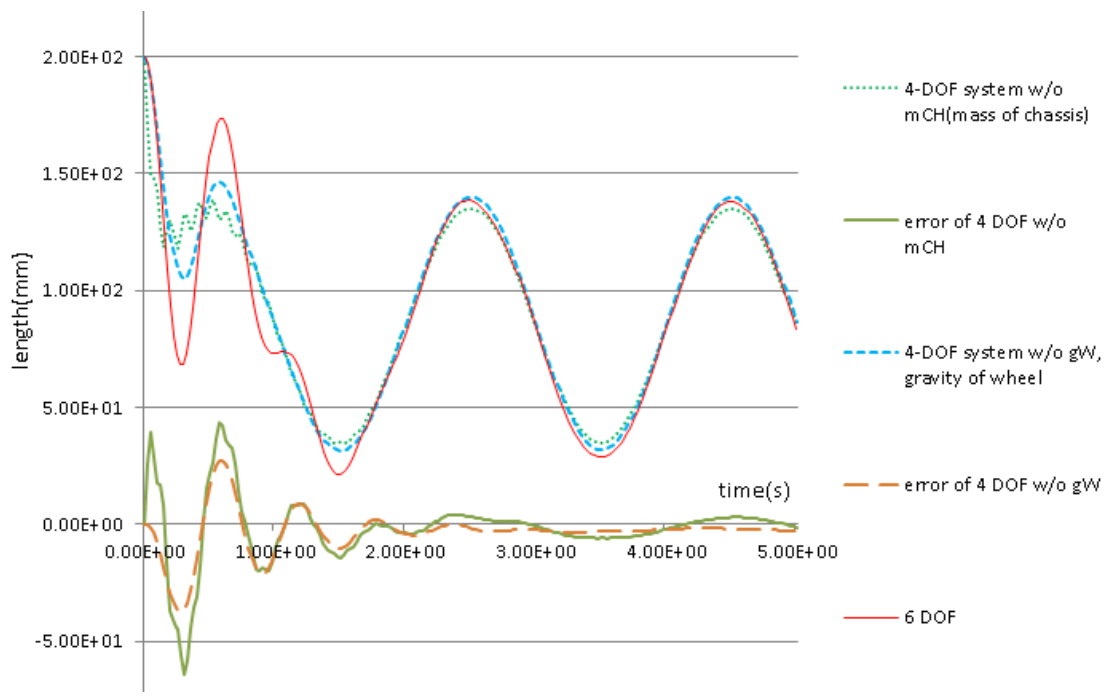

Figure 5.25: Comparison of Two 4 DOF Reduced Models without Mass of Chassis and without Gravity of Wheel

Comparison of 2NPR with IRP and Balanced Truncation: In order to compare the 2NPR and the truncation methods (including IRP and balanced truncation), the best reduced models of these two methods in term of minimizing the chassis displacement error are investigated. The best reduced model of truncation methods has only two first-order linear differential equations (equation (5.24)) while the 2 DOF reduced model (Figure5.22) with new values of remaining parameters via genetic algorithm in Table 5.6 is the best model of 2NPR. The vertical chassis displacement in these two reduced models is almost

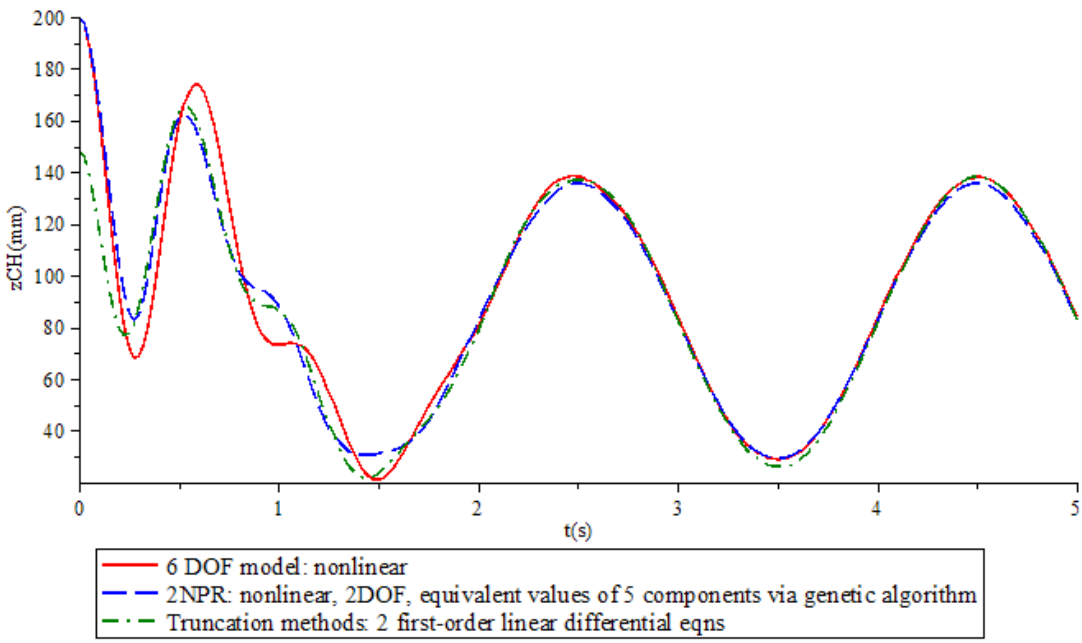

Figure 5.26: Comparison of 2NPR and Truncation Methods

equal to that of the 6 DOF suspension. The best reduced model of the truncation methods has only 2 first-order linear differential equations of motion in comparison to 4 differential-algebraic equations of the 2 DOF model in the 2NPR. Consequently, the simulation time of the reduced model via truncation methods is shorter than that of the 2 DOF model via the 2NPR. On the contrary, the 2 DOF model still keeps the topology of the original 6 DOF suspension, which is useful for the interpretation of the reduced models. In addition, the initial value of the chassis displacement in the reduced model of 2NPR is more accurate than that in the reduced model of truncation methods.

The output error between the nonlinear 6 DOF suspension and the 2DOF reduced

model in the 2NPR is shown in Figure 5.27.

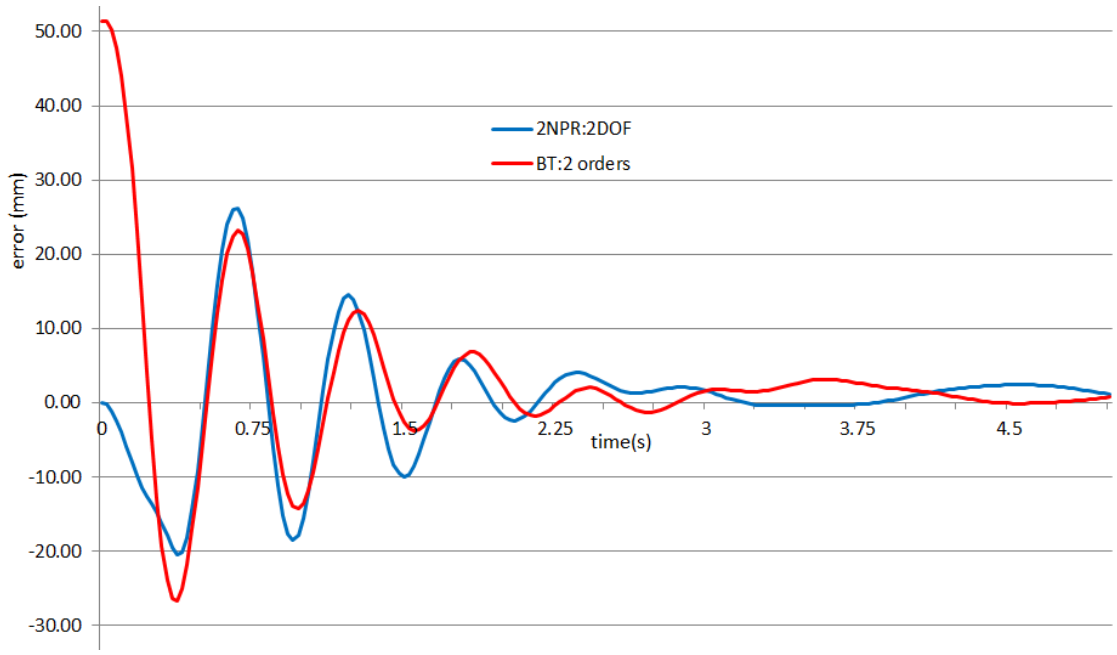

Figure 5.27: Output Error of Reduced Model with 2 States & 2 DOF Model of 2NPR

5.7 Application of Model Reduction Techniques to 5 DOF Double-Wishbone Suspension

Considering another 5 DOF double-wishbone suspension as shown in Figure 5.28, its input is the forces acting on the center of the wheel (point W) $F_{wy}(t) = 50\,\mathrm{e}^{-1.2\,t}\cos(3.815756806\,t) + 50\,\mathrm{N}$, and $F_{wz}(t) = 200\,\mathrm{e}^{-1.1\,t}\cos(10.94486181\,t) + 200\,\mathrm{N}$; the output is the vertical displacement of the wheel z_W.

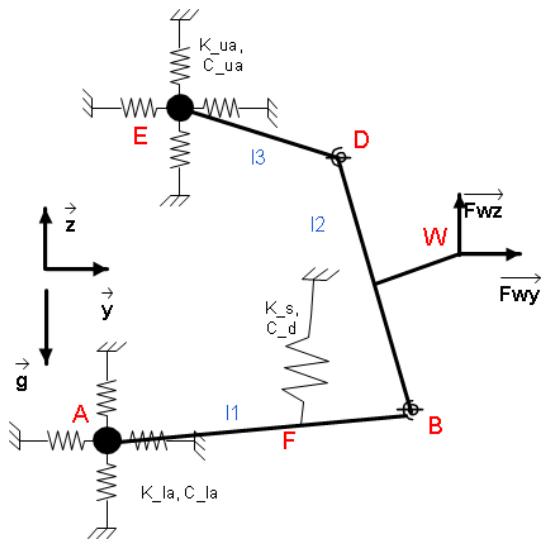

Figure 5.28: 5 DOF Planar Double-Wishbone Suspension

Applying IRP and balanced truncation, this 5 DOF suspension can be reduced to the smallest state-space model that has only two state (Figure 5.29). In addition, the 2NPR not only reduce the degrees of freedom from five to one, but also keep the original topology (Figure 5.29). The smallest reduced model of 2NPR has only one degree of freedom, and five out of twelve components.

In this mechanism, the 2NPR gives more accurate reduced model than IRP and balanced truncation.

For activity-based reduction (MORA), the activity of the upper arm gravity A_{g_3} and the activity of lower arm mass A_{m1} may not accurately reflect the importance of these components to system response. A_{g_3} is almost twice as larger as A_{m1} (Figure 5.30), so the gravity of upper arm g_3 is more important and having more effect to the system behavior

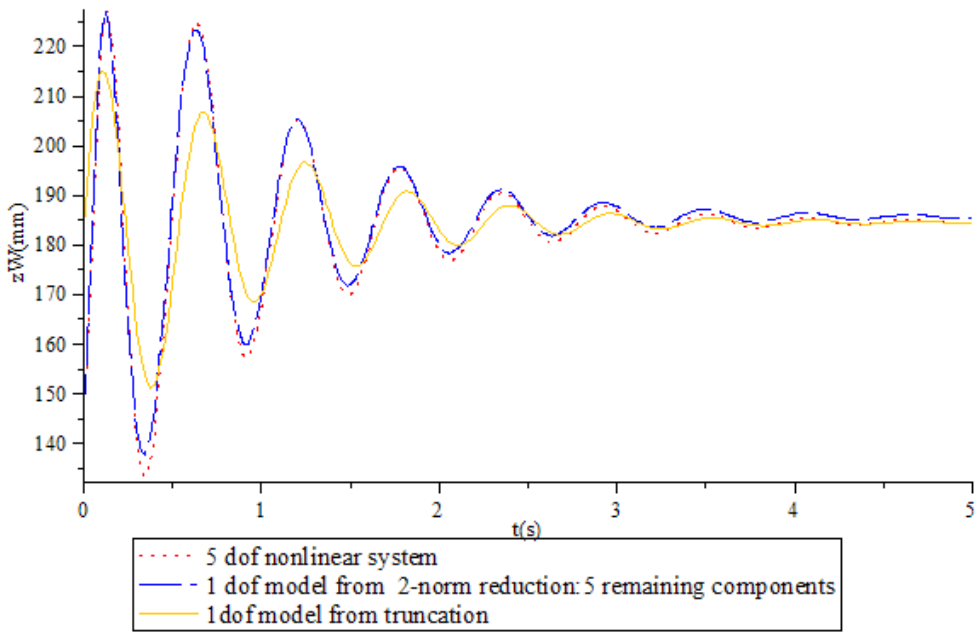

Figure 5.29: Vertical Displacement of Wheel Center: Truncation Methods and 2NPR

than the mass of lower arm m_1. However, the error of the reduced system where the gravity of upper arm g_3 is removed from is much smaller than that of the system removing the mass of lower arm m_1 (Figure 5.31).

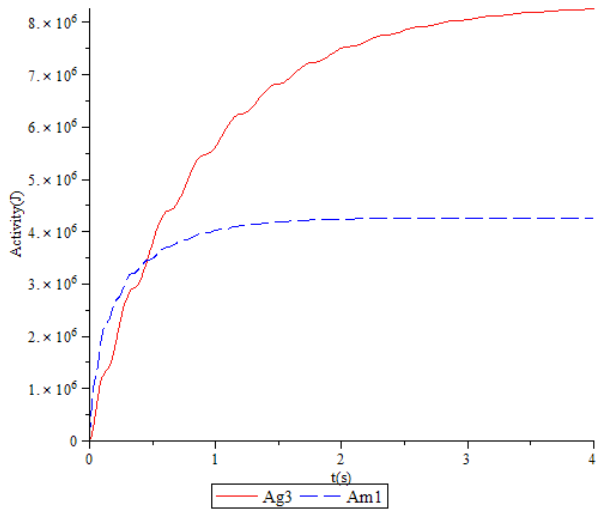

Figure 5.30: Activity of Gravity of Upper Arm (Ag3) and Mass of Lower Arm (Am1)

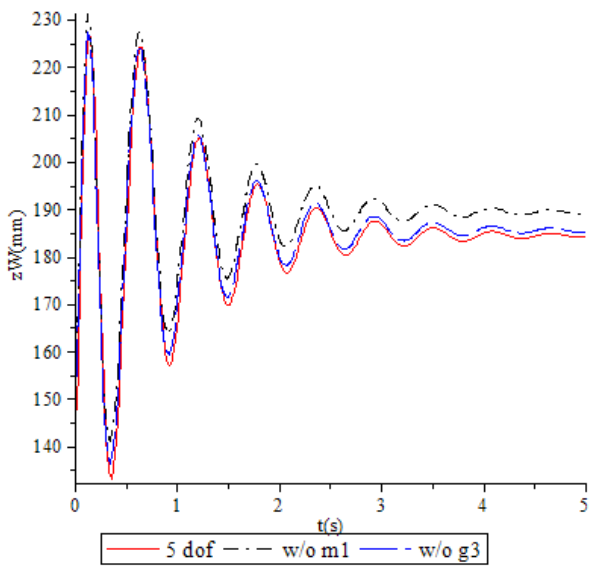

Figure 5.31: Comparison of Systems without Mass of Upper Arm $m1$ and without Gravity of Upper Arm g_3

5.8 Application of Model Reduction Techniques to a Piston-Crank System

Consider the piston-crank system illustrated in Figure 5.32.The system is on the horizontal plane (no gravity), with the crank length, $OA = l_1 = 0.15\,\mathrm{m}$, the connecting rod length $AB = l_2 = 0.35\,\mathrm{m}$, the crank mass $m_1 = 0.12\,\mathrm{kg}$, the connecting rod mass $m_2 = 0.5\,\mathrm{kg}$, the piston mass $m_3 = 2\,\mathrm{kg}$, the crank moment of inertia $I_1 = 0.001\,\mathrm{kg.m^2}$, and the connecting rod moment of inertia $I_2 = 0.004\,\mathrm{kg.m^2}$.

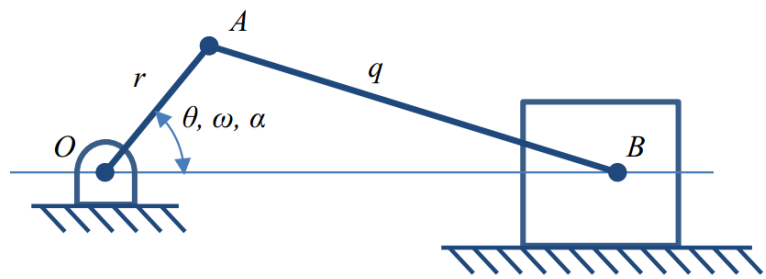

Figure 5.32: Schematic of Piston-Crank Assembly

The piston-crank system has one degree of freedom. Its input is the torque applying to the crank $T = 0.25\,\mathrm{e}^{-0.2\,t}\sin(\pi\,t)$ N.m. The output is the displacement of the piston $d(t) = OB$.

Considering the mechanism response in $[0, 5]$ second, the 2-norms of power of all five components are computed and shown in Figure 5.33.

Table 5.7: Values of m_2 and m_3

Components	Original Model	Reduced Model via 2NPR
connecting rod mass m_2 (kg)	0.5	0.7437254902
piston mass m_3 (kg)	2	0.9254901961

Based on the Figure 5.33, two most important components are the piston mass m_3, and the connecting rod mass m_2. Applying 2NPR, a reduced model is obtained by removing three other components, namely the crank mass m_1, the crank moment of inertia I_1, and the connecting rod moment of inertia I_2. In addition, in the reduced model, the equivalent values of m_2 and m_3 are described in Table 5.7. The actual displacement of the piston in the reduced model is quite different from that of the original model (Figure 5.34).

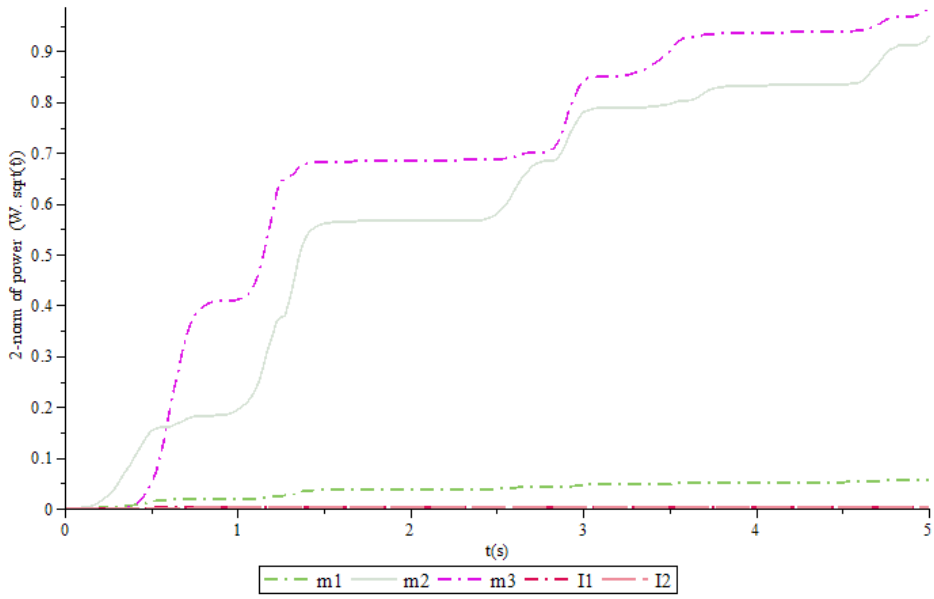

Figure 5.33: 2-Norm of Power of All Components

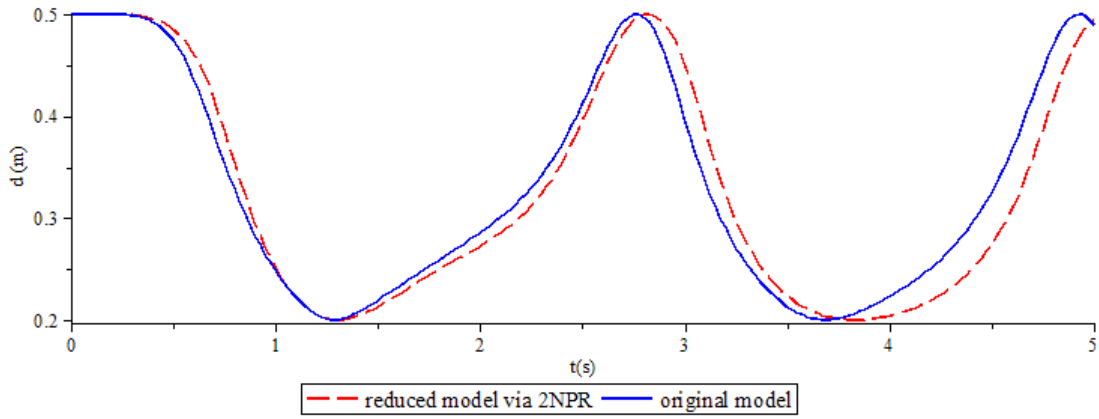

Figure 5.34: Displacement of Piston in Reduced Model Before Finding Equivalent Values of Remaining Components

5.9 MapleSim Template of Model Reduction

The balanced truncation and IRP discussed above has been implemented in MapleSim to build the MapleSim template of model reduction (Figure 5.35). This template is attached to MapleSim interface and has three main functions. The first function is to create a Maple worksheet connecting to MapleSim model for linearizing the MapleSim model to a state-space representation. Second, both IRP and balanced truncation are applied to the state-space representation in order to reduce its order. The output of the reduced model can also be plotted in the template. Finally, the template can create the MapleSim model of the reduced system.

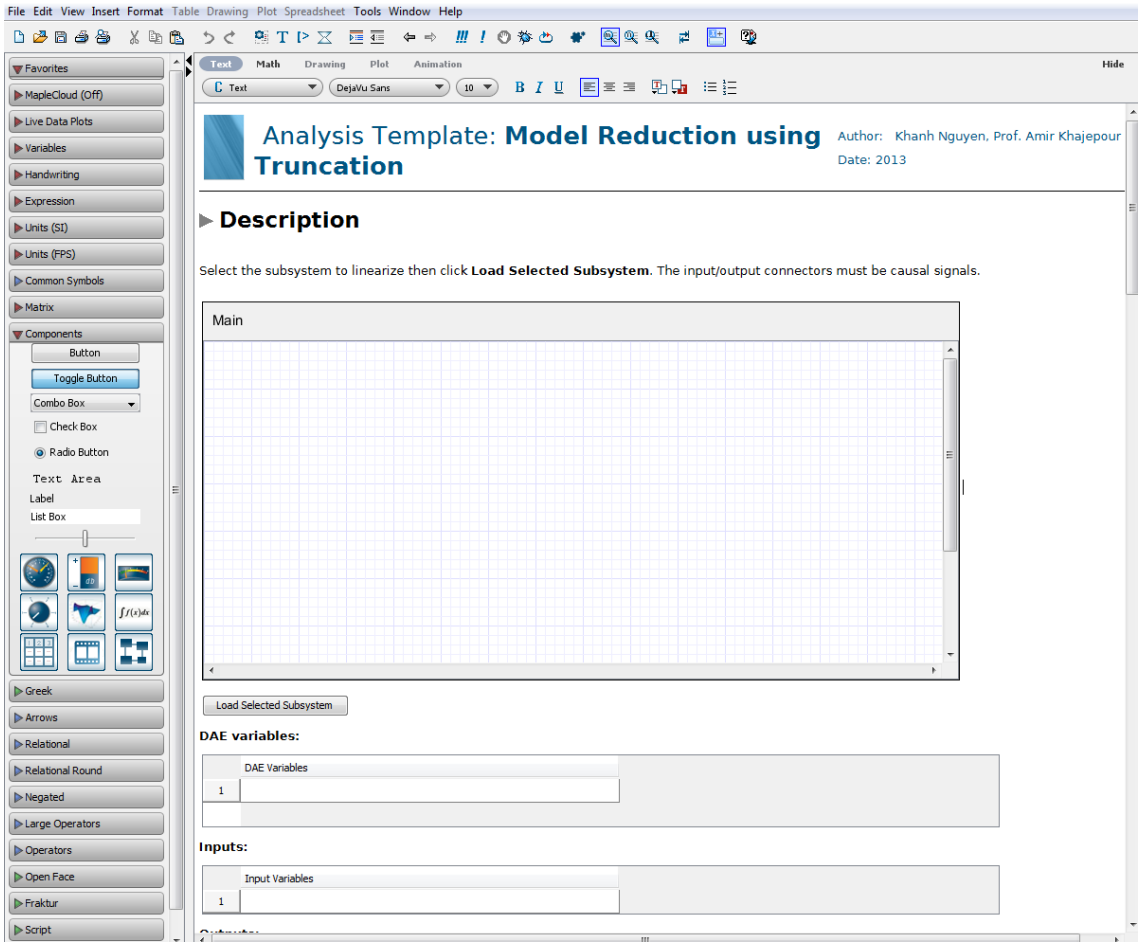

Figure 5.35: MapleSim Template of Model Reduction

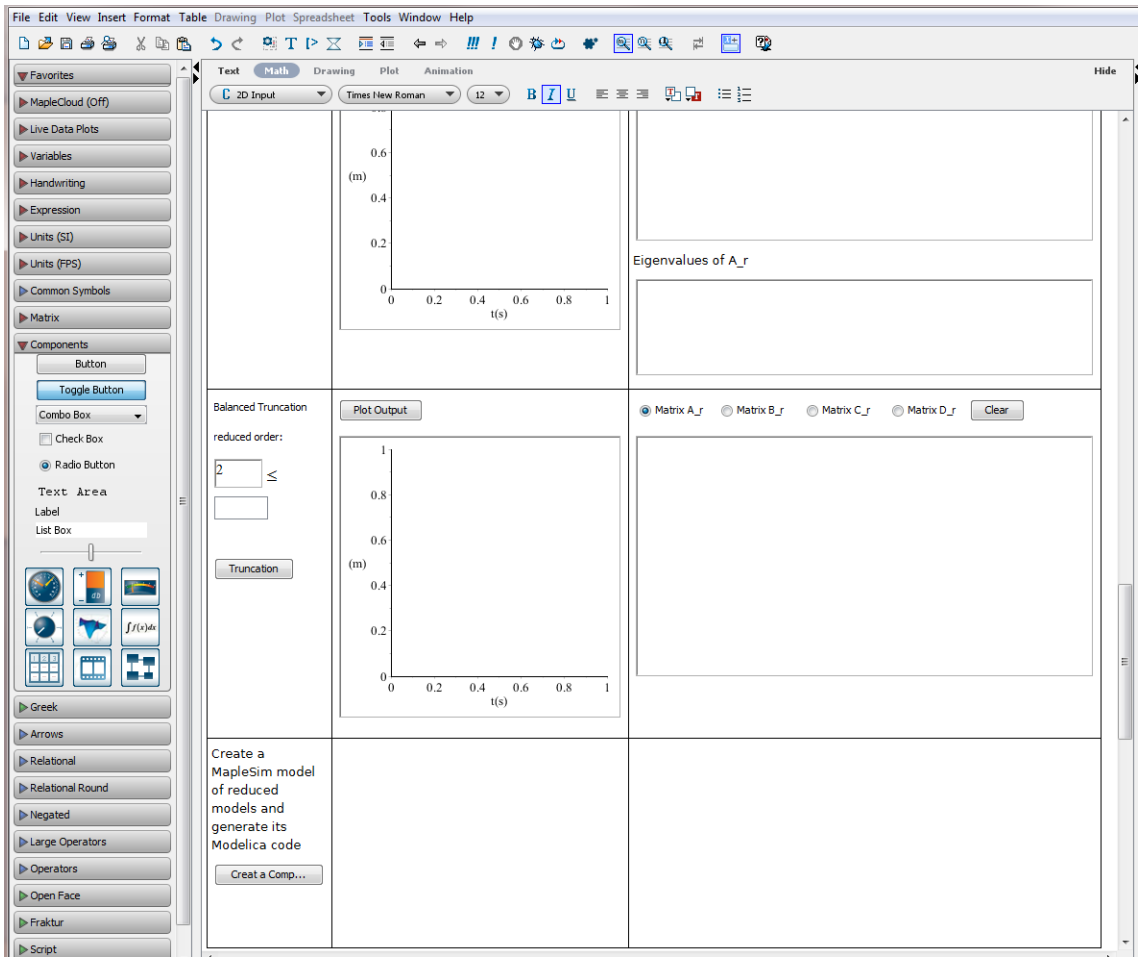

Figure 5.36: MapleSim Template of Model Reduction

Chapter 6

Conclusion and Future Work

6.1 Discussion

Disadvantages of Truncation Methods: There are some important disadvantages of truncation methods. First, in truncation methods, the initial values of the states in the reduced model are not clear. Although in Section 5.2 two methods of approximating the initial values of new states, in some cases, the outputs of the reduced models start at very different points from the original output. Therefore, the output error between the reduced models and the original model is quite significant at start (Figure 5.13). Second, most truncation methods such as IRP and balanced truncation are only applied to several types of linear systems, so nonlinear systems need to be linearized before applying truncation. Hence, the error due to the linearization is inevitable. Finally, the topology of a multi-body system is lost by the truncation methods because its reduced model is a set of differential equations.

Advantages of 2-Norm Power Reduction: The most important advantage of 2-norm power-based reduction (2NPR) is that 2NPR preserves the topology of a system. In addition, because 2NPR is based on the physical properties of a system, the reduced model of 2NPR has useful interpretation. For instance, users can know how each component connects to others in the reduced models, or which component strongly affects the system behavior. Third, 2NPR directly applies to nonlinear systems without linearization, so the error of linearization does not effect to the reduced model. 2-norm of power in 2NPR can identify important components to system response more accurately than the activity in Louca's model reduction technique (activity-based model reduction).

6.2 Summary and Thesis Contribution

The thesis presented several reduction techniques for linear and nonlinear systems such as IRP, balanced truncation, and activity-based model reduction. In addition, a new reduction method, namely 2NPR, was introduced and implemented along with two truncation methods to a 6 DOF double-wishbone suspension with bushings and a 5 DOF suspension. According to the simulation results, the 6 DOF double-wishbone suspension was reduced to a model consisting of two first-order linear differential equation (which is equivalent to a 1 DOF model) by IRP and balanced truncation, and a 2 DOF model by 2NPR. The output errors between theses reduced models and the 6 DOF suspension are acceptable (Figure 5.26). Furthermore, two methods of determining initial values of the reduced model for IRP and balanced truncation were proposed. A MapleSim template is also built to reduce MapleSim dynamic models by IRP and balanced truncation.

The main contribution of this thesis is a new model reduction method 2NPR that combines both 2-norm of power and genetic algorithms. This method not only removes less important components, but also determines the equivalent values of the remaining components in the reduced system. The advantages of a 2-norm metric over the activity metric in Louca's model reduction technique and the comparison of 2NPR to truncation methods were also demonstrated in a 6 DOF double-wishbone suspension and a 5 DOF suspension. Second, a new reduction technique for constrained multi-body systems via proper orthogonal decomposition is proposed in Chapter 4. This method handles Lagrange's multipliers and does not require the linearization of the constrained multi-body systems.

6.3 Future Work

Many nonlinear systems can be decomposed into linear subsystems and nonlinear subsystems, for example the interconnected system in Figure 2.2. As a next step, balanced truncation and 2NPR, respectively, will be used to simplify the linear and nonlinear subsystems in a multi-body system.

The implementation of two proposed model reduction methods in Chapters 3 and 4 to real vehicles is really important. First of all, the empirical data on suspension vehicle corresponding to different inputs will be measured. After that, suitable reduced suspension models need to be determined by the proposed method. Further investigation and experimentation in real vehicles with reduced suspension models are strongly recommended.

Finally, 2NPR can be potentially extended to electric circuits because the behaviors of electrical components is quite similar to that of mechanical components (see Figure 6.1).

Mechanical system	*Electrical system*	*Voltage drop*
F Force (N)	V Voltage	–
m Mass (kg)	L Inductance	$V = \frac{Ldi}{dt} = \frac{Ld^2q}{dt^2}$
c Damping coefficient	R Resistance	$V = iR = R\frac{dq}{dt}$
k Stiffness	$\frac{1}{c}$ Capacitance	$V = \frac{1}{c}\int idt = \frac{q}{c}$
x Displacement	q Charge	–
$\frac{dx}{dt}$ Velocity	i Current	–

Figure 6.1: Equivalent Components of Mechanical And Electrical Circuits [65]

APPENDICES

Appendix A

Definitions

A.1 Moments of a Transfer Function

Considering a descriptor system of the form

$$G_d : \begin{cases} E\dot{x}(t) &= Ax(t) + Bu(t), \quad u \in \mathbb{L}_2[0,\infty), x(t) \in \mathbb{R}^n \\ y(t) &= Cx(t) \end{cases} \tag{A.1}$$

with $E, A \in \mathbb{R}^{n\times n}, and\ B, C \in \mathbb{R}^n$, its transfer function $H(s)$ is defined as follows:

$$H(s) = C^T(sE - A)^{-1}B \tag{A.2}$$

If the pencil $(sE - A)$ is regular, the transfer function can be rewritten in a polynomial form for an arbitrary $s_0 \in \mathbb{C}$:

$$H(s) = \sum_{k=0}^{\infty} (-1)^k M_k(s_0)(s - s_0)^k \tag{A.3}$$

The coefficients $M_k(s_0)$ are called the moments of the transfer function.

A.2 QR Decomposition

QR decomposition of a matrix A is a method to decompose the matrix A into a product $A = QR$ where Q is an orthogonal matrix, and R is an upper triangular matrix.

Appendix B

Linear System Control

B.1 Linear State-Space Systems

Considering linear state-space systems

$$G : \begin{cases} \dot{x}(t) &= Ax(t) + Bu(t), \quad x(0) = x_0 \\ y(t) &= Cx(t) + Du(t) \end{cases} \tag{B.1}$$

, where $x(t) \in \mathbb{R}^n$: the state; $u(t) \in \mathbb{R}^m$: the input; and $y(t) \in \mathbb{R}^p$: the output. The state $x(t)$ and the output $y(t)$ of the linear state-space systems are rewritten as follows

$$x(t) = e^{At}x_0 + \int_0^t e^{A(t-\tau)}Bu(\tau)\, d\tau, \tag{B.2}$$

$$y(t) = Cx(t) + Du(t). \tag{B.3}$$

The transfer function is

$$G(s) = C(sI - A)^{-1}B + D \in C^{m\times p} \tag{B.4}$$

Its H_∞-norm of G operator is

$$\|G\|_\infty = \underset{s\in C_+}{sup}\|G(s)\| = \underset{\omega}{sup}\|G(j\omega)\| \tag{B.5}$$

$\|G\|_\infty$, is finite, if and only if $G(s)$ is stable.

Here are some important definitions that we will consider through the report:

- The realization of the system is the quadruple of matrices $[A(t), B(t), C(t), D(t)]$.
- The realization is <u>observable</u> if for any $y(t)$ and $u(t), t \in [t_0, T]$, there exists a unique $x(t_0)$.
- The realization is <u>controllable</u> if and only if, the $x(T)$ uniquely determines $u(t), t \in [t_0, T]$.
- The realization is <u>minimal</u> if other realizations with the same transfer function have higher state dimensions.

As we known, the realization is minimal if and only if it is not only controllable, but also observable [40].

B.2 Optimization in Hilbert Space

In order to solve optimal estimation problems, and optimal control problems, to define the controllability and observability Gramians, and to find projection matrices for balanced truncation, the following theorem is considered.

Theorem B.2.1 *(Luenberger [39]) Suppose $A : U \to Y$ is a bounded linear operator, where U and Y are Hilbert spaces.*

1. *For fixed $y \in Y$, the vector $u \in U$ that minimizes $\|y - Au\|_Y$ satisfies the normal equations*
$$A^* A u = A^* y \tag{B.6}$$
If $(A^* A) : U \to U$ is invertible, the unique optimal solution is $u = (A^* A)^{-1} A^* y$.

2. *Suppose A has closed range in Y. Then the vector $u \in U$ with the smallest norm $\|u\|_U$ satisfying $y = Au$ is given by*
$$u = A^* z, \tag{B.7}$$
for any $z \in Y$ that satisfies $AA^* z = y$.
If $(AA^*) : Y \to Y$ is invertible, the unique optimal solution is $u = A^*(AA^*)^{-1} y$

B.3 Signals

The measurable function mapping the real number to a real vector is called a signal. The set of signal is

$$S = \{f : \mathbb{R} \mapsto \mathbb{R}^n\} \tag{B.8}$$

Let

$$S_+ = \{f \in S : f(t) = 0 \quad \text{for all t} < 0\} \tag{B.9}$$
$$S_- = \{f \in S : f(t) = 0 \quad \text{for all t} > 0\} \tag{B.10}$$

The finite-horizon Lebesgue 2-space is:

$$L_2[0,T] = \left\{f \in S_+ : \|f\|_{2,[0,T]} < \infty\right\} \tag{B.11}$$

in which

$$\|f\|_{2,[0,T]} = \left\{\int_0^T \|f(t)\|^2 \, dt\right\}^{1/2} \tag{B.12}$$

is the finite-horizon 2-norm of the signal f

The infinite-horizon 2-norm is defined as follows

$$\|f\|_2 = \left\{\int_{-\infty}^{\infty} \|f(t)\|^2 \, dt\right\}^{1/2} \tag{B.13}$$

The infinite-horizon Lebesgue 2-space is:

$$L_2[-\infty,\infty] = \{f \in S_+ : \|f\|_2 < \infty\} \tag{B.14}$$

B.4 The Controllability Gramian

Considering the state-space system B.1, let R_T be its controllability operator:

$$\begin{aligned} R_T : L_2[0,T] &\to \mathbb{R}^n \\ u(t) &\mapsto x(T) \\ x(T) &= \int_0^T e^{A(T-t)} B u(t) \, dt = R_T u \end{aligned} \tag{B.15}$$

If the realization is controllable, for any $x(T) = x_T \in \mathbb{R}^n$, there are $u \in \mathbb{L}_2[0,T]$ such that $x(T) = R_T u$.

Let R_T^* be the Hilbert adjoint of R_T:

$$\begin{aligned} R_T^* &: \mathbb{R}^n \to L_2[0,T] \\ R_T^* &= B^T e^{A^T(T-t)} \end{aligned} \tag{B.16}$$

Define the controllable gramian $P(T)$as follows [44]:

$$P(T) = R_T R_T^* = \int_o^T e^{A\tau} B B^T e^{A^T \tau}\, dt, \tag{B.17}$$

If the system is controllable, $P(T)^{-1}$ exists for all $T > 0$. The input is rewritten from eqn B.15 by pseudo-inverse

$$u(t) = R_T^*(R_T R_T^*)^{-1} x_T = B^T e^{A^T(T-t)} P(T)^{-1} x_T, \tag{B.18}$$

Hences, the finite-horizon 2-norm of u is

$$\|u\|_{2,[0,T]} = \sqrt{x_T^T P(T)^{-1} x_T} \tag{B.19}$$

Let $U_P \Sigma_P^2 U_P^T$ be a singular value decomposition of P(T), with $\Sigma_P = diag\,\{\sigma_1, \cdots, \sigma_n\}$ and $U_P = (u_1 \cdots u_n)$is unitary matrix:

$$P(T) = U_P \Sigma_P^2 U_P^T \tag{B.20}$$

If we fix the domain of the input $\|u\|_{2,[0,T]} \leq 1$, the range of the controllable operator R_T is

$$\mathbb{R} = \left\{x : x = U_P \Sigma_P z, \|z\|_{2,[0,T]} = 1\right\} \tag{B.21}$$

Therefore, we have the following theorem

Theorem B.4.1 *(Bruce Moore [44]): A realization $[A, B, C, D]$ of G is controllable if, and only if, $P_T(0)$ is invertible for all $T > 0$. The controllable subspace is spanned by the component vector $u_1, \cdots, u_r$ in U_P that correspond to the $r \leq n$ strictly positive singular values in Σ_P. The singular value σ_i quantifies how far one can reach in the direction u_i using the input energy $\|u\|_{2,[0,T]} \leq 1$.*

B.5 The Observability Gramian

The observability Gramian is definded by [44]:

$$Q_T(0) = \int_0^T x_0^T e^{A^T} C^T C e^{At} x_0 \, dt, \tag{B.22}$$

The energy of the output is

$$\|y\|_{2,[0,T]}^2 = \int_0^T y(t)^T y(t) \, dt = \int_0^T x_0^T e^{A^T} C^T C e^{At} x_0 \, dt = x_0 Q_T(0) x_0 \tag{B.23}$$

The system is observable if, only if, $Q_T(0)$ is nonsingular for all $T > 0$.

In practice, it is easier to obtain the observability gramian by solving the Lyapunov differential equation. If $T \to \infty$, the observability gramian $Q(= Q_\infty(0))$ is determined through the algebraic Lyapunov equation

$$A^T Q + QA + C^T C = 0 \tag{B.24}$$

Similar to the controllable Gramian, using the singular value decomposition of $Q_T(0)$ is to determine which states affect the energy of the output most: $Q_T(0) = U_Q \Sigma_Q^2 U_Q^T$, where $U_Q = (u_1 \cdots u_2)$ is unitary matrix, and $\Sigma_P = diag\{\sigma_1, \cdots, \sigma_n\}$. The direction that produces the largest energy of the ouput is the vector u_1. If the range of the observability operator

Theorem B.5.1 *(Bruce Moore [44]): A realization $[A, B, C, D]$ of G is observable if, and only if, $Q_T(0)$ is invertible for all $T > 0$. the unobservable subspace is spanned by the component vectors $u_{r+1}, \cdots, u_n$ in U_Q that correspond to the possible zero singular values in Σ_Q. The singular value σ_i quantifies how much energy $\|y\|_{2,[0,T]}$ there if $x_0 = u_i$.*

Appendix C

Least Squares Estimation (LSE) for Nonlinear Systems

Kim C. developed least square estimation for ordinary differential equations [9]. However, this method is inapplicable to the equations of motion containing unknown Lagrange's multipliers, which are not measured by experiments. This section is the extension of least square estimation for multi-body systems with differential-algebraic equations and Lagrange's multipliers.

Applying Lagrang's theory, the differential equations of a multi-body system are equation (C.1), and the algebraic equations are the constraint equation (C.2).

$$M\ddot{q} + \Phi_q^T \lambda = Q_B(\dot{q}, q, u). \tag{C.1}$$

$$\Phi = 0. \tag{C.2}$$

The constraint equations are the geometrical constraint of the multi-body systems, so do not contain any component that has power such as mass, moment of inertia, or forces. Therefore, parameter estimation only uses differential equations (C.1).

Because λ is a vector of Lagrange's multipliers, which cannot be obtained from experiments, λ need to be removed from equation (C.1). The first step of this parameter estimation method is to find the equilibrium or nominal position of the system, q^*, so $\Phi_q^T \simeq \Phi_{q|q=q^*}^T = \Phi_{q^*}^T$. Equation (C.1) is approximated by:

$$M\ddot{q} + \Phi_{q^*}^T \lambda = Q_B. \tag{C.3}$$

Let (Q_1, R_1) be QR decomposition of Φ_{q*}^T and $Q_1 = (Q_{11} \;\; D)$, where matrix Q_{11} has the same number of columns as the number of Lagrange's multipliers. Hence, $D^T \Phi_{q*}^T = 0$.

Multiplying both sides of equation (C.3) with D^T, Lagrange's multipliers are removed; the equations of motion are simplified as:

$$D^T M\ddot{q} = D^T Q_B. \tag{C.4}$$

Let n be the size of the variables vector q, so equation (C.4) has n differential equations, and rewritten in the following forms:

$$\theta^T \phi_i - f_i = 0, \tag{C.5}$$

where $i \in \{1, 2, \cdots, n\}$; and ϕ_i, f_i, and θ be, respectively, the vector, the function of measured states, and a parameter vector. From the generated simulation data or experiments, ϕ_i and f_i are known.

Let $\hat{\theta}$ be an estimated parameter vector. The errors of approximated equations are defined as follows: $\epsilon_i = \hat{\theta}^T \phi_i - f_i$.

The objective function for m numbers of measured variables is defined as follows:

$$E = \sum_{k=1}^{m} \left[\sum_{i=1}^{n} \epsilon_i^2 (k) \right] = \sum_{k=1}^{m} \left[\sum_{i=1}^{n} \left(\hat{\theta}^T \phi_i - f_i \right)^2 (k) \right]. \tag{C.6}$$

The estimated parameters satisfy the condition $\frac{\delta E}{\delta \widehat{\theta}} = 0$ in order to minimize E. Therefore,

$$\widehat{\theta} = \left\{ \sum_{k=1}^{m} \left[\sum_{i=1}^{n} \phi_i (k) \phi_i^T (k) \right] \right\}^{-1} \left\{ \sum_{k=1}^{m} \left[\sum_{i=1}^{n} \phi_i^T (k) f_i (k) \right] \right\} \tag{C.7}$$

Finally, from equation (C.7), the estimated parameters are calculated from the measured data.

Appendix D

Parameter Estimation for Nonlinear Systems via Genetic Algorithms

The least square estimation is effective for a linear system, however, it is difficult to apply the least square estimation to minimize the squared output error for a nonlinear system. For example, LSE in Appendix C is only able to minimize the squared error between the original equations and the approximated equations (see equation (C.6)). On the contrary, genetic algorithms (GAs) provide a robust, efficient and flexible method for an optimization problem. Specially, GAs do not require the derivative of the objective function like LSE. Therefore, GAs for parameter estimation are investigated in this section.

Considering the following nonlinear systems:

$$\begin{aligned} g\left(t, p, u, q, \dot{q}, \ddot{q}\right) &= 0, \\ y &= h\left(q\right), \end{aligned} \tag{D.1}$$

where p is parameters, u is inputs, q is states, and y is outputs. The equations of motion of a multi-body system (equation (C.1) and (C.2)) are easily rewritten into the form (D.1).

The goal of GAs is to find the unknown parameters p that minimize the squared errors (equation D.2) between the outputs y and desired outputs $\hat{y}_k$, $k \in \{1, \cdots, m\}$, at m points along the output trajectory. Therefore, the fitness function of GAs is the inverse of the square errors $f = \frac{1}{E}$.

$$E = \sum_{k=1}^{m} \left(y_k - \hat{y}_k\right)^2. \tag{D.2}$$

The flow chart of GAs for parameter estimation is described in Figure D.1.

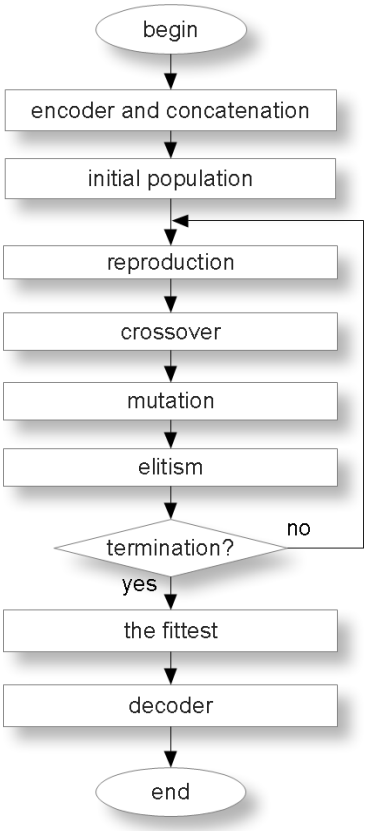

Figure D.1: Parameter Estimation via Genetic Algorithms

Appendix E

Dynamics of a 6 DOF Planar Double-Wishbone Suspension

E.1 Analytical Model

Although some simulation software can generate the equations of motion of this suspension, its results are extremely disorderly and cannot be used for model reduction. Therefore, the analytical model of the 6 DOF suspension is derived by hand.

Let $q = [y_A, z_A, \alpha_1, \alpha_2, y_E, z_E, \alpha_3, z_{CH}]^T$ and $[y_{A0}, z_{A0}, \alpha_{10}, \alpha_{20}, y_{E0}, z_{E0}, \alpha_{30}, z_{CH0}]^T$ be an initial position. Denote $s_i = \sin(\alpha_i)$, and $c_i = \cos(\alpha_i)$ with $i \in \{1, 2, 3, 10, 20, 30\}$

The kinetic energy of each component is defined as follows:

- lower arm AB

$$T_{LA} = \frac{1}{2}m_1\left(\dot{y}_A - \frac{1}{2}l_1 s_1 \dot{\alpha}_1\right)^2 + \frac{1}{2}m_1\left(\dot{z}_A + \frac{1}{2}l_1 c_1 \dot{\alpha}_1\right)^2 + \frac{1}{2}I_{X1}\dot{\alpha}_1^2, \quad \text{(E.1)}$$

- upper arm DE

$$T_{UA} = \frac{1}{2}m_3\left(\dot{y}_E + \frac{1}{2}l_3 s_3 \dot{\alpha}_3\right)^2 + \frac{1}{2}m_3\left(\dot{z}_E - \frac{1}{2}l_3 c_3 \dot{\alpha}_3\right)^2 + \frac{1}{2}I_{X3}\dot{\alpha}_3^2, \quad \text{(E.2)}$$

- knuckle DBW

$$
\begin{aligned}
T_{SP} = & \frac{1}{2} m_2 \left(\dot{y}_A - l_1 s_1 \dot{\alpha}_1 - \left(\left(\frac{1}{2} l_2 + y_{C2} \right) s_2 + z_{C2} c_2 \right) \dot{\alpha}_2 \right)^2 \\
& + m_2 \left(\dot{z}_A + \frac{1}{2} l_1 c_1 \dot{\alpha}_1 + \left(\left(\frac{1}{2} l_2 + y_{C2} \right) c_2 - z_{C2} s_2 \right) \dot{\alpha}_2 \right)^2 \\
& + \frac{1}{2} J_{XX2} \dot{\alpha}_2^2,
\end{aligned}
\tag{E.3}
$$

- chassis

$$
T_{CH} = \frac{1}{2} m_{CH} \left(\dot{z}_{CH} \right)^2, \tag{E.4}
$$

- wheel HH'

$$
\begin{aligned}
T_{WH} = & \frac{1}{2} m_W \left(\dot{y}_A - l_1 s_1 \dot{\alpha}_1 - \left(\left(\frac{1}{2} l_2 + y_{KW} \right) s_2 + z_{KW} c_2 \right) \dot{\alpha}_2 \right)^2 \\
& + \frac{1}{2} m_W \left(\dot{z}_A + l_1 c_1 \dot{\alpha}_1 + \left(\left(\frac{1}{2} l_2 + y_{KW} \right) c_2 - z_{KW} s_2 \right) \dot{\alpha}_2 \right)^2 \\
& + \frac{1}{2} J_{XXw} \dot{\alpha}_2^2.
\end{aligned}
\tag{E.5}
$$

The total kinetic energy T is:

$$
T = T_{LA} + T_{UA} + T_{SP} + T_{WH}. \tag{E.6}
$$

The potential energy of following components is calculated as follows:

- chassis

$$
V_{gCH} = m_{CH} g z_{CH}, \tag{E.7}
$$

- lower arm

$$
V_{g1} = m_1 g \left(z_A + \frac{1}{2} l_1 s_1 \right), \tag{E.8}
$$

- knuckle

$$
V_{g2} = m_2 g \left[z_A + l_1 s_1 + \left(\frac{1}{2} l_2 + y_{C2} \right) s_2 + z_{C2} c_2 \right], \tag{E.9}
$$

- upper arm

$$V_{g3} = m_3 g \left(z_A + l_1 s_1 + l_2 s_2 + \frac{1}{2} l_3 s_3 \right), \tag{E.10}$$

- wheel

$$V_{gW} = m_W g \left[z_A + l_1 s_1 + \left(\frac{1}{2} l_2 + y_{KW} \right) s_2 + z_{KW} c_2 \right], \tag{E.11}$$

- springs at A

$$V_{sLA} = \frac{1}{2} k_{LA} \left(z_A - z_{A0} - z_{CH} + z_{CH0} \right)^2 + \frac{1}{2} k_{LA} \left(y_A - y_{A0} \right)^2, \tag{E.12}$$

- springs at E

$$V_{sUA} = \frac{1}{2} k_{UA} \left(z_E - z_{E0} - z_{CH} + z_{CH0} \right)^2 + \frac{1}{2} k_{UA} \left(y_E - y_{E0} \right)^2, \tag{E.13}$$

- suspension spring

$$V_{ssus} = \frac{1}{2} k_{sus} \left(l_s - l_{s0} \right)^2, \tag{E.14}$$

where l_{s0} is the initial length of the suspension spring, and l_s is the length of the suspension spring at time t

$$l_s = \sqrt{\left(y_A + l_f c_1 - y_{A0} - l_f c_{10} \right)^2 + \left(z_{CH} + z_{A0} + l_f s_{10} - z_{CH0} + l_{s0} - z_A - l_f s_1 \right)^2},$$

- tire spring

$$V_{sTire} = \frac{1}{2} k_t \left(l_{tt} - l_{t0} \right)^2, \tag{E.15}$$

where l_{t0} is the initial length of the tire spring, and l_{tt} is the length of the tire spring:

$$l_{tt} = \sqrt{\left(z_A + l_1 s_1 + \left(\frac{1}{2} l_2 + y_{KH} \right) s_2 + z_{KH} c_2 - z_G \right)^2 + \left(y_A + l_1 c_1 + \left(\frac{1}{2} l_2 + y_{KH} \right) c_2 - z_{KH} s_2 - y_G \right)^2}.$$

The total potential energy V is:

$$V = V_m + V_{sUA} + V_{sLA} + V_{ssus} + V_{sTire}. \tag{E.16}$$

The Lagrangian L is defined as follows:

$$L = T - V. \tag{E.17}$$

The generalized forces of each component are:

- suspension damper

$$Q_{sus} = \begin{bmatrix} 0 \\ -C_d\left(\dot{z}_A + l_f c_1 \dot{\alpha}_1 - \dot{z}_{CH}\right) \\ -l_f c_1 C_d\left(\dot{z}_A + l_f c_1 \dot{\alpha}_1 - \dot{z}_{CH}\right) \\ 0 \\ 0 \\ 0 \\ 0 \\ C_d\left(\dot{z}_A + l_f c_1 \dot{\alpha}_1 - \dot{z}_{CH}\right) \end{bmatrix}, \tag{E.18}$$

- dampers at A

$$Q_{LA} = \begin{bmatrix} -C_{LA}\dot{y}_A \\ -C_{LA}\left(\dot{z}_A - \dot{z}_{CH}\right) \\ 0 \\ 0 \\ 0 \\ 0 \\ 0 \\ C_{LA}\left(\dot{z}_A - \dot{z}_{CH}\right) \end{bmatrix}, \tag{E.19}$$

- dampers at E

$$Q_{UA} = \begin{bmatrix} 0 \\ 0 \\ 0 \\ 0 \\ -C_{UA}\dot{y}_E \\ -C_{UA}\left(\dot{z}_E - \dot{z}_{CH}\right) \\ 0 \\ C_{UA}\left(\dot{z}_E - \dot{z}_{CH}\right) \end{bmatrix}. \tag{E.20}$$

The total generalized force is calculated as follows

$$Q_G = Q_{UA} + Q_{LA} + Q_{sus}. \tag{E.21}$$

Because the suspension has 6 DOF while the number of variables is eight, two constraint equations are required:

$$\overrightarrow{AB} + \overrightarrow{BD} + \overrightarrow{DE} = \overrightarrow{AE}, \tag{E.22}$$

or

$$\begin{aligned} y_A + l_1c_1 + l_2c_2 - y_E + l_3c_3 = 0, \\ z_A + l_1s_1 + l_2s_2 - z_E + l_3s_3 = 0, \end{aligned} \tag{E.23}$$

or

$$\Phi = 0, \tag{E.24}$$

where

$$\Phi = \begin{bmatrix} y_A + l_1c_1 + l_2c_2 - y_E + l_3c_3 \\ z_A + l_1s_1 + l_2s_2 - z_E + l_3s_3 \end{bmatrix}. \tag{E.25}$$

Lagrange's equations are:

$$\frac{d}{dt}\left(\frac{\partial L}{\partial \dot{q}}\right) - \frac{\partial L}{\partial q} + \Phi_q^T\lambda = Q. \tag{E.26}$$

Because in this suspension, the equations of motion consisting of Lagrange's equations (E.26) and the constraint equation (E.24) cannot be numerically solved, the constraint

equation need to be replaced by other equations. One of these equations is the second time derivative of constraint equations defined as follows:

$$\begin{aligned} &\ddot{y}_A - l_1 s_1 \ddot{\alpha}_1 - l_2 s_2 \ddot{\alpha}_2 - \ddot{y}_E - l_3 s_3 \ddot{\alpha}_3 - l_1 c_1 \dot{\alpha}_1^2 - l_2 c_2 \dot{\alpha}_2^2 - l_3 c_3 \dot{\alpha}_3^2 = 0, \\ &\ddot{z}_A + l_1 c_1 \ddot{\alpha}_1 + l_2 c_2 \ddot{\alpha}_2 - \ddot{z}_E + l_3 c_3 \ddot{\alpha}_3 - l_1 s_1 \dot{\alpha}_1^2 - l_2 s_2 \dot{\alpha}_2^2 - l_3 s_3 \dot{\alpha}_3^2 = 0. \end{aligned} \tag{E.27}$$

The constraint equation (E.22) is replaced by its second time derivative (equation(E.27)). Therefore, the equations of motion are re-written in a descriptor form:

$$\begin{bmatrix} M & \Phi_q^T \\ \Phi_q & 0 \end{bmatrix} \begin{bmatrix} \ddot{q} \\ \lambda \end{bmatrix} = \begin{bmatrix} Q_B \\ \gamma \end{bmatrix}, \tag{E.28}$$

where

$$\gamma = \begin{bmatrix} 260 \left(\frac{d}{dt}\alpha_1\right)^2 \cos(\alpha_1) + 280 \left(\frac{d}{dt}\alpha_2\right)^2 \cos(\alpha_2) + 180 \left(\frac{d}{dt}\alpha_3\right)^2 \cos(\alpha_3) \\ 260 \left(\frac{d}{dt}\alpha_1\right)^2 \sin(\alpha_1) + 280 \left(\frac{d}{dt}\alpha_2\right)^2 \sin(\alpha_2) + 180 \left(\frac{d}{dt}\alpha_3\right)^2 \sin(\alpha_3) \end{bmatrix}. \tag{E.29}$$

One of equations (E.28) is:

$$\begin{aligned}
&4.4153500000\,10^6 \left(\frac{d^2}{dt^2}\alpha_1(t)\right) + \left(-1.040000000\,10^6 \sin\left(-\alpha_2(t) + \alpha_1(t)\right) + 2.249520000\,10^6 \cos\left(-\alpha_2(t) + \alpha_1(t)\right)\right) \left(\frac{d^2}{dt^2}\alpha_2(t)\right) - 17147.00000 \left(\frac{d^2}{dt^2} y_A(t)\right) \sin\left(\alpha_1(t)\right) \\
&\quad + 17147.00000 \left(\frac{d^2}{dt^2} z_A(t)\right) \cos\left(\alpha_1(t)\right) + \left(5.1300000\,10^7 + 5.1300000\,10^7 \cos\left(2\,\alpha_1(t)\right)\right) \left(\frac{d}{dt}\alpha_1(t)\right) + 8.660000\,10^6 z_{CH0} \cos\left(\alpha_1(t)\right) + 2.841439511\,10^{10} \sin\left(\alpha_1(t)\right) - 8.0600000\,10^7 \cos\left(\alpha_1(t)\right) z_G(t) \\
&\quad - 1.988115890\,10^9 \cos\left(\alpha_1(t)\right) - 7.215992316\,10^9 \cos\left(-\alpha_2(t) + \alpha_1(t)\right) + 4.820625832\,10^9 \sin\left(-\alpha_2(t) + \alpha_1(t)\right) - 1.732000000\,10^9 \sin\left(-\alpha_1(t) + \alpha_{10}\right) + 5.13000\,10^5 \left(\frac{d}{dt} z_A(t)\right) \cos\left(\alpha_1(t)\right) \\
&\quad - 8.660000\,10^6 z_{A0} \cos\left(\alpha_1(t)\right) - 8.9260000\,10^7 y_A(t) \sin\left(\alpha_1(t)\right) + 8.660000\,10^6 \sin\left(\alpha_1(t)\right) y_{A0} - 8.660000\,10^6 z_{CH}(t) \cos\left(\alpha_1(t)\right) - \left(5.412500\,10^6 \left(-400.\, y_A(t) \sin\left(\alpha_1(t)\right) + 400.\, \sin\left(\alpha_1(t)\right) y_{A0}\right.\right. \\
&\quad \left.\left. - 400.\, z_{CH}(t) \cos\left(\alpha_1(t)\right) - 400.\, z_{A0} \cos\left(\alpha_1(t)\right) + 400.\, z_{CH0} \cos\left(\alpha_1(t)\right) + 400.\, z_A(t) \cos\left(\alpha_1(t)\right) - 1.00000\,10^5 \cos\left(\alpha_1(t)\right) - 80000.\, \sin\left(-\alpha_1(t) + \alpha_{10}\right)\right)\right) \Big/ \\
&\left(142500 - 500\, z_{CH0} + 500\, z_{A0} - 100000 \sin\left(\alpha_1(t)\right) - 500\, z_A(t) + 500\, z_{CH}(t) - 80000 \cos\left(-\alpha_1(t) + \alpha_{10}\right) + 100000 \sin\left(\alpha_{10}\right) + y_{A0}^2 + z_{A0}^2 - 2\, z_{A0} z_{CH0} + z_{CH0}^2 + 400\, y_A(t) \cos\left(\alpha_1(t)\right) - 2\, y_A(t)\, y_{A0}\right. \\
&\quad - 400\, y_A(t) \cos\left(\alpha_{10}\right) - 400 \cos\left(\alpha_1(t)\right) y_{A0} + 400\, y_{A0} \cos\left(\alpha_{10}\right) + 2\, z_{CH}(t)\, z_{A0} + 400\, z_{CH}(t) \sin\left(\alpha_{10}\right) - 2\, z_{CH}(t)\, z_{CH0} - 2\, z_{CH}(t)\, z_A(t) - 400\, z_{CH}(t) \sin\left(\alpha_1(t)\right) + 400\, z_{A0} \sin\left(\alpha_{10}\right) - 2\, z_{A0} z_A(t) \\
&\quad - 400\, z_{A0} \sin\left(\alpha_1(t)\right) - 400 \sin\left(\alpha_{10}\right) z_{CH0} - 400 \sin\left(\alpha_{10}\right) z_A(t) + 2\, z_{CH0} z_A(t) + 400\, z_{CH0} \sin\left(\alpha_1(t)\right) + 400\, z_A(t) \sin\left(\alpha_1(t)\right) + y_A(t)^2 + z_{CH}(t)^2 + z_A(t)^2\Big)^{1/2} \\
&\quad - \left(5.4314682230\,10^6 \left(1.833186781\,10^5 \sin\left(\alpha_1(t)\right) + 31100.81182 \sin\left(-\alpha_2(t) + \alpha_1(t)\right) - 46554.78914 \cos\left(-\alpha_2(t) + \alpha_1(t)\right) - 520.\, y_A(t) \sin\left(\alpha_1(t)\right) + 520.\, z_A(t) \cos\left(\alpha_1(t)\right) - 520.\, \cos\left(\alpha_1(t)\right) z_G(t)\right)\right) \Big/ \\
&\left(-705.0718390\, y_A(t) - 1.833186781\,10^5 \cos\left(\alpha_1(t)\right) - 63123.98228 \sin\left(\alpha_2(t)\right) + 42169.82036 \cos\left(\alpha_2(t)\right) + z_G(t)^2 - 31100.81182 \cos\left(-\alpha_2(t) + \alpha_1(t)\right) - 46554.78914 \sin\left(-\alpha_2(t) + \alpha_1(t)\right)\right. \\
&\quad + 2.034740629\,10^5 + 520\, y_A(t) \cos\left(\alpha_1(t)\right) + 520\, z_A(t) \sin\left(\alpha_1(t)\right) + y_A(t)^2 + z_A(t)^2 - 119.6185070\, z_A(t) \sin\left(\alpha_2(t)\right) - 179.0568813\, z_A(t) \cos\left(\alpha_2(t)\right) - 2\, z_A(t)\, z_G(t) - 520 \sin\left(\alpha_1(t)\right) z_G(t) \\
&\quad + 119.6185070 \sin\left(\alpha_2(t)\right) z_G(t) + 179.0568813 \cos\left(\alpha_2(t)\right) z_G(t) - 119.6185070\, y_A(t) \cos\left(\alpha_2(t)\right) + 179.0568813\, y_A(t) \sin\left(\alpha_2(t)\right)\Big)^{1/2} + 8.9260000\,10^7 z_A(t) \cos\left(\alpha_1(t)\right) + \left(1.040000000\,10^6 \cos\left(-\alpha_2(t)\right.\right. \\
&\quad \left.\left. + \alpha_1(t)\right) + 2.249520000\,10^6 \sin\left(-\alpha_2(t) + \alpha_1(t)\right)\right) \left(\frac{d}{dt}\alpha_2(t)\right)^2 + 260.\, \lambda_2(t) \cos\left(\alpha_1(t)\right) - 260.\, \lambda_1(t) \sin\left(\alpha_1(t)\right) - 5.13000\,10^5 \cos\left(\alpha_1(t)\right) \left(\frac{d}{dt} z_{CH}(t)\right) = 0
\end{aligned}$$

Linearization: Applying the linearization method discussed in Section 5.1.3, the state-space representation $\left[\hat{I}, \hat{A}, \hat{B}, \hat{C}\right]$ of the analytical model (equation (E.28)) is obtained as follows:

$$\begin{aligned} \dot{X} &= \hat{A}X + \hat{B}u \\ Y &= \hat{C}X, \end{aligned} \tag{E.30}$$

where $X = \begin{bmatrix} \Delta q \\ \Delta \dot{q} \end{bmatrix}$, $Y = z_{CH}$,

$$\hat{A} = \begin{bmatrix}
0.0 & 0.0 & 0.0 & 0.0 & 0.0 & 0.0 & 0.0 & 0.0 & 1.0 & 0.0 & 0.0 & 0.0 & 0.0 & 0.0 & 0.0 & 0.0 \\
0.0 & 0.0 & 0.0 & 0.0 & 0.0 & 0.0 & 0.0 & 0.0 & 0.0 & 1.0 & 0.0 & 0.0 & 0.0 & 0.0 & 0.0 & 0.0 \\
0.0 & 0.0 & 0.0 & 0.0 & 0.0 & 0.0 & 0.0 & 0.0 & 0.0 & 0.0 & 1.0 & 0.0 & 0.0 & 0.0 & 0.0 & 0.0 \\
0.0 & 0.0 & 0.0 & 0.0 & 0.0 & 0.0 & 0.0 & 0.0 & 0.0 & 0.0 & 0.0 & 1.0 & 0.0 & 0.0 & 0.0 & 0.0 \\
0.0 & 0.0 & 0.0 & 0.0 & 0.0 & 0.0 & 0.0 & 0.0 & 0.0 & 0.0 & 0.0 & 0.0 & 1.0 & 0.0 & 0.0 & 0.0 \\
0.0 & 0.0 & 0.0 & 0.0 & 0.0 & 0.0 & 0.0 & 0.0 & 0.0 & 0.0 & 0.0 & 0.0 & 0.0 & 1.0 & 0.0 & 0.0 \\
0.0 & 0.0 & 0.0 & 0.0 & 0.0 & 0.0 & 0.0 & 0.0 & 0.0 & 0.0 & 0.0 & 0.0 & 0.0 & 0.0 & 1.0 & 0.0 \\
0.0 & 0.0 & 0.0 & 0.0 & 0.0 & 0.0 & 0.0 & 0.0 & 0.0 & 0.0 & 0.0 & 0.0 & 0.0 & 0.0 & 0.0 & 1.0 \\
-35713.0 & 46370.0 & -698350.0 & -552400.0 & -689.12 & 103.14 & -12.585 & -50388.0 & -595.82 & 951.32 & 9859.9 & -0.0 & -10.371 & 1.5522 & -0.0 & -952.87 \\
46872.0 & -123210.0 & 86979.0 & -253670.0 & 497.74 & -221.59 & 15.489 & 121900.0 & 897.03 & -2301.0 & -24810.0 & 0.0 & 7.4907 & -3.3348 & -0.0 & 2304.3 \\
-202.67 & 512.55 & -4133.9 & -23.913 & -18.639 & 6.1516 & -0.48666 & -525.06 & -3.8884 & 9.7080 & 78.872 & -0.0 & -0.28051 & 0.092579 & -0.0 & -9.8006 \\
-51.103 & -40.214 & -1551.8 & -2729.8 & 37.799 & 7.7569 & 0.10668 & 14.910 & -0.56712 & -0.35282 & 13.130 & -0.0 & 0.56886 & 0.11674 & 0.0 & 0.23608 \\
196.59 & 810.56 & -161800.0 & 95472.0 & -27516.0 & 63823.0 & -1005.7 & -64242.0 & -20.503 & -9.6352 & -4439.6 & -0.0 & -414.10 & 960.50 & -0.0 & -950.87 \\
638.53 & 1507.0 & 396550.0 & 176380.0 & 63823.0 & -245200.0 & 3663.5 & 245450.0 & 3.0686 & 0.98955 & 1377.1 & 0.0 & 960.50 & -3690.2 & -0.0 & 3689.2 \\
-9.8602 & -21.695 & -7414.8 & -2536.4 & -389.33 & 1418.2 & -21.653 & -1424.2 & -0.14495 & -0.060495 & -43.389 & -0.0 & -5.8593 & 21.343 & -0.0 & -21.283 \\
10.730 & 1351.3 & 18634.0 & -0.0 & -0.0 & 757.50 & -0.0 & -2108.8 & -0.0 & 28.950 & 1164.7 & -0.0 & -0.0 & 11.400 & -0.0 & -40.350
\end{bmatrix},$$

$$\hat{B} = \begin{bmatrix} 0.0 \\ 0.0 \\ 0.0 \\ 0.0 \\ 0.0 \\ 0.0 \\ 0.0 \\ 0.0 \\ 3915.4 \\ 1527.0 \\ 6.3627 \\ 17.547 \\ -390.92 \\ -1749.5 \\ 27.688 \\ -0.0 \end{bmatrix}, \qquad \hat{C} = \begin{bmatrix} 0 & 0 & 0 & 0 & 0 & 0 & 0 & 1 & 0 & 0 & 0 & 0 & 0 & 0 & 0 & 0 \end{bmatrix}.$$

The linear model has 16 first-order diferential equations, so its order is 16. The output of the linear model (equation (E.30)) in comparison with the nonlinear model is shown in Figure E.1.

From Table E.1, there are two unstable poles of the system $\left[\hat{I}, \hat{A}, \hat{B}, \hat{C}\right]$ (equation E.30), namely $0.106\,10^{-4}$ and $0.505\,10^{-6}$. Because the number of digits in the fractional part of the calculation in Maple is 10 digits and $\det(A) = -98.6$, these eigenvalues cannot be considered as zero or numerical errors of the calculation. In fact, the model $\left[\hat{I}, \hat{A}, \hat{B}, \hat{C}\right]$ is unstable because the constraint equation (E.24) is replaced by its second time derivatives.

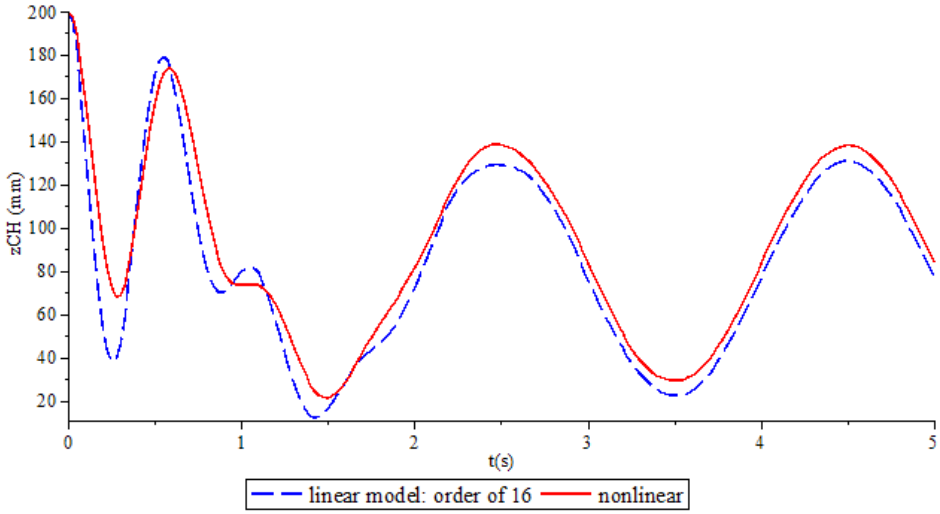

Figure E.1: Chassis Displacement of Linear and Nonlinear Models

Table E.1: Poles of Linear System $\left[\hat{I}, \hat{A}, \hat{B}, \hat{C}\right]$

$\left[\hat{I}, \hat{A}, \hat{B}, \hat{C}\right]$
-3894.4
-2565.2
-86.82+90.757*i
-86.82-90.757*i
-89.87+59.361*i
-89.87-59.361*i
-11.096+55.427*i
-11.096-55.427*i
-56.417
-67.6
-1.665+11.1*i
-1.665-11.1*i
0.106 10^{-4}
-0.106 10^{-4}
0.505 10^{-6}
-0.505 10^{-6}

E.2 Baumgarte Constraint Stabilization

In previous section, the constraint equation is replaced by its second time derivative (equation (E.27)) in order to be able to numerically solve the equations of motion (E.28). However, the linearized model (equation (E.30)) of this nonlinear model (equation (E.28)) is unstable because there are two eigenvalues of matrix $\hat{A}$ are positive number (see Table E.1). Therefore, in order to derive a stable analytical model, instead of using the acceleration equation (E.27), the following Baumgarte constraint equations replaces the constraint equation (E.24) [25]:

$$\ddot{\Phi} + 2\alpha\dot{\Phi} + \beta^2\Phi = 0, \tag{E.31}$$

with $\alpha > 0$ and $\beta \neq 0$ are constant.

Equation (E.31) is rewritten as follows:

$$\Phi_q\ddot{q} = \Big(-\left(\Phi_q\dot{q}\right)_q\dot{q} - 2\Phi_{qt}\dot{q} - \Phi_{tt}\Big) - 2\alpha\left(\Phi_q\dot{q} + \Phi_t\right) - \beta^2\Phi \equiv \hat{\gamma}. \tag{E.32}$$

Noting that the notation of this section is as same as Haug's notation in [25].

The equations of motion of the 6 DOF suspension is rewritten as follows:

$$\begin{bmatrix} M & \Phi_q^T \\ \Phi_q & 0 \end{bmatrix} \begin{bmatrix} \ddot{q} \\ \lambda \end{bmatrix} = \begin{bmatrix} Q_B \\ \hat{\gamma} \end{bmatrix}, \tag{E.33}$$

In the analytical model (equation(E.33)), choosing $\alpha = 1$, and $\beta = 1$. This analytical model has almost same output as that of the analytical model (equation (E.28)) using the second time derivative of the constraint equations (see Figure E.2).

After linearizing the nonlinear model (equation (E.33)) with the method discussed in Section 5.1.3, its state-space representation $[I, A, B, C]$, is obtained as follows:

$$\begin{aligned} \dot{X} &= AX + Bu \\ Y &= CX, \end{aligned} \tag{E.34}$$

where

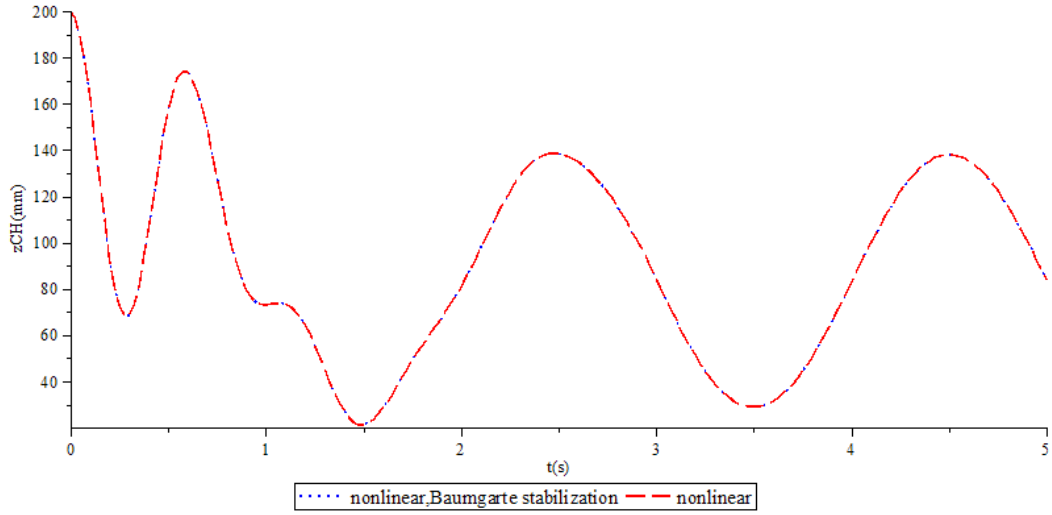

Figure E.2: Comparison of Chassis Displacement between Two Analytical Models (equations (E.33) & (E.28))

$$A = \begin{bmatrix}
0 & 0 & 0 & 0 & 0 & 0 & 0 & 0 & 1 & 0 & 0 & 0 & 0 & 0 & 0 & 0 \\
0 & 0 & 0 & 0 & 0 & 0 & 0 & 0 & 0 & 1 & 0 & 0 & 0 & 0 & 0 & 0 \\
0 & 0 & 0 & 0 & 0 & 0 & 0 & 0 & 0 & 0 & 1 & 0 & 0 & 0 & 0 & 0 \\
0 & 0 & 0 & 0 & 0 & 0 & 0 & 0 & 0 & 0 & 0 & 1 & 0 & 0 & 0 & 0 \\
0 & 0 & 0 & 0 & 0 & 0 & 0 & 0 & 0 & 0 & 0 & 0 & 1 & 0 & 0 & 0 \\
0 & 0 & 0 & 0 & 0 & 0 & 0 & 0 & 0 & 0 & 0 & 0 & 0 & 1 & 0 & 0 \\
0 & 0 & 0 & 0 & 0 & 0 & 0 & 0 & 0 & 0 & 0 & 0 & 0 & 0 & 1 & 0 \\
0 & 0 & 0 & 0 & 0 & 0 & 0 & 0 & 0 & 0 & 0 & 0 & 0 & 0 & 0 & 1 \\
-35713.4 & 46369.7 & -698346.9 & -552402.7 & -689.1 & 103.1 & -12.3 & -50388.3 & -595.8 & 951.3 & 9859.6 & 3.6 & -10.4 & 1.6 & 0.643 & -952.9 \\
46871.9 & -123205.3 & 86979.2 & -253666.9 & 497.7 & -221.6 & 15.1 & 121899.9 & 897 & -2301 & -24808.8 & -2.23 & 7.48 & -3.341 & -0.7915 & 2304.3 \\
-202.6 & 512.5 & -4133.89 & -23.86 & -18.639 & 6.15 & -0.474 & -525.06 & -3.8887 & 9.7077 & 78.852 & 0.0889 & -0.28019 & 0.092808 & 0.02487 & -9.80056 \\
-51.1021 & -40.2139 & -1551.8 & -2729.87 & 37.79 & 7.7567 & 0.1039 & 14.90994 & -0.56629 & -0.3525 & 13.10049 & -0.2309 & 0.568 & 0.116 & -0.00545 & 0.23608 \\
197.38 & 810.895 & -161803.4 & 95250.58 & -27516.81 & 63822.4 & -1026.94 & -64242.37 & -18.915 & -8.962 & -4453.496 & -443.244 & -415.69 & 959.8 & -42.469 & -950.86 \\
638.875 & 1506.65 & 396425.7 & 176287.85 & 63822.40 & -245202.74 & 3743.66 & 245445.6 & 3.7540 & 0.2520 & 1128.367 & -193.2 & 959.8 & -3689.4 & 160.3 & 3689.19 \\
-9.862 & -21.687 & -7412.76 & -2535.8 & -389.3 & 1418.2 & -23.099 & -1424.2 & -0.14927 & -0.045 & -39.26 & 1.239 & -5.8549 & 21.3279 & -2.8934 & -21.282 \\
10.7299 & 1351.3 & 18634.035 & -0.0 & 0.0 & 757.5 & -0.0 & -2108.79 & -0.0 & 28.95 & 1164.65 & -0.0 & 0.0 & 11.4 & -0.0 & -40.35
\end{bmatrix},$$

$$B = \begin{bmatrix} 0 \\ 0 \\ 0 \\ 0 \\ 0 \\ 0 \\ 0 \\ 0 \\ 3915.42 \\ 1527.011 \\ 6.36 \\ 17.54 \\ -390.9 \\ -1749.5 \\ 27.687 \\ -0.0 \end{bmatrix}, \quad C = \begin{bmatrix} 0 & 0 & 0 & 0 & 0 & 0 & 0 & 1 & 0 & 0 & 0 & 0 & 0 & 0 & 0 & 0 \end{bmatrix}.$$

The linear model $[I, A, B, C]$ is asymptotically stable (see Table E.2).

Table E.2: Poles of $[I, A, B, C]$ and $\left[\hat{I}, \hat{A}, \hat{B}, \hat{C}\right]$ Models

$[\hat{I}, \hat{A}, \hat{B}, \hat{C}]$	$[I, A, B, C]$
-3894.4	-3894.4
-2565.2	-2565.2
-86.82+90.757*i	-86.82+90.757*i
-86.82-90.757*i	-86.82-90.757*i
-89.87+59.361*i	-89.87+59.361*i
-89.87-59.361*i	-89.87-59.361*i
-11.096+55.427*i	-11.096+55.427*i
-11.096-55.427*i	-11.096-55.427*i
-56.417	-56.417
-67.6	-67.6
-1.665+11.1*i	-1.665+11.1*i
-1.665-11.1*i	-1.665-11.1*i
0.106 10^{-4}	-1+0.47 10^{-4}*i
-0.106 10^{-4}	-1 -0.47 10^{-4}*i
0.505 10^{-6}	-1 +0.227 10^{-4}*i
-0.505 10^{-6}	-1 -0.227 10^{-4}*i

Appendix F

Demo of Using MapleSim Template of Model Reduction

There are 2 video demonstrating how to use the MapleSim temple described in Section 5.9 to reduce a 2 DOF double-wishbone suspension (http://youtu.be/sav4oZD33ro) and a centrifuge (http://youtu.be/aO09WK4GzU4)

References

[1] M. Celik A. Odabasioglu and L.T. Pileggi. Prima: passive reduced-order interconnect macromodeling algorithm. *Computer-Aided Design of Integrated Circuits and Systems, IEEE Transactions on*, 17(8):645–654, 1998.

[2] A.C. Antoulas. *Approximation of Large-Scale Dynamical Systems*. Society for Industrial and Applied Mathematics, 2005.

[3] P. Astrid. *Reduction of process simulation models: A proper orthogonal decomposition approach*. PhD thesis, Technische Universiteit Eindhoven (The Netherlands), 2004.

[4] Z. Bai. Krylov subspace techniques for reduced-order modeling of large-scale dynamical systems. *Applied Numerical Mathematics*, 43(12):9–44, 10 2002.

[5] G. Berkooz, P. Holmes, and J.L. Lumley. The proper orthogonal decomposition in the analysis of turbulent flows. *Annual Review of Fluid Mechanics*, 25(1):539–575, 1993.

[6] B. Besselink, N. Wouw, and H. Nijmeijer. Model reduction of nonlinear systems with bounded incremental 2 gain. In *Decision and Control and European Control Conference (CDC-ECC), 2011 50th IEEE Conference on*, pages 7170–7175. IEEE, 2011.

[7] V. Buljak. *Proper Orthogonal Decomposition and Radial Basis Functions for Fast Simulations*, pages 85–139. Inverse Analyses with Model Reduction. Springer, 2012.

[8] M. Burkhardt and R. Seifried. Simulation and feed-forward control of a flexible parallel manipulator. *PAMM Proceedings in Applied Mathematics and Mechanics*, 11(1):39–40, 2011.

[9] P. Ro C. Kim and H. Kim. Effect of the suspension structure on equivalent suspension parameters. *Proceedings of the Institution of Mechanical Engineers, Part D: Journal of Automobile Engineering*, 213(5):457–470, 1999.

[10] S. Chaturantabut and D.C. Sorensen. Nonlinear model reduction via discrete empirical interpolation. *SIAM Journal on Scientific Computing*, 32(5):2737–2764, 2010.

[11] J.D. Cobb. Feedback and pole-placement in descriptor variable systems. *International Journal of Control*, 33:1135–1146, 1981.

[12] T. Colonius C.W. Rowley and R.M. Murray. Model reduction for compressible flows using pod and galerkin projection. *Physica D: Nonlinear Phenomena*, 189(1):115–129, 2004.

[13] P.M. Van Dooren. The generalized eigenstructure problem in linear system theory. *IEEE Trans. Automat. Control AC*, 26, 1981.

[14] F. Ebert. A note on pod model reduction methods for daes. *Mathematical and Computer Modelling of Dynamical Systems*, 16(2):115–131, 2010.

[15] J. Edgar. *Front Suspension Designs*, 2006. http://www.autospeed.com/cms/article.html?&A=2934.

[16] P. Feldmann and R.W. Freund. Efficient linear circuit analysis by pade approximation via the lanczos process. *Computer-Aided Design of Integrated Circuits and Systems, IEEE Transactions on*, 14(5):639–649, 1995. ID: 1.

[17] P. Feldmann and R.W. Freund. Reduced-order modeling of large linear subcircuits via a block lanczos algorithm. In *Proceedings of the 32nd annual ACM/IEEE Design Automation Conference*, pages 474–479. ACM, 1995.

[18] A. Feliachi and C. Bhurtun. Model reduction of large-scale interconnected systems. *International Journal of Systems Science*, 18(12):2249–2259, 1987.

[19] P. Mantegazza G. Quaranta and P. Masarati. Assessing the local stability of periodic motions for large multibody non-linear systems using proper orthogonal decomposition. *Journal of Sound and Vibration*, 271(3):1015–1038, 2004.

[20] K.A. Gallivan, E. Grimme, and P.M. Van Dooren. *Model Reduction of Large-Scale Systems Rational Krylov Versus Balancing Techniques*, pages 177–190. Error control and adaptivity in scientific computing. Springer, 1999.

[21] G. Golub and W. Kahan. Calculating the singular values and pseudo-inverse of a matrix. *Journal of the Society for Industrial & Applied Mathematics, Series B: Numerical Analysis*, 2(2):205–224, 1965.

[22] D. Gratton and K. Willcox. *Reduced-order, trajectory piecewise-linear models for nonlinear computational fluid dynamics*, 2004.

[23] W. Steven Gray and J. Scherpen. On the nonuniqueness of singular value functions and balanced nonlinear realizations. *Systems & Control Letters*, 44(3):219–232, 2001.

[24] E.J. Grimme. *Krylov projection methods for model reduction*. PhD thesis, University of Illinois at Urbana-Champaign, Urbana, IL, USA, 1997.

[25] E.J. Haug. *Computer aided kinematics and dynamics of mechanical systems*, volume 1. Allyn and Bacon Boston, 1989.

[26] T. Reis J. Mockel and T. Stykel. Linear-quadratic gaussian balancing for model reduction of differential-algebraic systems. *International Journal of Control*, 84(10):1627–1643, Oct 2011.

[27] E. Jonckheere and L. Silverman. A new set of invariants for linear systems–application to reduced order compensator design. *Automatic Control, IEEE Transactions on*, 28(10):953–964, 1983.

[28] T. Katayama and K. Minamino. Linear quadratic regulator and spectral factorization for continous-time descriptor systems. In *Decision and Control, 1992., Proceedings of the 31st IEEE Conference on*, pages 967–972. IEEE, 1992.

[29] A. Kawamoto, K. Takaba, and T. Katayama. On the generalized algebraic riccati equation for continuous-time descriptor systems. *Linear algebra and its applications*, 296(1):1–14, 1999.

[30] L. Knockaert and D. Zutter. Laguerre-svd reduced-order modeling. *Microwave Theory and Techniques, IEEE Transactions on*, 48(9):1469–1475, 2000.

[31] A.J. Krener. *Reduced order modeling of nonlinear control systems*, pages 41–62. Analysis and Design of Nonlinear Control Systems. Springer, 2008.

[32] S. Lall and C. Beck. Error-bounds for balanced model-reduction of linear time-varying systems. *Automatic Control, IEEE Transactions on*, 48(6):946–956, 2003.

[33] P. Lancaster and L. Rodman. *Algebraic riccati equations*. Oxford University Press, 1995.

[34] Y. Liang. *Parametric identification of chaotic/nonlinear systems and reduced order models based on proper orthogonal decomposition*. PhD thesis, 2005.

[35] Z. Liu and J. Wagner. Nonlinear model reduction for dynamic and automotive system descriptions. *Journal of Dynamic Systems, Measurement and Control, Transactions of the ASME*, 124(4):637–647, 2002. Cited By (since 1996):7.

[36] L.S. Louca. *An energy-based model reduction methodology for automated modeling.* PhD thesis, 1998.

[37] L.S. Louca, J.L. Stein, and G.M. Hulbert. Energy-based model reduction methodology for automated modeling. *Journal of Dynamic Systems, Measurement and Control, Transactions of the ASME*, 132(6), 2010.

[38] L.S. Louca and B.U. Yildir. Modelling and reduction techniques for studies of integrated hybrid vehicle systems. *Mathematical and Computer Modelling of Dynamical Systems*, 12(2-3):203–218, 2006.

[39] D.G. Luenberger. *Optimization by Vector Space Method.* John Wiley, 1969.

[40] D.J.N. Limebeer M. Green. *Linear Robust Control.* Prentice Hall, 1995.

[41] V. Mallet and S. Zhuk. Reduced minimax filtering by means of differential-algebraic equations. In *Proc. of 5th Int. Conf. on Physics and Control (PhysCon 2011). IPACS Electronic Library*, 2011.

[42] V. Mehrmann and T. Stykel. Balanced truncation model reduction for large-scale systems in descriptor form. *Dimension Reduction of Large-Scale Systems*, pages 83–115, 2005.

[43] D. G. Meyer and S. Srinivasan. Balancing and model reduction for second-order form linear systems. *Automatic Control, IEEE Transactions on*, 41(11):1632–1644, 1996.

[44] B.C. Moore. Principal component analysis in linear systems: Controllability, observability, and model reduction. *Automatic Control, IEEE Transactions on*, 26(1):17–32, 1981. ID: 1.

[45] P.E. Nikravesh. *Computer-aided analysis of mechanical systems.* Prentice-Hall, Inc., 1988.

[46] M. Lanz P. Masarati, G. Quaranta and P. Mantegazza. Dynamic characterization and stability of a large size multibody tiltrotor model by pod analysis. In *ASME 2003 International Design Engineering Technical Conferences and Computers and Information in Engineering Conference*, pages 1145–1154. American Society of Mechanical Engineers, 2003.

[47] K. Pearson. Liii. on lines and planes of closest fit to systems of points in space. *The London, Edinburgh, and Dublin Philosophical Magazine and Journal of Science*, 2(11):559–572, 1901.

[48] L.T. Pillage and R.A. Rohrer. Asymptotic waveform evaluation for timing analysis. *Computer-Aided Design of Integrated Circuits and Systems, IEEE Transactions on*, 9(4):352–366, 1990. ID: 1.

[49] J.W. Polderman and J.C. Willems. *Introduction to mathematical systems theory: a behavorial approach*, volume 26. Springer, 1998.

[50] T. Reis and T. Stykel. Stability analysis and model order reduction of coupled systems. *Mathematical and Computer Modelling of Dynamical Systems*, 13(5):413–436, 2007.

[51] T. Reis and T. Stykel. Balanced truncation model reduction of second-order systems. *Mathematical and Computer Modelling of Dynamical Systems*, 14(5):391–406, 10/01; 2013/12 2008. doi: 10.1080/13873950701844170; M3: doi: 10.1080/13873950701844170; 14.

[52] M.J. Rewieski. *A Trajectory Piecewise-Linear Approach to Model Order Reduction of Nonlinear Dynamical Systems*. PhD thesis, 2003.

[53] M. Ripepi and P. Masarati. Reduced order models using generalized eigenanalysis. *Proceedings of the Institution of Mechanical Engineers, Part K: Journal of Multi-body Dynamics*, 225(1):52–65, 2011.

[54] A.L. Ros and A. Messina. Order-reduction strategy of non-linear differential-algebraic equation models with application on power systems. *Electric Power Components and Systems*, 40(15):1690–1707, 2012.

[55] RC Rosenberg and T. Zhou. Power-based model insight. In *Proc. 1988 ASME Winter Annual Meeting, Symposium on Automated Modeling for Design*, pages 61–67, 1988.

[56] J.E. Marsden S. Lall and S. Glavaaki. Empirical model reduction of controlled nonlinear systems. International Federation of Automatic Control, 1999.

[57] J.E. Marsden. S. Lall and S. Glavaki. A subspace approach to balanced truncation for model reduction of nonlinear control systems. *International Journal of Robust and Nonlinear Control*, 12(6):519–535, 2002.

[58] L. Ozkan S. Weiland, J. Wildenberg and J. Ludlage. A lagrangian method for model reduction of controlled systems. In *Proceedings of the 17th IFAC World Congress, Seoul*, 2008.

[59] Y. Saad. *Iterative methods for sparse linear systems*. Siam, 2003.

[60] H. Sandberg and A. Rantzer. Balanced truncation of linear time-varying systems. *Automatic Control, IEEE Transactions on*, 49(2):217–229, 2004.

[61] J. Scherpen. Balancing for nonlinear systems. *Systems & Control Letters*, 21(2):143–153, 1993.

[62] J. Scherpen. H balancing for nonlinear systems. *International Journal of Robust and Nonlinear Control*, 6(7):645–668, 1996.

[63] J. Scherpen and A.V.D. Schaft. Normalized coprime factorizations and balancing for unstable nonlinear systems. *International Journal of Control*, 60(6):1193–1222, 1994.

[64] A.A. Shabana. *Computational dynamics*. Wiley. com, 2009.

[65] CS Sharma and K. Purohit. *Theory of Mechanisms and Machines*. PHI Learning Pvt. Ltd., 2006.

[66] S. Shokoohi, L. Silverman, and P. Van Dooren. Linear time-variable systems: Balancing and model reduction. *Automatic Control, IEEE Transactions on*, 28(8):810–822, 1983.

[67] T. Stykel. Gramian-based model reduction for descriptor systems. *Math. Control Signals Systems*, 16, 2004.

[68] C. Sun and J. Hahn. Reduction of stable differential-algebraic equation systems via projections and system identification. *Journal of Process Control*, 15(6):639–650, 2005.

[69] F. Trltzsch and S. Volkwein. Pod a-posteriori error estimates for linear-quadratic optimal control problems. *Computational Optimization and Applications*, 44(1):83–115, 2009.

[70] A. Ubaidm and F. Genef. An error bound for a discrete reduced order model of a linear multivariable system. *Automatic Control, IEEE Transactions on*, 32(9):815–819, 1987.

[71] A. Vandendorpe and P.V. Dooren. *Model reduction of interconnected systems*, pages 305–321. Model Order Reduction: Theory, Research Aspects and Applications. Springer, 2008.

[72] A. Varga. Computation of irreducible generalized state-space realizations. *Kybernetika*, 26(2):89–106, 1990.

[73] D. Vasilyev, M. Rewienski, and J. White. A tbr-based trajectory piecewise-linear algorithm for generating accurate low-order models for nonlinear analog circuits and mems. In *Design Automation Conference, 2003. Proceedings*, pages 490–495. IEEE, 2003.

[74] D. Vasilyev, M. Rewienski, and J. White. *Macromodel generation for BioMEMS components using a stabilized balanced truncation plus trajectory piecewise linear approach*, pages 169–187. Design Automation Methods and Tools for Microfluidics-Based Biochips. Springer, 2006.

[75] E. Verriest and T. Kailath. On generalized balanced realizations. *Automatic Control, IEEE Transactions on*, 28(8):833–844, 1983.

[76] Thomas Vob. Model reduction for nonlinear differential-algebraic equations. In *Communications to SIMAI Congress*, volume 2, 2007.

[77] X. Xin. Strong solutions and maximal solutions of generalized algebraic riccati equations. In *Decision and Control, 2008. CDC 2008. 47th IEEE Conference on*, pages 528–533. IEEE, 2008.

[78] A. Vandendorpe Y. Chahlaoui, D. Lemonnier and P.V. Dooren. Second-order balanced truncation. *Linear algebra and its applications*, 415(2):373–384, 2006.

[79] Y. Yang and K. Shen. Nonlinear heat-transfer macromodeling for mems thermal devices. *Journal of Micromechanics and Microengineering*, 15(2):408, 2005.

[80] R. Li Z. Bai and Y. Su. A unified krylov projection framework for structure-preserving model reduction. In WilhelmusH.A. Schilders, HenkA. Vorst, and Joost Rommes, editors, *Model Order Reduction: Theory, Research Aspects and Applications*, volume 13 of *Mathematics in Industry*, pages 75–93. Springer Berlin Heidelberg, 2008.

[81] K. Zhou, G. Salomon, and E. Wu. Balanced realization and model reduction for unstable systems. *International Journal of Robust and Nonlinear Control*, 9(3):183–198, 1999.